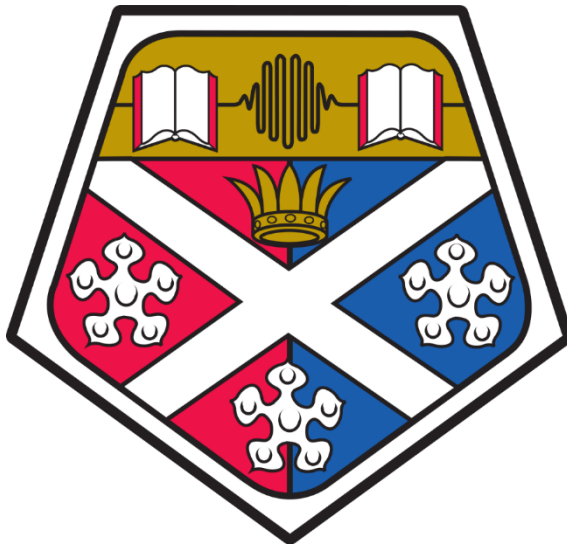


*DEVELOPMENT OF A MICROBIALLY
INDUCED CALCITE AND SILICA BIO-
GROUT FOR THE SEALING OF FINE
APERTURE FRACTURES*



Erica MacLachlan

Department of Civil and Environmental Engineering

A thesis submitted by Erica MacLachlan to the Department of Civil and Environmental Engineering, University of Strathclyde for the degree of Doctor of Philosophy

June 2017

Word Count = 42044 words.

Acknowledgements

“Gratitude is one of the least articulate of the emotions, especially when it is deep.”

Felix Frankfurter

Life doesn't stand still or wait for you to finish your thesis, instead it challenges you throughout your PhD years. Sometimes I wasn't sure if I could rise to these challenges but because of the invaluable support of a several people I was able to. Without these supporters, especially the select few I'm about to mention, I may not have been able to complete my PhD, at least not sanely.

It has been my privilege to work with Professor Rebecca Lunn and Dr Grainne El Mountassir. I have enjoyed the opportunity to watch and learn from their knowledge and experience. Their frequent insights and patience with me is fully appreciated. I am very proud of what we have achieved together, thank you both. I would also like to thank both of you for your help and understanding during a particularly difficult period of time during my Ph.D, without your help I may have never completed this wonderful experience. I would never have really known about this topic without the introduction to it by Dr Vernon Phoenix and Dr Dominique Tobler from Glasgow University, who accepted me to work with them on the subject during my undergraduate degree. I have also enjoyed many useful and entertaining discussions with Dr Charles Knapp who has always had an available ear for bending when I had a question.

Finally, I am indebted to my partner Paul, my daughter Fiona and my nephew Iain who not only supported and encouraged me throughout the last few years but showed me that there is more to life than hiding and studying. Without you my life would be boring 😊

“If you’re not part of the solution, you’re part of the precipitate”

Henry J Tillman

Declaration

This thesis is the result of the author's original research. It has been composed by the author and has not been previously submitted for examination which has led to the award of a degree.'

The copyright of this thesis belongs to the author under the terms of the United Kingdom Copyright Acts as qualified by University of Strathclyde Regulation 3.50. Due acknowledgement must always be made of the use of any material contained in, or derived from, this thesis.'

Signed: _____

Date: _____

—

Erica MacLachlan BSc (hons), MSc

Abstract

Geological repositories are being considered as the best feasible solution for the storage of hazardous materials such as high level nuclear waste throughout the world, including the UK. However; when crystalline rock is the chosen storage medium, the construction of the underground tunnels and caverns can enhance discontinuities within the rock. These discontinuities can be pathways by which radio-nuclides can reach the biosphere, due to their higher permeability, connectivity and density (Blyth and Freitas, 1992). Thus, depending on aperture, density and predicted travel times, it may be necessary to grout all fractures, even small aperture ones, which over thousands of years can contribute significantly to subsurface flow.

Conventional cementitious and chemical grouts are unsuitable within some regions of a geological disposal facility due to concerns regarding longevity, toxicity, reactions with other barriers and/or workability issues. The four main requirements of a grout are; to be of low viscosity as the lower the viscosity the easier it is to achieve good penetration, to have a controllable gel/setting time, to be chemically inert to prevent reactions within the subsurface or have any toxic consequences during preparation, and to be durable thus able to withstand exposure to varying physico-chemical condition. MICP (Microbially Induced Calcite Precipitation) and Colloidal Silica are novel grouts which may be suitable for the sealing of fine aperture fractures in rock. MICP research has been predominantly focussed on its application in sediments, whilst colloidal silica has shown its potential for reducing the liquefaction potential of non-cohesive soils and for sealing fractures.

This research examines the influence of hydraulic controls (velocity, flow rate, aperture) on the spatial distribution of microbially induced calcite precipitation (MICP) within simulated fractures using flocculated *Sporosarcina pasteurii*. The experimental results show that under flowing conditions, the spatial distribution of microbially induced calcite precipitate on fracture surfaces is controlled by fluid velocity. Even for a uniform initial fracture aperture with a steady flow rate, a feedback mechanism existed between velocity and precipitation that resulted in a precipitate distribution that focussed flow into a small number of self-organizing channels which remained stable. Ultimately, this feedback mechanism controlled the final aperture profile which governed flow within the fracture.

To use MICP for field scale sealing operations (e.g., in aquifers and host rock surrounding nuclear waste storage sites), it is important to develop an injection strategy that ensures microbially precipitated calcite is distributed homogeneously throughout the rock body to avoid preferential flow through high porosity pathways. *Sporosarcina pasteurii* was found to be able to hydrolyse urea for several days before the bacteria became encased within calcite preventing access to the cementing fluid. The higher rates of urea hydrolysis occurred within the first 9 hours, though significant rates of urea hydrolysis still occurred after this period. By reducing the size of bacterial flocs it is possible to reduce the impact of sedimentation and straining, promoting a more even distribution of bacteria thus calcite precipitate throughout the plate. By increasing the length of time that the bacteria flow through the fracture, more bacteria can become entrained upon the fracture surface giving a better distribution.

The introduction of a filler (colloidal silica) that can also act as a nucleation site for calcite precipitation was examined as a way of reducing the time it takes for the sealing of a fracture. Both *Sporosarcina pasteurii* and colloidal silica have negative surface charges thus colloidal silica could be used as a nucleation surface, this plus its nanometre size which could allow for a better distribution of and could enhance calcite precipitation.

A clear difference in the mass of grout retained within the fracture was seen, with MICP alone showing the greatest weight increase. During the 8 grouting cycles with MICP + colloidal silica there appeared to be pieces of calcite travelling through the open channels. This would indicate that the calcite is unable to attach to the fracture surface. Thus, adding a small amount of colloidal silica to the cementing solution as a filler was not an efficient way to produce calcite fill. However, *Sporosarcina pasteurii* produces ammonium ions from the hydrolysis of the non-ionic urea, which as a cation can destabilise the silica sol resulting in gelation.

Batch tests were used to determine what differences in gel point, gel rate and shear strength were created by different cations, including the chemical addition of ammonium ions and the biological production of ammonium ions by the bacterium *Sporosarcina pasteurii*. The sensitivity of colloidal silica to calcium chloride can result in dramatic differences in gel time with small changes in molarity having great impact on whether the colloidal silica gels or not. The direct addition of ammonium salts requires ten times the concentration, compared to CaCl_2 , to achieve similar shear

strength values. However; this concentration produces very short gel times, potentially reducing the radius of penetration. The bacterial in-situ production of ammonium ions gives the greatest gel times yet still produces the same shear strength as that of a sodium chloride accelerator. This increasing of gel times, without adversely impacting grout properties, could be beneficial for penetrating greater distances into fractured rock reducing the number of injection points required. This would be particularly useful for subsurface engineering applications where large volumes of rock are required to be grouted.

Contents

1. INTRODUCTION.....	22
1.1 GROUTING	22
1.2 COMMON GROUTS	23
1.3 GROUTING FOR THE GEOLOGICAL DISPOSAL OF NUCLEAR WASTE	26
1.4 AIMS AND OBJECTIVES.....	29
1.5 THESIS OUTLINE.....	30
2. LITERATURE REVIEW: MICROBIALLY INDUCED CALCITE PRECIPITATION	32
2.1 INTRODUCTION	32
2.2 PRESENCE OF CALCIUM CARBONATE IN NATURAL ROCK FRACTURES.....	32
2.3 THE MICP PROCESS	35
2.4 APPLICATIONS OF MICP	39
2.4.1 <i>Permeability reduction in porous media</i>	39
2.4.2 <i>Strength improvement of porous media</i>	40
2.4.2 <i>Permeability reduction in fractured media</i>	43
2.4.3 <i>Solid-phase capture of contaminants</i>	45
2.4.4 <i>Construction materials</i>	45
2.5 IMPROVEMENT OF THE SPATIAL DISTRIBUTION OF CALCIUM CARBONATE PRECIPITATION	46
2.5.1 <i>Biofilm growth (nutrients vs no nutrients)</i>	47
2.5.2 <i>Injection strategies</i>	48
2.5.3 <i>Flocculation</i>	49
2.5.4 <i>Fixer</i>	49
2.6 CONCLUSION	53
3. MICP IN FRACTURES	54

3.1 INTRODUCTION	54
3.2 BACKGROUND	54
3.3 METHODOLOGY	55
3.3.1 <i>Flow-plate setup</i>	55
3.3.2 <i>Fracture velocities</i>	56
3.3.3 <i>Bacterial Solution</i>	57
3.3.4 <i>Injection Strategy</i>	58
3.3.5 <i>SEM Analysis</i>	60
3.4 PREVIOUS WORK COMPLETED BY MSC STUDENT	60
3.5 INFLUENCE OF VELOCITY.....	61
3.6 RESULTS	65
3.6.1 <i>Initial Observations</i>	65
3.6.2 <i>Bacterial Density</i>	67
3.6.3 <i>Flow Rate Reduction</i>	70
3.6.4 <i>SEM Analysis</i>	73
3.7 DISCUSSION.....	74
3.8 CONCLUSIONS	78
4. IMPROVING THE UNIFORMITY OF MICP DISTRIBUTION IN ROCK FRACTURES	79
4.1 INTRODUCTION	79
4.2 MATERIALS AND METHODS.....	80
4.2.1 <i>Bacterial and Cementing Solutions</i>	80
4.2.2 <i>Determination of cation concentrations</i>	81
4.2.3 <i>Scanning Electron Microscopy</i>	81
4.2.4 <i>Laser Scanner</i>	81
4.3 BATCH TESTS.....	82

4.3.1 <i>Batch Test Results, which Informed Flow-plate Set-up</i>	83
4.4 FLOW-PLATE EXPERIMENT	86
4.4.2 <i>Hydraulic aperture and fracture velocity</i>	87
4.4.3 <i>Injection Strategy for Flow-plate 3</i>	89
4.5 FLOW-PLATE 3 RESULTS AND DISCUSSION	91
4.5.1 <i>Chemical Analysis of Effluent</i>	93
4.5.2 <i>Fracture Topography</i>	96
4.5.3 <i>SEM Analysis</i>	99
4.5.4 <i>Discussion and Conclusion</i>	100
5. THE DEVELOPMENT OF A COMBINED BACTERIAL CALCITE AND SILICA GROUT.	102
5.1 INTRODUCTION TO COLLOIDAL SILICA GROUT.....	102
5.2 COLLOIDAL SILICA AS A GROUT FOR IMPARTING STRENGTH.....	104
5.3 COLLOIDAL SILICA AS A GROUT TO REDUCE HYDRAULIC CONDUCTIVITY.....	108
5.3.1 <i>Reduction in the Hydraulic Conductivity of Soils</i>	108
5.3.2 <i>Colloidal Silica as a Grout for the Reduction of Hydraulic Conductivity of Fractured Rock</i>	109
5.4 PENETRATION OF COLLOIDAL SILICA.....	110
5.5 CHOICE OF ACCELERATORS FOR THE GELLING OF COLLOIDAL SILICA.....	112
5.6 IS IT POSSIBLE TO USE COLLOIDAL SILICA AS A FILLER DURING MICP?.....	113
5.6.1 <i>Methods and Materials</i>	113
5.6.2 <i>Results</i>	114
5.6.3 <i>Discussion and Conclusion</i>	117
5.7 VARYING THE ACCELERATOR FOR COLLOIDAL SILICA GROUTING	120
5.7.1 <i>Materials and Methods</i>	120
5.7.2 <i>Results</i>	125
5.9 IMPLICATIONS FOR GROUTING.....	140

5.10 CONCLUSION.....	141
6. DISCUSSION FOR INDUSTRIAL APPLICATIONS	142
6.1 WHAT CURRENT GROUTING PROBLEMS COULD THIS RESEARCH SOLVE?.....	142
6.2 WHAT FURTHER RESEARCH IS REQUIRED TO ENABLE THIS WORK TO BE APPLIED AT A FIELD SCALE?.....	146
6.3 HOW WOULD THIS RESEARCH BE APPLIED AT A FIELD SCALE?.....	147
7 CONCLUSIONS AND FUTURE WORK	150
7.1 CONCLUSIONS	150
7.2 FUTURE WORK	154

List of Tables

- TABLE 2.1: CONCENTRATIONS OF BACTERIA AND CEMENTING AGENTS USED FOR DIFFERENT PURPOSES AND RESULTS. 51
- TABLE 3.1: SUMMARY OF PREPARATION AND CONSTITUENTS OF INJECTION SOLUTIONS 57
- TABLE 3.2: FLOW RATE, OPTICAL DENSITY, PUMPED INJECTION VOLUME, DURATION AND NUMBER OF INJECTION CYCLES. 59
- TABLE 4.1: BATCH TEST SETUP, EXAMINING THE IMPACT OF DIFFERENT RATIOS OF BACTERIAL VOLUME TO CEMENTING SOLUTION VOLUME AND CALCIUM CARBONATE MORPHOLOGY. 82
- TABLE 4.2: INJECTION STRATEGY FOR THE FLOW-PLATE, CONSISTING OF A BACTERIA STAGE, A WATER PULSE TO CLEAR THE TUBING, THE CEMENTING SOLUTION STAGE AND FINAL WATER PULSE BEFORE THE FOLLOWING CYCLE. THE FRACTURE VOLUME IS THE TOTAL VOLUME INJECTED PER STAGE DIVIDED BY THE INITIAL FRACTURE LIQUID VOLUME. * AFTER THREE HOURS, THE EFFLUENT WAS RECIRCULATED TO CREATE A CLOSED SYSTEM THAT COULD BE LEFT RUNNING OVERNIGHT WITHOUT CESSATION OF FLOW. 90
- TABLE 4.3: UREA HYDROLYSIS AND CALCIUM UTILISATION CALCULATED FROM THE REDUCTION IN RE-CIRCULATED CEMENTING FLUID AT THE END OF EACH CYCLE. UREA HYDROLYSIS CALCULATED FROM THE AMMONIUM PRODUCED OVER THE CYCLE DIVIDED BY THE MAXIMUM POSSIBLE AMOUNT OF AMMONIUM THAT COULD BE PRODUCED HAD ALL OF THE UREA PRESENT HAD BEEN HYDROLYSED. 95
- TABLE 5.1: COMPOSITION OF BATCH TESTS AND MASS OF CALCITE PRODUCED BY EACH INDIVIDUAL TEST, CS = COLLOIDAL SILICA. 114
- TABLE 5.2: COMPARISON OF GROUT WEIGHTS BETWEEN MICP AND MICP WITH 25ML PER LITRE OF CEMENTING SOLUTION. 116
- TABLE 5.3: THE FINAL OPTICAL DENSITIES OF BACTERIA AND HOW THEY WERE ACHIEVED. THE BACTERIALLY-INDUCED AMMONIUM IONS WAS ACHIEVED BY MIXING 20ML OF REQUIRED BACTERIAL SUSPENSION AND 20ML OF 1.74M UREA TOGETHER AND THEN MIXING WITH 200ML OF COLLOIDAL SILICA. TO ACHIEVE OPTICAL DENSITIES >1 , LARGER VOLUMES OF LOWER CONCENTRATION

SUSPENSIONS WERE CENTRIFUGED, AND THE SUPERNATANT RE-SUSPENDED IN
SMALLER VOLUMES OF STERILE WATER. 121

TABLE 5.4: THE GEL TIME FOR DIFFERENT SODIUM CHLORIDE CONCENTRATION
COLLOIDAL SILICA GROUTS. 125

TABLE 5.5: COMPOSITION AND CONCENTRATION OF DIFFERENT ACCELERATORS TESTED
AND CORRESPONDING COLLOIDAL SILICA GROUT PROPERTIES. 127

TABLE 6.1: PERFORMANCE CRITERIA OF MICP, COLLOIDAL SILICA AND OPC.
144

List of Figures

FIGURE 1.1: CARTOON OF FRACTURE GROUTING SHOWING GROUT PENETRATION AND ASSOCIATED PROBLEMS. 22

FIGURE 1.2: FILTER CAKE FORMATION OF A CEMENT GROUT AT THE OPENING OF A DISCONTINUITY (AFTER EKLUND AND STILLE, 2008). 23

FIGURE 1.3: SKB'S TWO DISPOSAL PLANS FOR THE GEOLOGICAL DISPOSAL OF HIGH LEVEL NUCLEAR WASTE IN THE CRYSTALLINE (GRANITE) BEDROCK, SWEDEN (POSIVA, 2012). 27

FIGURE 2.1: CALCITE VEINING PRESENT WITHIN A ROCK OUTCROP AT CAPE FORCHU, YARMOUTH (IMAGE COURTESY OF GARY DEVILLER YCMHS HIGH SCHOOL) 33

FIGURE 2.2: A) CALCIUM IONS IN THE SOLUTION ARE ATTRACTED TO THE BACTERIAL CELL WALL DUE TO THE NEGATIVE CHARGE OF THE LATTER. UPON ADDITION OF UREA TO THE BACTERIA, DISSOLVED INORGANIC CARBON (DIC) AND AMMONIUM (AMM) ARE RELEASED IN THE MICROENVIRONMENT OF THE BACTERIA (A). IN THE PRESENCE OF CALCIUM IONS, THIS CAN RESULT IN A LOCAL SUPERSATURATION AND HENCE HETEROGENEOUS PRECIPITATION OF CALCIUM ARBONATE ON THE BACTERIAL CELL WALL (B). AFTER A WHILE, THE WHOLE CELL BECOME ENCAPSULATED (C), LIMITING NUTRIENT TRANSFER, RESULTING IN CELL DEATH (DEMUYNCK, 2010). 2B) SEM IMAGES FROM MY MSC DISSERTATION (MCLACHLAN, 2011); SHOWING CALCIUM CARBONATE PRECIPITATE SURROUNDING THE NEGATIVE FOOTPRINT OF THE BACTERIA. 38

FIGURE 2.3: BACTERIALLY CEMENTED SAND APPROXIMATELY 43 M³ IN VOLUME SHOWING A WEDGE SHAPE CREATED BY THE HYDROLOGICAL FLOW FROM INJECTION TO EXTRACTION (COLUMNS CLOSEST IN THE FIELD OF VIEW) (VAN PAASSEEN ET AL, 2010). 42

FIGURE 2.4: PHOTOGRAPHS SHOWING THE CHANGE IN CRYSTAL SIZE AND DISTRIBUTION OF CALCIUM CARBONATE WITHIN A FLOWING SYSTEM (SCHULTZ ET AL. 2011). 43

FIGURE 3.1: EXPERIMENTAL SETUP: (A) PLAN VIEW OF TOP POLYCARBONATE SHEET, (B) PLAN VIEW OF LOWER ETCHED POLYCARBONATE SHEET, (C) CROSS SECTION OF FRACTURES OF DIFFERENT WIDTHS AND APERTURES IN FLOW-PLATE 1 (VERTICAL EXAGGERATION OF APERTURES IS 10X), (D) CROSS SECTION OF FRACTURES OF

DIFFERENT WIDTHS AND APERTURES IN FLOW-PLATE 2 (VERTICAL EXAGGERATION OF APERTURES OF 10X), AND (E) SCHEMATIC OF FLOW ARRANGEMENT. 56

FIGURE 3.2: OIL IMMERSION OLYMPUS FLUORESCENCE MICROSCOPE IMAGES OF FLOCCULATED BACTERIA AT (A) 1.00OD600 AND (B) 0.25 OD600. 58

FIGURE 3.3: INFLUENCE OF VELOCITY AND APERTURE ON CALCITE PRECIPITATION (FLOW-PLATE 1) AFTER FIVE INJECTION CYCLES AT (A) $Q = 1.12$ ML/MIN, (B) $Q = 4.48$ ML/MIN. W IS THE WIDTH OF AN INDIVIDUAL FRACTURE PERPENDICULAR TO THE FLOW DIRECTION AND MARKED IN (A), B IS THE FRACTURE APERTURE AND V_1 IS THE INITIAL AVERAGE FRACTURE VELOCITY, I.E. PRIOR TO PRECIPITATION. IT SHOULD ALSO BE NOTED THAT THE FLOW-PLATE WAS NOT FULLY SEALED BETWEEN CHANNELS (SEE B) AND ACROSS CELL FLOW WAS OBSERVED BETWEEN FRACTURES; THE ACTUAL VOLUME OF ACROSS CELL FLOW WAS VERY LOW, AS EACH FRACTURE WAS CALIBRATED FOR THE DESIRED FLOW RATE BOTH PRIOR TO ENTERING THE FRACTURE INLET AND AT THE FRACTURE OUTLET. FIGURES (C) AND (D) SHOW THE DEVELOPMENT OF OPEN FASTER FLOWING CHANNELS IN FRACTURE 8 AFTER 5 INJECTION CYCLES AT $Q = 1.12$ ML/MIN AND $Q = 4.48$ ML/MIN: (I) DIGITAL PHOTOGRAPH OF AREAS IN FRACTURE 8 MARKED ON FIGURE 3.1, (II) DIGITAL ESTIMATION OF DEPTH OF CALCITE PRECIPITATION (IMAGE ANALYSIS CONDUCTED USING MATLAB), WHERE BLUE INDICATES THAT THE FRACTURE IS FULLY CLOSED AT THAT LOCATION (I.E. APERTURE = 0), FOR THE RED CHANNELS THE APERTURE IS 0.1MM (FULLY OPEN) AND FOR THE GREEN CHANNELS THE APERTURE IS 0.05MM

63

FIGURE 3.4: EVOLUTION OF MICROBIALY INDUCED CALCITE PRECIPITATION IN FRACTURE 5 OF FLOW-PLATE 2: DIGITAL PHOTOGRAPHS (A) DURING THE INJECTION OF CEMENTATION FLUID ($T=3$ MINS) IN INJECTION CYCLE 1, (B) AT THE END OF INJECTION CYCLE 1 ($T=30$ MINS), (C) AT THE END OF INJECTION CYCLE 2, (D) AT THE END OF INJECTION CYCLE 3, AND (E) AT THE END OF INJECTION CYCLE 4. 66

FIGURE 3.5: INFLUENCE OF BACTERIAL DENSITY ON CALCITE PRECIPITATION AT $Q=1.2$ ML/MIN (FLOW-PLATE 2): (A) AFTER FIVE INJECTION CYCLES AT 1.00D₆₀₀ AND (B) AFTER 20 INJECTION CYCLES AT 0.25OD₆₀₀. 69

FIGURE 3.6: COMPARISON OF CYCLES 24 (A) AND 25 (B) IN EXPERIMENT 4A. STABLE CHANNEL FORMATION HAS OCCURRED. 71

FIGURE 3.7: THE EFFECT OF REDUCING VELOCITY ON FRACTURE INFILLING. BRAIDED CHANNELS HAVE DEVELOPED IN THREE OF THE FRACTURES AND IN FRACTURE 5 (THE SLOWEST INITIAL FLOW VELOCITY) PREVIOUSLY STABLE CHANNELS HAVE BECOME INFILLED. 72

FIGURE 3.8: SEM IMAGES OF CALCITE SAMPLED FROM FRACTURE 5 IN EXPERIMENT 3. SAMPLE LOCATIONS ARE SHOWN IN FIGURE 4A. (A) IS PROXIMAL TO AN OPEN CHANNEL (WHERE THE VELOCITIES ARE HIGHER), (B) IS SET BACK SLIGHTLY FROM AN OPEN CHANNEL AND (C) IS FAR FROM AN OPEN CHANNEL. THE MICROBE-CALCITE AGGREGATES APPEAR TO BE HIGHLY UNIFORM IN SIZE, AROUND 30 - 40 MM. (D) IS A HIGHER MAGNIFICATION OF LOCATION B SHOWING DISTINCT CRYSTAL GROWTH IN THE FORM OF CALCITE PLATES (THE BEGINNING OF RHOMBOHEDRONS) ARE ALSO VISIBLE IN AMONGST THE MASS OF CALCITE COATED BACTERIA. 73

FIGURE 4.1: PLOT OF THE AVERAGE CUMULATE AMMONIUM CONCENTRATION PRODUCED BY EACH TRIPPLICATE BATCH TEST OVER 96 HOURS. 83

FIGURE 4.2: PLOT OF THE PH PRODUCED BY EACH TRIPPLICATE BATCH TEST OVER 96 HOURS. 84

FIGURE 4.3: PLOT OF CALCIUM CARBONATE MASS PRODUCED AGAINST THE PERCENTAGE OF BACTERIA OF TOTAL VOLUME. 85

FIGURE 4.4: A) SCHEMATIC DIAGRAM OF THE FLOW-PLATE 3 SET-UP AND B) PLAN VIEW OF THE FLOW-PLATE. 87

FIGURE 4.5: PHOTOGRAPHS OF FLOW PATHS (AS INDICATED BY THE FLUORESCEIN DYE) AT 1, 6 AND 9 MINUTES. 88

FIGURE 4.6: PHOTOGRAPHS OF THE FULL FLOW-PLATE SURFACE. CALCIUM CARBONATE CAN CLEARLY BE SEEN COATING THE ENTIRE FRACTURE SURFACE. 91

FIGURE 4.7: PLOT OF THE CHANGES IN FRACTURE TRANSMISSIVITY AT THE END OF EACH CYCLE. EACH CYCLE WAS COMPOSED OF FOUR STAGES (SEE TABLE 4.2) AND EACH CYCLE LASTED A DAY. TRANSMISSIVITY WAS CALCULATED FROM PRESSURE DROP READINGS TAKEN ACROSS THE LOW-PLATE AT THE END OF EACH 2 HOUR INJECTION CYCLE ACCOUNTING FOR THE REDUCTION IN FLOW-RATE WHICH OCCURRED WHEN INJECTION PORTS BECAME BLOCKED (AS INDICATED BY THE DASHED RED LINES).

FIGURE 4.8: BACTERIAL BREAKTHROUGH CURVES FOR EACH CYCLE THROUGHOUT THE THREE HOURS OF BACTERIAL INJECTION PER CYCLE. BACTERIAL CONCENTRATION IS NORMALISED BY THE ORIGINAL CONCENTRATION OF 0.5 OD600 THUS A VALUE OF 1 IS EQUAL TO FULL BREAKTHROUGH AND NO RETENTION OF BACTERIA WITHIN THE FRACTURE. 93

FIGURE 4.9: CHANGES IN AMMONIUM AND CALCIUM CONCENTRATION OF THE FLOW-PLATE EFFLUENT. THE X-AXIS MEASURES FRACTURE LIQUID VOLUME INJECTED WHICH IS N=BASED ON THE INITIAL MEASUREMENT OF HYDRAULIC APERTURE. 94

FIGURE 4.10: A) CHANGE IN ELEVATION DUE TO CALCIUM CARBONATE PRECIPITATION RELATIVE TO THE DOLERITE BASE, B) VARIATION IN THE ELEVATION OF THE CLEAN DOLERITE BASE, C) VARIATION IN THE ELEVATION OF CALCIUM CARBONATE PRECIPITATE ALONG THE LINE A-A, AND D) AVERAGE ELEVATION OF CALCIUM CALCIUM CARBONATE PRECIPITATE MEASURED OF 4MM THICK BANDS FROM INLET TO OUTLET. 97

FIGURE 4.11: SEM ANALYSIS OF SAMPLES TAKEN FROM BASE PLATE IN THE MIDDLE OF THE PRECIPITATE AT A POINT CLOSE TO THE INLET (LOCATION 8) WHERE THERE IS A LARGE THICK PATCH OF PRECIPITATE, AND A POINT CLOSE TO THE OUTLET (LOCATION 17) WHERE THE PRECIPITATE IS SMOOTHER. THE RED BORDERED IMAGE IS A CLOSE-UP VIEW OF LOCATION 8. 99

FIGURE 5.1: VAN DER WAALS ATTRACTION IS THE RESULTS OF FORCES BETWEEN MOLECULES IN EACH COLLOIDAL PARTICLE. ONE MOLECULE OF THE COLLOID HAS A VAN DER WAALS ATTRACTION TO EACH MOLECULE IN THE OTHER COLLOID. IN A REGIME WHERE THERE IS REPULSION, THERE IS AN ENERGY PREVENTING FURTHER ATTRACTION. WE CAN DECREASE THE ENERGY BARRIER BY INCREASING THE IONIC STRENGTH OR CHANGING THE PH. 102

FIGURE 5.2: CARTOON OF HOW COLLOIDAL SILICA CAN BE GELLED USING COUNTER-IONS. 103

FIGURE 5.3: AS THE % WEIGHT COLLOIDAL SILICA INCREASE FROM 5% TO 27.5% THERE IS A LINEAR INCREASE IN THE UNCONFINED COMPRESSIVE STRENGTH (PERSOFF ET AL, 1998). 104

FIGURE 5.4: SHOWS THE CHANGE IN VOLUME (SHRINKAGE) OVER SIX MONTHS, WHEN THE COLLOIDAL SILICA IS IN A 100% RELATIVE HUMIDITY THE SHRINKAGE IS THE

SMALLEST WHILST THE LOWEST HUMIDITY (75%) HAD THE HIGHEST SHRINKAGE. IN FIGURE 5.5B) WITH A RELATIVE HUMIDITY OF 75%, THE RATE IN THE STRENGTH INCREASE OF STRENGTH OCCURS SOONER THAN IN THE 95% RELATIVE HUMIDITY; SPECIMENS KEPT AT 100% RELATIVE HUMIDITY THERE WAS VERY LITTLE CHANGE IN THE STRENGTH. 105

FIGURE 5.5: NEWTONIAN FLUID GROUTS HAVE A RAPID SETTING (GELLING) RATE WHILST 3B) BINGHAM FLUID GROUTS HAVE A SLOW SETTING (GEL) RATE WHICH BEGINS IMMEDIATELY. COLLOIDAL SILICA IS IN BETWEEN THESE TWO GROUTS WHERE INITIALLY THE VISCOSITY REMAINS LOW (SIMILAR TO CHEMICAL GROUTS) AND THEN AS GELLING BEGINS THE VISCOSITY INCREASE IS MORE AKIN TO CEMENTITOUS BINGHAM GROUTS (AFTER MONGILARDI AND TORNAGHI, 1986; BRUCE ET AL, 1993). NOTE THE RED DATA FOR THE 'GEL POINT' (KIM AND CORAPCIOLGU, 2002). 111

FIGURE 5.6: COMPARISON BETWEEN MICP (A) AND MICP WITH COLLOIDAL SILICA (B). CALCITE CAN BE DISTINGUISHED FROM COLLOIDAL SILICA BY COLOUR, THE GREY WHITE COLOUR IS CALCITE WHILST THE BLUE WHITE COLOUR IS COLLOIDAL SILICA. 115

FIGURE 5.7: SEM IMAGES OF SAMPLES TAKEN FROM LOCATIONS 2 AND 15. 118

FIGURE 5.8: GRAPH SHOWING THE GEL POINT AND THE GEL TIME OF A COLLOIDAL SOLUTION. 122

FIGURE 5.9: VISCOSITY-TIME CURVES FOR THE GELATION OF SILICA SOL DESTABILISED USING SODIUM CHLORIDE ACCELERATORS. FOR EACH CONCENTRATION, THE EXPERIMENT WAS PERFORMED IN TRIPLICATE. GEL TIME (TGEL) IS DEFINED AS THE INTERCEPT OF THE EXTRAPOLATIONS FROM THE TWO STRAIGHT LINE PORTIONS OF THE VISCOSITY-TIMES CURVES (SUMMERS ET AL., 1988) AND THE RATE OF GELATION (RGEL) AS THE SLOPE OF THE CURVE AS MARKED ON THE FIGURE. VALUES OF TGEL AND RGEL REPORTED ARE AVERAGES OF EACH TRIPLICATE. 126

FIGURE 5.10: VISCOSITY-TIME CURVES FOR THE GELATION OF SILICA SOL DESTABILISED USING DIFFERENT ACCELERATORS. TABLE 5.4 SUMMARISES THE PROPERTIES OF EACH GROUT. 128

FIGURE 5.11: ILLUSTRATES THE DOUBLE DIFFUSE LAYER OF COUNTERIONS AROUND A NEGATIVELY CHARGED SILICA PARTICLES IN AN ELECTROLYTE OF MONOVALENT CATIONS, AND THE REDUCTION IN THE THICKNESS OF THE DIFFUSE LAYER AND THE REDUCTION IN ELECTROSTATIC REPULSION BETWEEN PARTICLES IN AN ELECTROLYTE OF DIVALENT CATIONS AT THE SAME CONCENTRATION. 130

FIGURE 5.12: VISCOSITY-TIME CURVES FOR THE GELATION OF SILICA SOL DESTABILISED USING DIFFERENT ACCELERATORS. TABLE 5.5 SUMMARISES THE PROPERTIES OF EACH GROUT MARKED ON THIS FIGURE. 131

FIGURE 5.13: INFLUENCE OF ION SPECIFICITY ON HYDRATION SPHERES SURROUNDING MONOVALENT IONS. 132

FIGURE 5.14: VISCOSITY-TIME CURVES FOR THE GELATION OF SILICA SOL DESTABILISED USING DIFFERENT ACCELERATORS. TABLE 5.5 SUMMARISES THE PROPERTIES OF EACH GROUT. 133

FIGURE 5.15: VISCOSITY-TIME CURVES FOR IN SITU DESTABILISATION VIA BACTERIAL UREOLYSIS AT TWO DIFFERENT BACTERIAL DENSITIES: 0.33OD600 AND 0.67OD600. EXPERIMENTS WERE PERFORMED IN TRIPLICATE. 135

FIGURE 5.16: AMMONIUM PRODUCTION AND K_{UREA} IN SILICA SOL AT TWO DIFFERENT EQUIVALENT BACTERIAL DENSITIES: 0.33OD600 AND 0.67OD600. INITIAL UREA CONCENTRATION USED FOR DETERMINATION OF K_{UREA} WAS 1.5M. CLOSED AND OPEN CIRCLES ARE AMMONIUM CONCENTRATIONS ESTIMATED FROM CONDUCTIVITY MEASUREMENTS. 135

FIGURE 5.17: COMPARISON BETWEEN GROUTS F(BACTERIA ONLY) AND G (BACTERIA AND CALCIUM CHLORIDE). NOTE THAT THE GEL RATE FOR BACTERIA ONLY IS GREATER THAN THE GEL RATE FOR THE SAME CONCENTRATION OF BACTERIA BUT WITH THE ADDED CALCIUM IONS. 137

FIGURE 5.18: XRD RESULTS USING A GOEBEL MIRROR ALIGNMENT. PEAKS INDICATE THAT CALCITE IS PRESENT WITHIN COLLOIDAL SILICA. COLLOIDAL SILICA SHOWS AS THE BROAD PEAK AT 230 DUE TO ITS AMORPHOUS NATURE. 138

FIGURE 5.19: XRD RESULTS USING TWIN DUAL OPTICS. A) COLLOIDAL SILICA SHOWS AS SLIGHT CURVE TO ITS AMORPHOUS NATURE. B) PEAKS INDICATE THAT CALCITE IS PRESENT WITHIN COLLOIDAL SILICA THOUGH THEY ARE NOT AS INTENSE AS THE GOEBEL MIRROR. 139

FIGURE 6.1: METHOD USED BY CUTHBERT ET AL (2013) TO EXTRACT AMMONIUM FROM A SMALL SCALE MICP FIELD SEALING EXPERIMENT. THE FRACTURE PLANE IS SHOWN IN BLUE; B2 IS THE INJECTION BOREHOLE, B5 THE EXTRACTION BOREHOLE AND BOREHOLES B3 & B4 WERE USED FOR HYDRAULIC TESTING. 149

List of Abbreviations and Acronyms

The following table describes the significance of various abbreviations and acronyms used throughout the thesis. The page on which each one is defined or first used is also given.

<i>Abbreviation</i>	<i>Meaning</i>	<i>Page</i>
OPC	Ordinary Portland Cement	15
MPa	Megapascals	16
MICP	Microbially Induced Calcite Precipitation	18
m/s	Metres per second	21
µm	micrometre	21
SEM EDS	Scanning electron microscopy energy dispersive spectroscopy	22
SEM	Scanning electron microscopy	23
SEM EDX	Scanning electron microscopy energy dispersive x-ray	23
(aq)	aqueous	24
DIC	Dissolved inorganic carbon	25
IAP	Ion activity product	30
K _{so}	Solubility product	30
AMM	Ammonium	32
cm	Centimetre	33
m	Metre	34
mg	Milligram	34
mg/g	Milligram per gram	35
kPa	Kilopascal	39
µg/L	Microgram per litre	41
EPS	Extracellular polymeric substance	41
AGW	Artificial groundwater	41
k _{urea}	Rate of urea hydrolysis	41

mM	Millimolar	41
ml/min	Millilitres per minute	43
Kg CaCo ₃ /m ³	Kilograms of calcium carbonate per metre cubed	45
Re	Reynolds number	53
OD600	Optical density at 600 nanometres	53
UV-Vis	Ultraviolet to visible	58
Q	Flowrate	58
cfu/ml	Colony forming units per millilitre	72
g/L	Grams per litre	72
FE-SEM	Field emission scanning electron microscopy	79
l/min	Litres per minute	117
M	Molar	127
mPa.s/min	Millipascal second per minute	129

1. INTRODUCTION

1.1 Grouting

Rock grouting is the process of infilling discontinuities within a geological formation by introducing the grout via a drilled borehole. The aim of rock grouting is to increase shear-strength, compressive strength, and to reduce the permeability of the rock (Moseley and Kirsch, 2004).

When using grouts in fractured rock; to achieve good penetration it is necessary to pump the grout into the rock via boreholes at a substantial overpressure (due to an increase in the grout viscosity). The voids are partially or complete infilled resulting in the displacement of ground water (represented by the cartoon shown in Figure 1.1). When the grout has set, the open joints or fissures are sealed. In the case of fractured rock zones, the rock fragments or larger blocks are cemented together as a rock mass.

Limited penetration; due to particle size, viscosity or gel time.

Even if sufficient penetration is achieved a slow gel rate/ curing time can result in erosion of the grout due to the shear force imparted by groundwater flow.

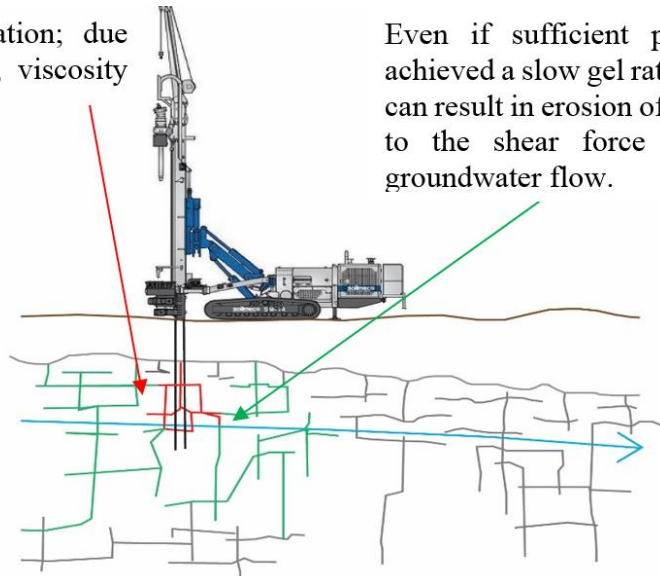


Figure 1.1: Cartoon of fracture grouting showing grout penetration and associated problems.

1.2 Common Grouts

The most common uses for rock grouting are the building or repair of dam foundations, reduction of inflow into tunnels and the stabilization of mine workings. The most common grout used is ordinary Portland cement (OPC). OPC is composed of Calcium oxide (60 – 67%), Silica (17 – 25%), Alumina (3 – 8%) and Iron (0.5 – 0.6%). According to ASTM C150 (ASTM, 2012), the average particle size of OPC is 70 μm , with a compressive strength after 1 day of 3 – 14 MPa. OPC is highly alkali, with a pore-water pH of up to 13.5.

It is considered possible to grout a discontinuity when its aperture exceeds three times the maximum grain size of the cement (Crawford, 1984). Thus the penetration of cementitious grouts is limited by particle size and their tendency to aggregate into filter cakes (Figure 1.2). In practice the fracture to be grouted should be at least four to five times larger than the characteristic particle size of the cement (Widmann, 1996) thus fracture apertures would have to be $> 280 \mu\text{m}$.

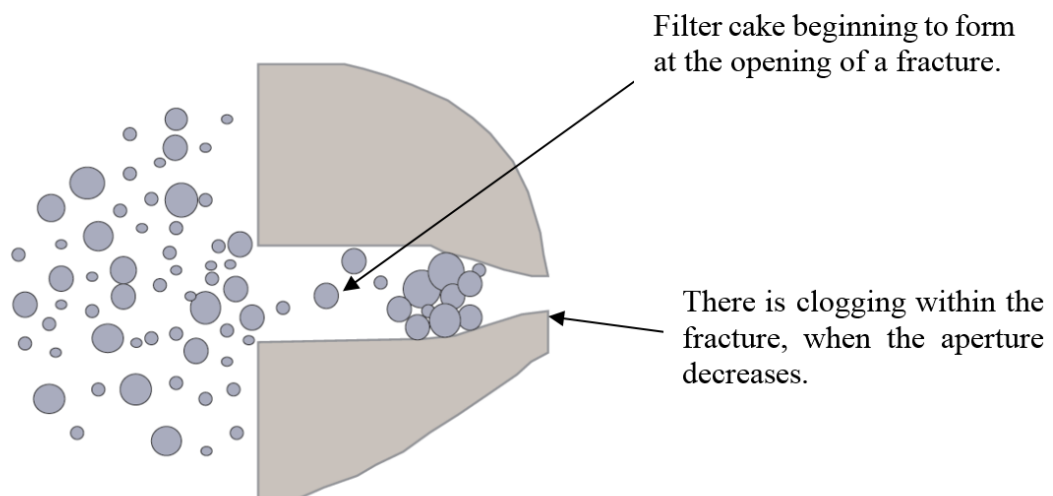


Figure 1.2: Filter cake formation of a cement grout at the opening of a discontinuity (after Eklund and Stille, 2008).

By mixing OPC with slag or pumice, it is possible to create an ultra-fine cement (by grinding) that has a particle size up to 10 μm with a D_{90} of 8 or 5 μm . This particle size would allow penetration of the grout into finer grained soils and smaller discontinuities (Henn et al, 2010). Although microfine ($d_{95} < 30 \mu\text{m}$), and ultrafine ($d_{95} < 15 \mu\text{m}$) cement grouts are being developed in order to penetrate fine aperture

fractures (Tolppanen, and Syrjänen, 2003), they are unable to penetrate fractures with apertures smaller than 50µm (Hernqvist et al, 2008; Eklund and Stille, 2008) (Figure 1.2) and the pore-water pH would still be unchanged.

All cementitious grouts increase in viscosity slowly over time, thus an increase in the pressure needed to pump the cement is also required. An over pressure of 1MPa, constitutes a load on the rock mass which can cause the fracture to propagate, potentially increasing the rock permeability and dilating (jack open) the fracture permanently by up to 1mm, (Gothall & Stille, 2009). In addition to this, cementitious grouts undergo volumetric shrinkage during setting, which may not be conducive to achieving very low hydraulic conductivities.

If the use of a cement grout is not suitable it may be preferred to use a chemical grout. Chemical grouting is the process of injecting a chemically reactive solution that behaves as a fluid but reacts after a predetermined time to form a solid, semisolid, or gel (Karol, 2003). Chemical grouts consist of injected solutions that initially behave as fluids and then after a pre-determined period of time, the chemically reactive solution forms a solid, semi-solid or gel (USACE, 1995).

Chemical grouts are not particulate-based and therefore are able to penetrate very fine aperture fractures that even microfine and ultrafine cements cannot access. However, there are concerns about the toxicity of some chemical grouts and their associated environmental impact as well as potential adverse health effects on the workforce handling them (Karol, 2003). For example, polyurethane is flammable, is an eye, skin and respiratory irritant, and contains toluene di-isocyanate which is classified as “very toxic” (Six and Richter, 2003).

There are 4 main requirements of chemical grouts:

- Be of Low Viscosity – Viscosity is the ability of a fluid to resist flow or resist internal shear forces. Viscosity is important as it determines the ability of a grout to flow into and through the pore spaces and small aperture fractures. The lower the viscosity the easier it is to achieve good penetration.
- Controllable gel time, the gel time is the interval between initial mixing of the grout components and formation of the gel. This is an important factor when grouting projects are designed as the longer the gel time, the greater the

penetrability. Gel time can be altered by varying the proportion of the components. Ideally a rapid gel rate is required, where the viscosity remains low until the desired penetration is achieved then the grout rapidly gains strength thus being able to resist the shear force of any flowing groundwater it comes in contact with.

- Low toxicity. Although most of the toxic grouts are no longer in use, there is the potential for certain materials to be or to become toxic or hazardous if not properly used.
- Durability is the ability of the grout after pumping to withstand exposure to hostile conditions. These include repeated cycles of wetting and drying or freeze/thaw cycles. Certain chemicals may also attack the grout and cause deterioration.

Currently chemical grouts such as silicates or acrylates are used for small (<50 μ m) aperture fractures. However; the changes in viscosity and/or unreliable setting times of these grouts can create limitations in penetrability (Karol, 2003). New grouts are needed that can withstand dissolution, shrinkage and erosion (unlike cement) (Graham, 1998), have a low viscosity and rapid gel/strengthening rate and also have a well-controlled gel time (unlike chemical grouts) (Karol, 1983). Two such grouts that are being considered in our research are colloidal silica and microbially induced calcite precipitation (MICP) as they both have the potential to penetrate fine aperture fractures and either have a well controlled gel time or hold sufficient shear strength to withstand erosion whilst sealing the fracture.

The ability of MICP to generate significant calcium carbonate precipitation has led to researchers exploring its potential in a wide range of geotechnical applications; from the reduction of hydraulic conductivity in porous media (Ferris and Stehmeier, 1992; Tobler et al, 2012), the sealing of cracks in concrete (Van Tittleboom et al., 2009), to improving the properties of bricks (Sarda et al, 2009).

1.3 Grouting for the Geological Disposal of Nuclear Waste

Geological disposal is based on the concept of multiple barriers, where both engineered and natural barriers work together to provide containment. For disposal in hard rocks, the engineered barrier components are the waste container (often multi-layered metals) and a buffer of backfill material (clay or cement), which fills the space between the container and the host rock. These barriers work together to provide containment and safety. Geological repositories are being considered as the best feasible solution for the storage of hazardous materials such as high level nuclear waste throughout the world including the UK.

Finland and Sweden plan to use high strength crystalline rocks for their geological disposal of nuclear waste, due to their low porosity and discontinuity (open joints and fractures) dominant fluid flow. The Swedish method for the disposal of high level waste is shown in Figure 1.3 (SKB, 2014). Their plan is to use the multi barrier method (copper canister, bentonite clay and impermeable host rock), thus the radioactive substances in the spent nuclear fuel would be prevented from re-entering the biosphere.

However; when crystalline rock is the chosen storage medium, the construction of the underground tunnels and caverns can enhance discontinuities within the rock inducing significant changes in flow and transport properties. These changes are irreversible, and can result in groundwater flowing radially inwards to the excavation zone. These discontinuities make it necessary to limit fluid flow as they can be pathways for contaminants, with the potential for quite a high permeability dependent upon aperture, connectivity and density (Blyth and Freitas, 1992).

The ingress of water during construction and operation of these repositories must be prevented, as well as the repository being able to isolate waste for tens of thousands of years. The isolation of the nuclear waste for such a long period of time is necessary because of the long half-life of some radionuclides i.e. Plutonium²³⁹ which has a half-life of 24,000 years (NRC, 1996). Subsurface hydrogeological transport is one of the main factors in the problem of disposing of high-level nuclear wastes in a deep geologic repository as fluid and/or gas flow are the mechanism by which

radionuclide's might reach the biosphere from a deep geological repository if engineered containment fails.

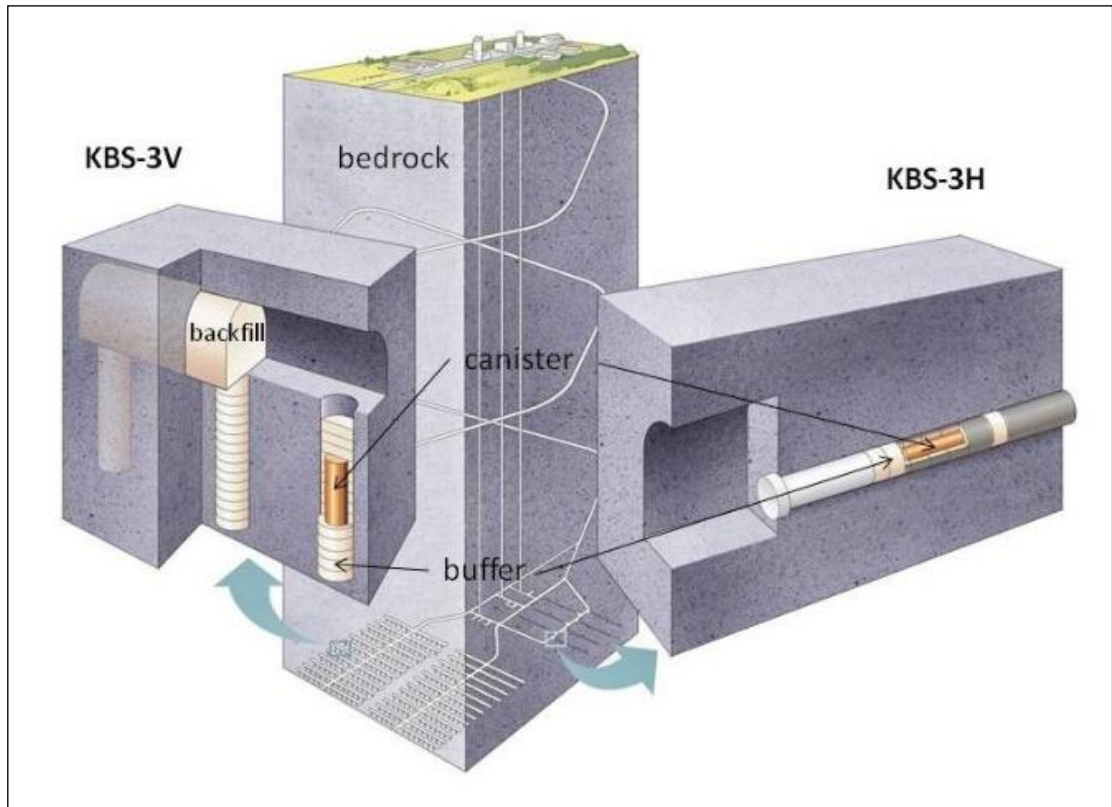


Figure 1.3: SKB's two disposal plans for the geological disposal of high level nuclear waste in the crystalline (granite) bedrock, Sweden (Posiva, 2012).

The engineered containment is composed of the metal waste canisters and the bentonite clay buffer. The continued reduction of hydraulic conductivity by the bentonite buffer is mainly dependent on the swelling pressure/dry density, but also on void ratio, groundwater salinity and temperature. Where the bentonite comes into contact with the host rock, where open discontinuities are present the bentonite particles could intrude into the openings, allowing chemical erosion to occur.

Chemical erosion is a process where rock fractures may provide pathways for the continued, localised, free swelling of the buffer material. These free swelling environments could lead to the continued hydration and expansion of the buffer until, ultimately, colloid sized particles separate by diffusion or shear (caused by flowing groundwater) from extruded gel fronts. However, this colloid formation is reduced or totally prevented by sufficiently high salinity levels (e.g. Laaksoharju & Wold 2005).

Although any site would be chosen with sufficient salinity levels, climate change could alter salinity levels in the future, such as the introduction of glacial melt-water (Posiva, 2010). To protect the bentonite buffer from erosion, it will be necessary to grout all discontinuities within the host rock.

Conventional cementitious grouts are unsuitable for use in nuclear waste repositories due to their pH and their durability (which is quite short geological speaking), with degradation occurring between 50 – 100 years (Pusch, 2008). They have a pH >11 which can accelerate the release of uranium; increase the mobility of uranium fission products and actinides. Furthermore, the use of high pH grouts in geological repositories for the storage of high level nuclear waste, should be strictly limited due to the adverse impact of high pH leachate on the bentonite backfill material (Bodén and Sievänen, 2005; Sievänen et al., 2005; Jin-Seop Kim, 2011). Super plasticisers are currently used within cement grouts to improve their flow characteristics. However, there are concerns that the presence of super plasticiser can also increase the mobility of radionuclides by preventing their sorption on to the cement (Young et al, 2013).

Hydraulic conductivities within crystalline bedrock can be quite variable, final required minimum permeability is 10^{-12} m/s. Of the three sites in Sweden that were considered for nuclear waste storage, the hydraulic conductivities of the host rocks were 10^{-8} m/s and at Aspo rock laboratory the fracture apertures are $\sim 266 \mu\text{m}$ (SR97, 99).

Non-cementitious grouts may be a better alternative to cementitious grouts since radionuclides stored within the subsurface need to be retained within the geological repository for periods greater than one hundred thousand years meaning it will be necessary to grout fractures smaller than $50 \mu\text{m}$ as even at these small apertures over a geological timescale it is possible for significant volumes of water to be transported through.

1.4 Aims and Objectives

This PhD looks at two distinct novel grouts, to achieve the aim of developing a grout that can be used in fine aperture fractures with a $\text{pH} < 11$. The main objectives are:

- Investigate the potential of microbially induced calcite precipitation for the sealing of fine aperture fractures.
- Investigate the potential of colloidal silica for the sealing of fine aperture fractures.
- Develop a combination grout composed of both bacteria and colloidal silica for the purpose of sealing fine aperture fractures.

These non-standard grouts will be investigated through batch scale, and flow-through tests, to answer the following questions:

- What are the effects of fracture aperture and fluid flow rate on the sealing efficacy of microbial biomineralisation? How does this affect sealing strategies?
- What does the effect of changing the ratio of bacteria to cementing solution have on calcium carbonate precipitation? Is there an optimum operating window for bacterial ureolysis?
- What changes in the operating time of cementing fluid, bacterial optical density and flow rate are required to maximise filling efficiency?
- Is it possible to use bacterial ureolysis as an accelerator for the gelation of colloidal silica? What effect does it have on the viscosity and shear strength of colloidal silica in comparison to the addition of salts such as calcium chloride, sodium chloride or ammonium chloride?
- Using a combined approach of *Sporosarcina pasteurii* and colloidal silica, what reduction in permeability can be seen? What injection strategy would give the most penetration with an even distribution?

Results will be analysed through ion chromatograph analysis of ammonium and calcium concentrations within the effluent, bacterial breakthrough curves, calculation of changes in the hydraulic conductivity through increases in back pressure, SEM EDS analysis of calcium carbonate, and time lapse videos of precipitation with associated imageJ analysis of flow velocities.

1.5 Thesis Outline

Chapter 2: Literature Review of MICP - Fundamental process, limitations of technology, what applications have been studied, (what are the gaps in literature).

Chapter 3: How does MICP fill a fracture. The influence of hydraulic controls on the spatial distribution of microbially induced calcite precipitation was investigated, for artificial rock fractures using fractures of varying widths but of the same aperture and bacteria-inclusive solutions. Analysis of results predominantly through time lapse photography and Fiji ImageJ post processing.

Chapter 4: Optimisation of MICP – batch tests to examine what effect different ratios of bacteria to cementing solutions has not only on K_{urea} , and the amount of calcium carbonate precipitated but also on the working time of the bacteria. New flow-plate - development of a methodology to prevent/reduce the formation of self-organised channels within the simulated fracture. Is it possible to fully fill using MICP alone? Analysis through Ion Chromatographic measurements of calcium and ammonium concentrations, from which we can calculate K_{urea} and the optimum working time of the bacteria, acid digestion to determine masses of calcium carbonate produced, SEM analysis of precipitate.

Chapter 5: Induction of Colloidal Silica Gelation using Bacterial Ureolysis - Low pH grouts that are capable of penetrating fine aperture fractures are increasingly being developed for use in engineering applications. Bacterial ureolysis using *Sporosarcina pasteurii* can be used as an accelerator for the in-situ destabilisation of colloidal silica (i.e. cations produced within silica suspension). A number of different accelerators have been investigated in this study including sodium chloride, calcium chloride, ammonium chloride and bacterially induced production of ammonium ions by ureolysis. For each accelerator, we experimentally determine the gel time and rate of gelation using viscosity measurements, and the shear strength of the grouts after 1 day and 7 days. We demonstrate that using bacterial ureolysis as a means of destabilising colloidal silica, leads to longer gel times than for the direct addition of a traditional chemical accelerator at the same concentration. In addition, for grouts with similar gel times we have illustrated that the bacterial grout has a higher rate of gelation and a higher final shear strength than a grout destabilised by a chemical accelerator. Does combining MICP and colloidal Silica within simulated fractures improve

efficiency? Analysis will be through breakthrough curve analysis, ion chromatographic measurement of ammonium and calcium concentrations, time lapse photography and SED EDX analysis of precipitate.

Chapter 6: Forward looking discussion, with a view to industrial applications

Chapter 7: Conclusions

References

2. LITERATURE REVIEW: MICROBIALLY INDUCED CALCITE PRECIPITATION

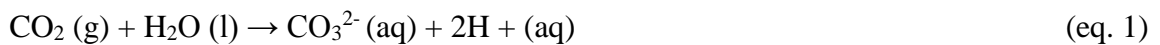
2.1 Introduction

The research presented within this thesis investigates the use of microbially induced calcium carbonate precipitation (MICP) as a method for grouting rock fractures. This chapter discusses first the natural occurrence of calcium carbonate (CaCO_3) within fractures. The MICP process is presented and its different applications, which have been studied to date, both in the laboratory and in the field, are reviewed. The main factors influencing the MICP process are identified, and the gaps in the literature are outlined.

2.2 Presence of calcium carbonate in natural rock fractures

Calcium carbonate occurs in nature in three different crystalline forms (polymorphs); calcite, aragonite and vaterite. Of the three, the more thermodynamically stable forms; calcite and aragonite, are found in nature. Calcite is the most thermodynamically stable and abundant calcium carbonate phase under the ambient pressure and temperature conditions of earth's surface, whilst aragonite is the most stable high-pressure polymorph.

Calcium carbonate precipitation occurs when carbon dioxide dissolves in water producing carbonate ions:

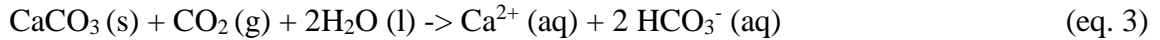


The carbonate ions can then react with calcium ions that are already in the water to produce calcium carbonate:



Under normal surface and near surface conditions calcium carbonate is water insoluble unless carbon dioxide is present and carbonic acid is formed resulting in the dissolution of calcium carbonate (Forbes et al, 2011).

The reaction mechanism the dissolution of calcium carbonate is:



Calcite is a common mineral found filling in rock fractures in nature. Figure 2.1 shows large calcite veins within basalt in Yarmouth.



Figure 2.1: Calcite veining present within a rock outcrop at Cape Forchu, Yarmouth (image Courtesy of Gary Deviller YCMHS High School)

The precipitation of calcite in the environment is often driven by a purely chemical process, which is controlled by environmental conditions (e.g. temperature, pressure and pH). The behaviour of calcium carbonate (for example, the mineral calcite) in a near-surface environment is controlled by equilibrium in the reaction, where CaCO_3 is a solid (calcite) and H_2CO_3 is carbonic acid (a weak naturally occurring acid that forms by the reaction between water and carbon dioxide):



Ca^{2+} (Calcium), is a positive ion (a cation) in solution and 2HCO_3^- is a negative ion (an anion) in solution - the bicarbonate ion. The equilibrium can be moved to the right by decreasing temperature. CO_2 is more soluble in cold water, thus with an increase in the amount of CO_2 , there is a greater production of H_2CO_3 ; thus, more calcium carbonate

becomes disassociated. The reverse can also occur and explains why we often see calcium carbonate in association with hot springs (Butler, 2013).

However; evidence exists for the presence of bacteria within calcite veins and their role in the formation of these veins (Hofmann, 2008). These calcite-filled fractures have been dated to be from hundreds of millions of years to thousands of years in age (Bons & Montenari, 2005; Hofmann & Farmer, 2000; Budai et al, 2002; Riding 2000). Bacteria can act as chemically reactive sites for the sorption of metal ions due to negative charges on their cell surfaces. This can then lead to nucleation and mineral precipitation (Beveridge and Doyle, 1989; Konhauser, 2007; Gadd, 2010). Bacteria can also play a more critical role by creating the local geochemical conditions necessary for mineral precipitation to occur, for example, by increasing pH leading to increased mineral saturation and subsequent precipitation (Mitchell and Ferris, 2006).

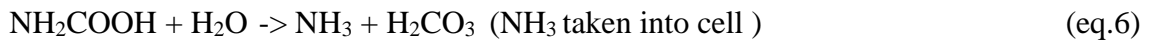
Pederson et al (1997) provided compelling evidence based on $\delta^{13}\text{C}$ values of calcite present within veins to suggest that microbial activity was responsible for calcite vein formation at depth (fracture in granite sampled from depth of 207m). The $\delta^{13}\text{C}$ values found were very low indicating microbiological activity as microbes preferentially utilise $\delta^{12}\text{C}$. Pederson et al (1997) also observed fossil microorganism structures within the calcite precipitate.

At depth in the subsurface, bacteria are typically present in low concentrations, due to the lack of nutrients. Calcite veins produced by microbial activity would have occurred over long periods of time, which would be considered to be unsuitable for modern engineering requirements. This research is focused on a process of triggering calcite precipitation by microbial activity, which is greatly speeded up relative to naturally occurring biogeochemical processes in the environment. The process studied here is driven by ureolysis and is commonly referred to as Microbially Induced Calcite Precipitation (MICP).

2.3 The MICP Process

MICP is a biogeochemical process where a bacterial suspension is used to produce calcium carbonate. This production of calcium carbonate is not biologically controlled (like aragonite found shells or the calcite plates produced in coccoliths) rather it is ‘biologically induced’, where the microorganism alters the chemistry of its local environment leading to calcium carbonate precipitation. There are two main metabolic pathways for the biogenic generation of calcium carbonate, aerobic and anaerobic.

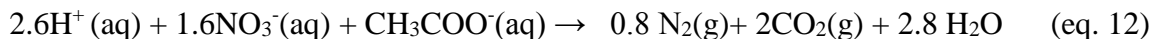
Aerobic microbially mediated calcite precipitation takes place as a result of urea hydrolysis to ammonium and bicarbonate. Urea hydrolysis causes the gradual increase in pH of the environment surrounding the bacteria and the production of both bicarbonate and ammonium within a groundwater that is already saturated with calcium (Stocks-Fischer et al, 1999):

$$\text{H}_2\text{NCONH}_2 + \text{H}_2\text{O} \rightarrow \text{NH}_2\text{COOH} + \text{NH}_3 \quad (\text{eq. 5})$$


Overall reaction:



The anaerobic pathway (microbial denitrification) is where anaerobic bacteria form calcite, through denitrification in a calcium-rich environment. Microbial metabolism increases the total carbonate (CO_3^{2-}) content and pH to the point of super-saturation with respect to calcite, thereby inducing calcite precipitation (Ehrlich 2002; Karatas 2008; van Paassen et al. 2009). The bacterium uses acetate as its carbon source and under anaerobic conditions, nitrate serves as an electron acceptor producing nitrogen, carbon dioxide and water, pH rises by the consumption of H^+ (Equations 12-14, (Hamden, 2011)). Carbon dioxide is converted to bicarbonate (Equation 13) and calcium carbonate is then precipitated (Equation 14).



The primary challenge of denitrification is the slower rate at which supersaturated conditions are created and the requirement of an optimum pH of 7 – 8 otherwise nitrite and nitrous oxide intermediates can form (van Paassen et al, 2010). These intermediates can inhibit denitrification thus limit the production of calcium carbonate (Lee and Rittmann, 2003).

The biomineralization process investigated in this study is microbially induced calcite precipitation via urea ($\text{CO}(\text{NH}_2)_2$) hydrolysis:

- This process relies on a bacterium hydrolyzing urea into ammonia and carbonic acid (equations 5 & 6).
- This is followed by the production of ammonium ions and an increase in the pH surrounding the bacterial cell, due to the net production of OH^- ions (equations 7 & 8).
- As the pH increases, carbonic acid (H_2CO_3) is converted to bicarbonate ions (HCO_3^-), subsequently forming carbonate ions (CO_3^{2-}) (equation 9).
- In the presence of calcium ions, the increase in pH promotes the precipitation of calcium carbonate (CaCO_3) (equation 10) (Ferris et al., 1992, 1996; Mitchell et al., 2010).

Sporosarcina pasteurii (Strain ATCC 11859), a gram-positive, spore-forming, ureolytic bacterium was used in this research to induce calcite precipitation as this model bacterium has been well studied in the laboratory (e.g., Gollapudi et al., 1995; Ferris et al., 2002; Mitchell and Ferris, 2006; Whiffin et al., 2007; Tobler et al., 2011). The rate of calcite (CaCO_3) precipitation is controlled by four main parameters; the calcium concentration, the concentration of dissolved inorganic carbon (DIC) as produced by ureolysis (equations 5–10), the pH, and the availability of nucleation sites (Hammes et al, 2003).

CaCO_3 precipitation requires the presence of sufficient calcium and carbonate ions such that the ion activity product (IAP) exceeds the solubility constant (K_{so}) leading to the solution becoming supersaturated with respect to calcium carbonate. The concentration of carbonate ions is related to the concentration of DIC and the pH of the environment. Microbial metabolic activity influences both these factors, as well as the bacteria providing nucleation sites (DeMuynck et al., 2010).

Classical nucleation theory assumes that nucleation on surfaces (termed “heterogeneous nucleation”) is energetically more favourable than nucleation within a uniform phase (termed “homogeneous nucleation”) (Cheong et al., 2013). Microbial cell surfaces are thought to reduce the nucleation activation energy barrier, which must be overcome for nucleation, by providing chemically reactive sites for sorption (Ferris et al., 2003; Gadd, 2010).

Sporosarcina pasteurii is a gram-positive bacterium thus its cell walls are composed of peptidoglycan with secondary polymers of teichoic acids, which give rise to electronegative charges on the cell surface (Schultze Lam et al., 1996). These negative charges attract positively charged ions (cations), such as calcium ions. Once the cation has complexed with the bacterial cell, it can serve as a heterogeneous nucleation site, enabling calcite mineralization on the cell surface (Schultze-Lam et al., 1996; Stocks-Fischer et al., 1999). Figure 2.2 shows the negative footprint of bacteria embedded within calcite supporting the hypothesis that the bacterial cell acts as a nucleation point.

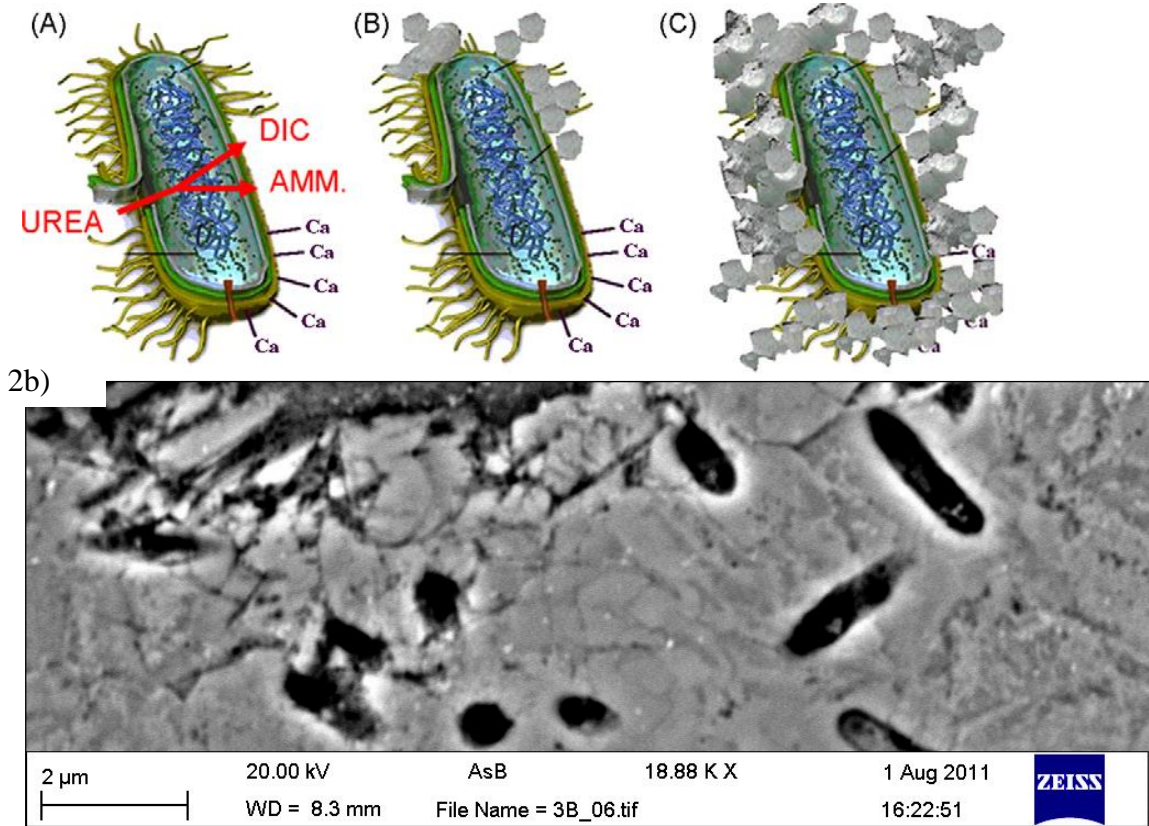


Figure 2.2: a) Calcium ions in the solution are attracted to the bacterial cell wall due to the negative charge of the latter. Upon addition of urea to the bacteria, dissolved inorganic carbon (DIC) and ammonium (AMM) are released in the microenvironment of the bacteria (A). In the presence of calcium ions, this can result in a local supersaturation and hence heterogeneous precipitation of calcium carbonate on the bacterial cell wall (B). After a while, the whole cell become encapsulated (C), limiting nutrient transfer, resulting in cell death (deMuynck, 2010). 2b) SEM images from my MSc dissertation (MacLachlan, 2011); showing calcium carbonate precipitate surrounding the negative footprint of the bacteria.

Homogeneous nucleation is also known to occur in solutions where geochemical changes have been induced by *Sporosarcina pasteurii*. Mitchell and Ferris (2006) demonstrated that calcium carbonate crystals were precipitated in both bacteria inclusive and bacteria-free environments, which had access to the same artificial groundwater solution (the two environments were separated by a cellulose dialysis membrane).

2.4 Applications of MICP

Over the last ten years microbially induced calcium carbonate precipitation (MICP) has been investigated for a range of different applications including ground improvement (increasing soil strength and stiffness) (DeJong et al., 2006; Whiffin et al., 2007; Van Paassen et al., 2010; Harkes et al., 2010), for permeability reduction in soils and rocks (Ferris et al., 1996), for solid-phase capture of contaminants (Fujita et al., 2008), and for surface treatment and repair of micro cracks in concrete (Bang et al., 2001; Van Tittleboom et al., 2010; De Muynck et al., 2010; De Muynck et al., 2011). These applications are discussed in more detail here and summaries presented in Table 2.1.

2.4.1 Permeability reduction in porous media

Early stage research focused on ex-situ methods. Ferris et al, (1992) mixed sand with bacteria, packed them into flow-cells and applied a continuous gravitational flow of urea and calcium ions (akin to permeation grouting). They found that after 50 to 100 pore volumes there was a >90% reduction in permeability. However, on examination of the cores all calcium carbonate precipitation occurred in the first 11cm of the 30cm cores.

Gollapudi et al (1995) also mixed the sand with bacteria before packing into columns and gravity fed a cementing solution. There was a 90% reduction in permeability with an initial bacterial culture volume of 300ml and a 100% reduction in permeability with an initial bacterial culture volume of 2000ml.

The plugging of sand and bacteria packed flow-cells was further investigated by Stocks-Fischer et al (1999) who found that as bacterial growth continued, the rate of calcium carbonate production per cell decreased. This reduction was explained as resulting from the bacterial cells becoming completely encased by calcium carbonate. This early stage research shows that although the ex-situ mixing of bacteria and sand (which allows for a homogeneous distribution of bacteria within the sand) can result in almost a complete reduction in permeability. However most uses for this grouting technique require an in-situ methodology to be developed.

Barouki et al (2009) used 0.5m long sand columns, bacteria and nutrient broth were injected into the top of the sand columns, followed by 8 hours of static conditions. Cementing solution was then injected as either a continuous flow, or pulsed flow from the base of the columns. Under continuous flow conditions, a depositional gradient of calcium carbonate was found with the greatest mass found closest to the injection port whilst the pulsed flow showed a more homogeneous distribution. At the end of the experiment hydraulic conductivity was reduced by 66%. It would be difficult to replicate this method in-situ.

Cunningham et al (2011) looked at this in relation to the geological storage of CO₂ and transport pathways created by borehole drilling and the use of *Sporosarcina pasteurii* biofilms to produce MICP. Their main aim was to develop a method that allowed them to direct the precipitation radially from the borehole producing a homogeneous calcium carbonate fill. Eventually, they were able to seal the sand column. Cunningham (2011) added bacteria and growth medium to 0.61m long sand columns and after 18 hours two pore volumes of cementing solution at 10ml/min were added and allowed to remain static for 24 hours then flushed with calcium free solution before another cycle was initiated. Overall there were 36 cycles per sand column. Although they found that hydraulic conductivity had been reduced by 66% there was a gradient of deposition from 479 ± 29 mg calcium carbonate per gram of sand at the injection point to an average of 239 ± 26 mg/g of calcium carbonate for the rest of the column.

2.4.2 Strength improvement of porous media

It is also possible to use MICP to increase the shear strength of a soil rather than reduce its permeability. Dejong et al (2006) compared MICP against the more traditional method such of gypsum cementation to improve the undrained shear strength. It was found that the gypsum-cemented sample gave a lower shear resistance than the microbially cemented samples.

Whiffin et al (2007) used 5m long flow cells to evaluate MICP via *Sporosarcina pasteurii* as a soil strengthening process by improving the load bearing capacity without significantly affecting the soil permeability under what was termed as realistic field conditions; where the grout was applied without disturbing the soil. Single stage drained

confined triaxial testing with a confining pressure of 50 kPa showed that a calcium carbonate concentration of less than 60 kg/m^3 had no significant effect on the strength of the sand, and the highest reported a compressive strength measurement of 570 kPa at $\sim 110 \text{ kg/m}^3$. In the section of the treated column with the highest cementation, porosity was reduced by 25% whilst the hydraulic conductivity over the entire column was only slightly reduced from $2 \times 10^{-5} \text{ m/s}$ to $9 \times 10^{-6} \text{ m/s}$.

Achal et al (2009), cemented cubes of sand with MICP. They found that the compressive strength of the bacteria and sand mortar cubes increased from 14MPa to 27MPa as treatment continued from 3 days to 28 days. In this study precipitation within sand columns occurred at their highest at the top of the sand column.

Van Paassen et al (2010) scaled up the bio-grouting process developed by Whiffin (2007). They used a similar injection to that developed by Whiffin et al. (2007) and Harkes et al. (2010), but in a $8.0\text{m} \times 5.6\text{m} \times 2.5\text{m}$ concrete container filled with poorly graded fine to medium grained sand with the placement of three injection wells and three extraction wells (shown in Figure 2.3).

The total amount of calcium carbonate precipitated was estimated to be 4500Kg over 12 days which was 50% of the theoretical maximum. Unconfined compressive strength testing was performed on samples cored from the cemented block. Strength varied between 0.7 and 12.4 Mpa with a calcium carbonate content which varied between 12.6 and 27.3%. Although there was a significant increase in the strength of the granular soil, there was a heterogeneous distribution of calcite within the granular soil with layered patterns parallel to the flow direction.



Figure 2.3: Bacterially cemented sand approximately 43 m³ in volume showing a wedge shape created by the hydrological flow from injection to extraction (columns closest in the field of view) (Van Paassen et al, 2010).

Van Paassen (2011) tested MICP in the field using as a method to reduce borehole instability within gravels during horizontal directional drilling. 6 injection wells surrounded by 14 extraction wells were installed in a plot of land 24m by 4m. 1.000m³ of soil at depths varying between 3m and 20m were treated with a cycle containing a bacterial suspension followed by cementing solution then 2 pore volumes of flush in between each cycle.

Horizontal drilling performed on the treated soil was achieved successfully. Samples extracted from the soil contained calcium carbonate of up to 6% of the total dry weight, again a heterogeneous distribution of calcium carbonate was found.

2.4.2 Permeability reduction in fractured media

Microbially induced calcium carbonate precipitation can also be used to seal fractures within a rock unit. Schultz et al (2011), investigated MICP within fully hydrated flow systems. Using a flow-plate which contained a hatched network of 1mm channels (shown in Figure 2.4). *Sporosarcina pasteurii* were injected into the flow-plate and left static for 1.5 hours to allow for attachment then a cementing solution was injected. The experiment was terminated once the flow-plate became fully plugged.

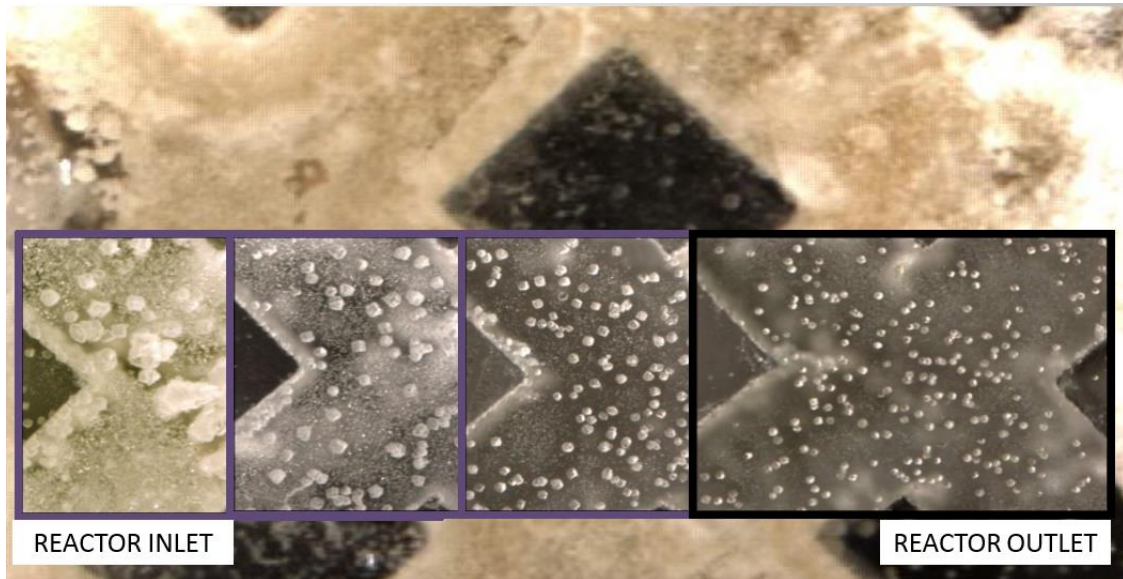


Figure 2.4: Photographs showing the change in crystal size and distribution of calcium carbonate within a flowing system (Schultz et al. 2011).

Similar to what occurs in soils, a gradient in calcium carbonate distribution was seen with the greatest amount of precipitate and the largest crystal sizes were seen closest to the injection inlet, this was attributed to a heterogeneous distribution of the bacterial cells and the presence of a geochemical gradient within the flow-plate. Thus indicating, that to improve the distribution of calcium carbonate, it will be necessary to be able to control the transport of bacteria and their trapping within rock fractures.

Phillips et al (2012) aimed to create a homogeneously distributed calcium carbonate seal of a hydraulically fractured 0.74m diameter sandstone core. The permeability of the fractured core was reduced by 4 orders of magnitude and was 3 times stronger. Phillips et al. (2012) injected *Sporosarcina pasteurii* into the core fracture

followed by growth medium to push the cells further into the fracture then left static for 4-5 hours. For 18 hours, growth medium was injected continuously to promote the development of a bio-film. After which, there were 45 cycles composed of two pore volumes of cementing solution and an overnight low flow rate injection of growth medium (bio-film resuscitation).

Although homogeneous distribution of calcium carbonate could not be confirmed, calcium carbonate was found at the beginning and the end of the flow path and the hydraulic conductivity of the fracture decreased from 1.9×10^{-4} m/s to 9.62×10^{-10} m/s. However, the creation of a bio-film creates the risk of bio-clogging. This is where the bacterial cells seal the fracture instead of the biologically produced calcium carbonate (Tobler et al, 2011).

To avoid the risk of bio-clogging; Cuthbert et al (2013) in the first field trial of sealing a rock fracture in-situ, mixed *Sporosarcina pasteurii* with calcium chloride instead of a growth medium. They were injected into the borehole at the same time (though in a separate injection line) as a solution of urea, this was then followed by continued injection of a urea and calcium chloride solution for two hours. Over 17 hours of treatment (8 cycles), approximately 750g of calcium carbonate precipitate was fixed in the subsurface and the transmissivity of the fracture over several m² achieved significant reduction.

Around the injection borehole there was a ~99% reduction in transmissivity, 2m from the borehole the reduction in transmissivity was ~35% and at the extraction borehole transmissivity was reduced by 14%. Although this field trial successfully demonstrated the potential of MICP as a viable alternative grout, given that the trial was in-situ it was not possible to observe where and how the calcium carbonate precipitated was distributed.

2.4.3 Solid-phase capture of contaminants

Microbiologically induced calcium carbonate precipitation has also been investigated for capture of inorganic contaminants into the calcium carbonate crystal lattice such as ^{90}Sr and UO_2 contamination of subsurface groundwater (an issue of concern in the Snake River Plain, USA).

Researchers have investigated the potential of MICP for capture of radionuclide's in the Snake River Plain Aquifer (Warren et al, 2001; Fujita et al, 2008; Fujita et al., 2004). Mitchell and Ferris (2006) concluded that MICP could still be a viable process for the clean-up of strontium contamination within the Snake River Plain Aquifer. Arnold (2007), used a similar method to investigate the phase capture of arsenic contaminants in groundwater. In this laboratory study, calcite and aragonite precipitated via *Sporosarcina pasteurii* in the presence of arsenic resulted in a decrease in arsenic concentrations of up to 88% from the initial $0.7\mu\text{g L}^{-1}$ concentration.

2.4.4 Construction materials

MICP could also be used to reinforce limestone mines without affecting permeability. MICP produced 9g of calcium carbonate per treated column, and treated cores were double the strength vs. untreated cores whilst permeability was only decreased by 50% (van Paassen et al, 2008).

De Muynck et al (2008) used pure (*Bacillus sphaericus*) and mixed cultures of ureolytic bacteria as a surface treatment for concrete. Concrete samples treated with MICP showed a decrease in permeability similar to that of silane/siloxane chemical grouts. Van Tittleboom et al (2010) looked at infilling cracks in concrete using *Bacillus sphaericus* in a protective silica gel. Hydraulic conductivity measurements showed that biological treatments performed nearly equal to that of more traditional epoxy treatments.

MICP has been evaluated by Okwadha and Li (2011), as a method to seal concrete surfaces that have been contaminated with PCB'S (polychlorinated biphenyls). Constant head tests showed that water permeability had decreased by 5 and 2 orders of magnitude. Chemical analysis showed that no PCB's were detected in the effluent.

Although the main aim of the paper was reached, there was a substantial difference between the decreases in permeability of the samples which was not evaluated. The research would indicate that somehow the bacteria found it easier to seal the concrete pores than the sand filled fracture aperture pores. Possibly the pore throats within the concrete were smaller than the pore throats within the sand allowing the bacteria to be retained more easily, or the pH differences could have affected the precipitation rates.

One of the most exciting aspects of research into the use of MICP as a concrete treatment is that of a ‘self healing’ concrete. Wang et al (2012) used silica gel to protect the bacteria (*Bacillus sphaericus*) from the high pH (>12) of the concrete. The bacterial/silica gel mix was placed in a glass tube, with a calcium nitrate/urea solution placed in another glass tube. These glass tubes were then glued together and placed within concrete samples which were then cured for 2 weeks. The concrete samples were then cracked and left in an air-conditioned room. The permeability decreased over the both the control and the silica gel with attenuated bacteria was 3 orders of magnitude greater than untreated samples.

2.5 Improvement of the spatial distribution of calcium carbonate precipitation

The transport of bacteria within porous media is influenced by physical, chemical and biological factors. Although bacterial transport through aquifers has been well studied (Torkzaban et al, 2008; Scholl et al, 1990; and Murphy and Ginn, 2000), the aim of these studies was not the improvement of spatial distribution. Controlling the spatial distribution of calcium carbonate precipitate can provide an invaluable tool for the development of strategies to manipulate porous media permeability and reactive transport on large scales.

The components of an engineered MICP system are a flow-cell, with an injection port, a flow-cell can be composed of a simulated fracture, a simulated fracture network or be filled with granular material. There can be concurrent injections of bacteria, cementing solution (typically calcium chloride and urea) and with or without a growth medium. Or, these different solutions can be injected sequentially known as a staged injection. Other

strategies involve static periods to encourage the growth of a bio-film or continuous flow to encourage a better distribution of calcium carbonate precipitate. These different strategies are shown in Table 1.

2.5.1 Biofilm growth (nutrients vs no nutrients)

Biofilms; particularly the extracellular polymeric substances (EPS), are generally highly hydrated and may create an environment where ions or molecules may accumulate in higher concentrations than the bulk fluid. The use of a biofilm could potentially lead to a greater rate of urea hydrolysis thus calcium carbonate precipitation.

Ferris et al (2003), examined MICP utilising an artificial groundwater (AGW) which contained urea and calcium ions. They calculated the rate of urea hydrolysis (K_{urea}) to be 0.91mM urea day⁻¹. Similarly Dupraz et al (2010) using an AGW calculated K_{urea} to be 0.996 urea day⁻¹. Okwadha and Li (2010), using similar urea and calcium concentrations utilised a growth medium within their injection solutions, their calculated K_{urea} was similar to that of Ferris et al (2003) and Dupraz et al (2010) at 0.93mM urea day⁻¹. These studies would indicate that the use of a growth medium containing urea and calcium ions instead of an artificial groundwater containing urea and calcium ions has little impact upon the ureolytic rates of *Sporosarcina pasteurii*.

An alternate use for growth medium during MICP is that of refreshing the bacterial biofilm present within the flow columns to produce a more homogeneous biofilm and prolong the effectiveness of the bacterium inoculation (Cunningham et al, 2011). However, an inherent problem with the use of growth medium in the subsurface is that of bio clogging. The subsurface is not a sterile environment, when a growth medium is introduced it would not only promote the growth of the bacteria used for the precipitation of calcium carbonate but also the growth of indigenous bacteria leading to the fractures becoming clogged with microbial matter instead of mineral precipitate (Tobler et al, 2011). This would reduce the hydraulic conductivity of the fracture during the short term but the microbial ‘clog’ would have a poor chemical and mechanical stability, which would lead to an unsealing of the fracture over the longer term.

2.5.2 Injection strategies

Stocks-Fischer et al, (1999) found that the concurrent injection of bacteria, calcium chloride and the urea together at low flow rates resulted in the clogging of the flow cell at the injection port most likely due to filtration (trapping bacteria at pore throats). Whiffin (2004) checked for filtration by flushing bacterial cells through a 1.6m sand column with <300um silica sand and found that the bacteria were relatively uniform throughout the sand column thus no filtration was occurring however there was a loss of ~30% of the bacteria from the column. Whiffin's results indicate that the what looks to have occurred in the Stocks-Fischer 1999 study is that precipitation on the bacterial surface began during the concurrent injection, increasing the density and size of the bacteria thus enabling filtration.

An interesting approach to improve the distribution of precipitate was taken by Barouki et al (2011) to even out the distribution of precipitate. Barouki et al (2011), used two sand columns, in one column the bacteria and the cementing solution were pumped in from the top, in another column the bacterial solution was pumped in from the top and the cementing/nutrient solution was pumped in from the bottom. This gave a gradient of bacteria from the top to the bottom and a gradient of cementing/nutrient solution from the bottom to the top thus the base bacteria there will have full access to the reactants, then as the reactants become depleted as it moves up the column, the bacteria will still produce precipitate but not as much, thus evening out the distribution. Bacteria were pumped in from the top of the column at 10ml/min and left static for six hours. In the top injection only column there was a continuous flow of cementing solution at 2ml/min and in the other column; the cementing solution flow was 10 ml/min for 30 mins the static for 2.5 hours. With continuous flow there was a greater concentration of calcium carbonate at the injection port and in the stop flow column there was a close to uniform distribution of calcium carbonate precipitate throughout the column.

Although Barouki et al (2011) results, managed to produce a more even distribution, unfortunately what produced these results is unclear. Is it the stop/flow procedure or the pumping of cementing solution in from the base? Injection from the

bottom would also be difficult to achieve in the field, due to gravity and the ambient groundwater flow.

2.5.3 Flocculation

Sporosarcina pasteurii has a negative cell surface charge, by adding a cation such as ammonium or calcium ions, the bacteria can be aggregated together creating bacterial flocs. These flocs are still permeable to fluids and have a greater density than individual bacteria. Tobler et al (2012) in an effort to prevent bio-clogging, injected *Sporosarcina pasteurii* at low optical densities into sand columns with either urea and calcium (concurrent injection) or one after the other (staged injection).

Concurrent injection where flocs would have been produced, resulted in extensive plugging of the first 10mm of the column whilst staged injection where there would be minimal flocculation gave a more homogeneous distribution of precipitate / bacteria. Cuthbert et al (2013) initially using a staged injection strategy, found that the shear stresses created by the laminar flow conditions dispersed the bacteria, thus resulting in less bacteria being retained within the fracture. They then applied a concurrent injection strategy, where the bacterial flocs were able to resist dispersion. The concurrent/floc strategy achieved a reduction in transmissivity of between 99% and 35%. Unfortunately, this field trial had no way of determining the effect flocculation had on the distribution of the calcium carbonate.

2.5.4 Fixer

Bacteria have a negative cell surface charge whilst silica (the most abundant mineral in rock) also has a slightly negative surface charge creating a repulsive force. By introducing cations after the bacteria have been injected into a fracture (a fixing solution), the negative repulsive force can be overcome. Thus increasing bacterial adsorption to the rock surface.

To avoid the loss of bacteria from the flow-cell, Whiffin (2007) used a continuous flow -staged injection strategy to not only immobilize the bacteria within the flow cell but to improve the distribution of calcium carbonate within the flow-cell. Bacteria were injected followed by a calcium chloride ‘fixing’ solution. Immediately after this the

cementing solution composed of calcium chloride and urea was injected. This produced an average calcium carbonate content of 59.2kg CaCO₃/m³; however, the majority of the calcium carbonate precipitate was in the first half of the flow-cell.

Harkes et al (2010) examined how different solutions affected bacterial retention within sand columns. The sand columns treated with a fixing solution resulted in between 92% and 100% of the bacteria being retained whilst demineralized water and the same bacterial concentration at the same flow rate resulted on 0% retention.

Table 2.1: concentrations of bacteria and cementing agents used for different purposes and results.

<i>Authors</i>	<i>Fractured or Porous Media</i>	<i>Growth Medium</i>	<i>Fixer</i>	<i>Flocculant</i>	<i>Staged Injection</i>	<i>Concurrent Injection</i>	<i>Static or Flowing</i>	<i>Comments</i>
Ferris et al (1992)	Sand	Yes	No	No	No	No	Flowing	Bacteria and sand were mixed together before packing. A precipitation gradient was evident.
Gollapudi et al (1995)	Sand and simulated Fractures	Yes	No	No	No	No	Flowing	Bacteria and sand were mixed together before packing. Final permeability reduction 90 to 100%. Precipitation did occur within the fractures.
DeJong et al (2006)	Sand	Yes	No	No	No	Yes	Static	MICP treated sand had a higher shear strength than gypsum treated sand.
Whiffin et al (2007)	Sand	No	Yes	No	Yes	No	Flowing	A calcium carbonate depositional gradient was found, with the majority of the solution being utilized within the top 2.85m of the column.
Cunningham et al (2009)	Glass Beads & simulated fractures	Yes	No	No	Yes	No	Static	Complete sealing occurred
Van Paassen et al (2010)	Sand	Yes	Yes	No	Yes	No	Flowing	An increase in shear strength was measured; however it was difficult to control the in-situ distribution of bacteria.
Barouki et al (2011)	Sand	Yes	No	No	Yes	No	Both	With continuous flow column there was a greater concentration of calcite at the injection port, in the stop flow column there was a close to uniform distribution of calcite precipitate throughout the column.
Cunningham et al (2011)	Sand	Yes	No	No	yes	No	Static	On average 16% of pore space occupied by calcite precipitate. Hydraulic conductivity decreased from 2.63×10^{-3} m/sec to 9.1×10^{-4} m/sec within 36 days, though there was a gradient in distribution.
Phillips et al (2013)	Sand and Fracture	Yes	Yes	No	Yes	No	Static	A reduction in permeability of between 61% and 99% seen and a more homogeneous distribution of precipitate.
Schultz et al (2011)	Simulated fracture	Yes	No	No	Yes	No	Flowing	The amount of calcium immobilized was 82 mg based on an effluent mass balance. A gradient of precipitate size was found and a higher proportion of dead cells were found at the base of the biofilms.
Tobler et al (2012)	Sand	No	No	No	Yes	Yes	Flowing	Concurrent injection resulted in a greater gradient of calcite distribution with a 34% reduction in permeability whilst staged injections gave a more homogeneous

Cuthbert et al (2013)	In-situ Fracture	No	Yes	Yes	No	Yes	Flowing	<p>distribution of precipitate and a 54% reduction in permeability. Bacteria were embedded within the calcite thus repeated bacterial injections are required.</p> <p>The use of a fixer did not retain bacteria within the fracture due to shear stress created by the flowing conditions dispersing the flocs. Urea was added to the fixer to start precipitation early on creating aggregation and filtration within the fracture. Flocked bacteria were injected via a borehole at 250ml/min for 15 min then cementing solution was injected for 105 minutes at the same flow rate. This was repeated three times. Approximately 750g of calcium carbonate precipitate was fixed in the subsurface and the transmissivity of a single fracture over several m² achieved significant reduction.</p>
-----------------------	------------------	----	-----	-----	----	-----	---------	---

2.6 Conclusion

Much of the literature surrounding ureolytic MICP focuses on controlling the physico-chemical conditions that influence precipitation. The wide range of variables such as pH, temperature, bacterial concentration, cation concentration, urea concentration, and shear stress created by slowing conditions for specific MICP applications indicates there is not one “recipe” for controlling MICP in engineered applications. The success of MICP treatment depends on the ability to control where and when calcium carbonate precipitation occurs.

From the discussion on injection strategy in section 2.4.2, it is evident that the following factors strongly influence the level of treatment that can be achieved: bacterial density, calcium concentration and urea concentration. With regards to bacterial density, research (Tobler et al, 2012; Dupraz et al, 2010) has shown that; as expected, by increasing the bacterial density the ureolytic activity is increased. Sufficient levels of calcium and urea concentration also need to be present in the system to ensure that they do not become the limiting factor (where not enough of one of these solutions limits the rate or total production of precipitate).

The review of the literature has shown that one of the main challenges with applying MICP to ground is that of the limitation in where the maximum precipitation occurs is often close to injection points. Further, for such techniques to be transferred into engineering practice the zone of treatment must be predictable and controllable. It is clear that in order to investigate the potential of MICP to be used for grouting rock fractures there is a need for further experimental work to understand how this process can be carried out in rock fractures.

This thesis investigates (i) the role of bacterial flocculation on the spatial distribution of calcite precipitation in rock fractures (Chapter 3), (ii) the influence of flow rate on fracture sealing (Chapter 3) and (iii) the influence of ratio of bacteria to cementing solution and concentrations of treatment solutions on mass of calcite precipitated (Chapter 4). Based on these results the procedure for grouting rock fractures to achieve a more evenly distributed calcite precipitation was developed (Chapter 4).

3. MICP IN FRACTURES

3.1 Introduction

The potential of microbially induced calcite precipitation (MICP) for use as a grouting technique in engineering practice depends on the controllability of the process. The literature review in Chapter 2 highlighted that considerably more work has been carried out on understanding and demonstrating the potential of MICP within porous media, compared to fractures.

This chapter presents an experimental investigation of the of the processes and controls on MICP within fractures. Experiments were carried out in transparent fracture flow cells to enable observation of the spatial distribution of calcite precipitated.

This chapter examines the influence of hydraulic controls (velocity, flow rate, fracture aperture) and bacterial density on the spatial distribution of MICP within fractures. The research presented in this chapter has been published in *Water Resources Research*: El Mountassir G., Lunn R.J., Moir H., MacLachlan E.C. (2014). Hydrodynamic coupling in microbially mediated fracture mineralization: formation of self-organized groundwater flow channels. *Water Resources Research* Vol 50, No. 1, pp. 1-16 <http://dx.doi.org/10.1002/2013WR013578>).

3.2 Background

Previous research (as discussed in Chapter 1) has predominantly focused on porous media and what research there has been on fractures has involved rock cores or in-situ where it is not possible to visually assess the influence that hydraulic controls has on the spatial distribution of microbially induced calcite precipitation. It is the hydraulic controls upon surface attachment, shear mobilization and filtering which can have strong implications for not only the penetration of the solutions but also the distribution of the calcite.

3.3 Methodology

3.3.1 Flow-plate setup

MICP was investigated in fractures of varying widths and aperture, these terms are defined in Figure 3.1. Fracture flow-plates were constructed using two sheets of polycarbonate. Lexan polycarbonate is hydrophobic and has a negative surface charge when in contact with electrolytes over a range of pH's (pH 4 – 10) (Kirby and Hasslebrink, 2004).

Fracture flow-plates of length 20 cm and width 14 cm were used to enable visual observation of microbially induced calcite precipitation on the fracture surfaces over time. Each flow-plate comprised a smooth top sheet (Figure 3.1a) and a lower etched sheet designed to represent more than one fracture (Figure 3.1b). The fracture flow-plates were manufactured using a precision computer numerical control (CNC) milling machine which has an operating tolerance of $\pm 5\mu\text{m}$. Flow-plate 1 had eight fractures all with different widths and apertures (Figure 3.1c). Flow-plate 2 consisted of five etched fractures all of which had an aperture of 0.3 mm but were of varying width (Figure 3.1d).

Figure 3.1e shows a schematic of the experimental setup. Calcite precipitation within the fractures was monitored over time using a Canon Powershot G9 camera. The fracture flow-plates were in the horizontal position in all of the experiments presented here, with the digital camera mounted above the flow-plates (Figure 1e) at a distance of 425 mm, allowing the full fracture flow-plate to be photographed at a resolution of 12.1 megapixels. Reflection from the upper polycarbonate surface was minimized using a Hoya 58 mm circular polarizing filter. Digital photographs were taken every 15 seconds during each injection cycle.

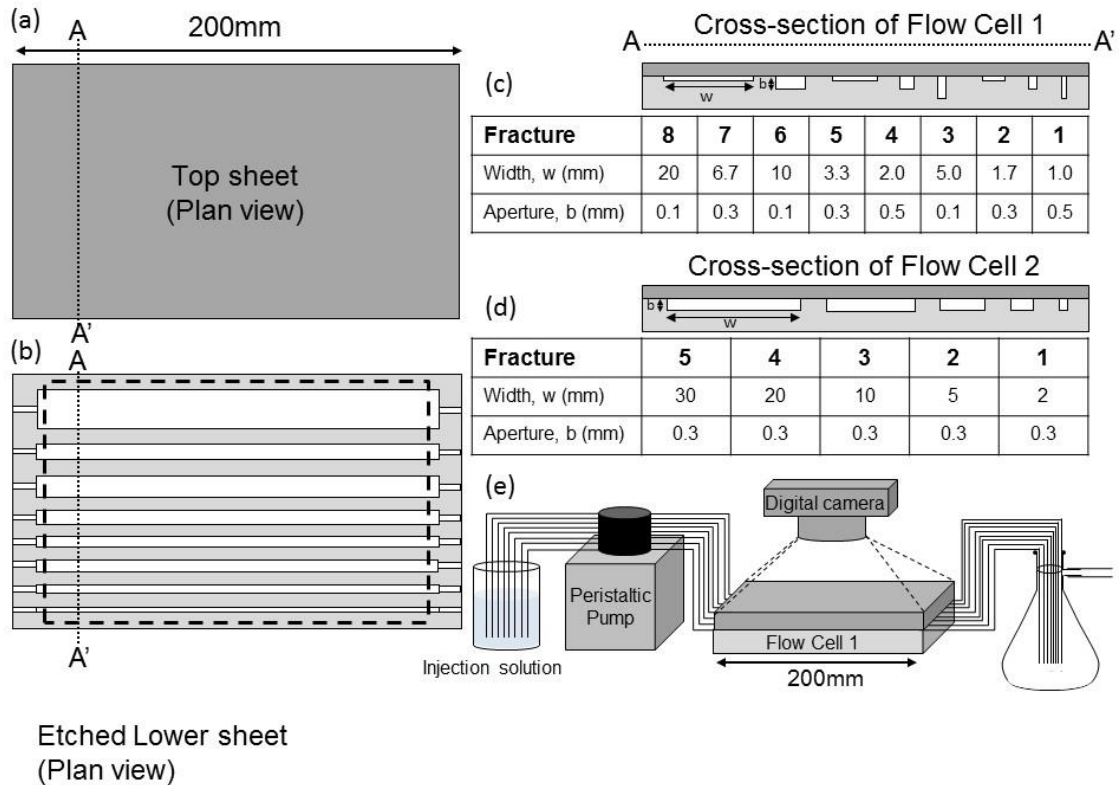


Figure 3.1: Experimental setup: (a) plan view of top polycarbonate sheet, (b) plan view of lower etched polycarbonate sheet, (c) cross section of fractures of different widths and apertures in Flow-plate 1 (vertical exaggeration of apertures is 10X), (d) cross section of fractures of different widths and apertures in Flow-plate 2 (vertical exaggeration of apertures of 10X), and (e) schematic of flow arrangement.

3.3.2 Fracture velocities

The initial average flow velocity in each individual fracture at the beginning of each experiment, v_i , i.e., prior to any calcite precipitation, was calculated as: $v_i=Q/A$, where Q is the flow rate and A is the initial cross-sectional area of each fracture (A =width x aperture).

For Flow-plate 1, Fractures 1 to 3 had the same A_i and thus for a given Q the same v_i ; Fractures 4 to 6 had half that v_i and Fractures 7 and 8, half that v_i again. At the velocities tested here, the Reynolds numbers of the fractures investigated in Flow-plates 1 and 2 remained well within the laminar flow regime ($Re < 100$). The initial average fracture velocities in these experimental fractures ranged from 1×10^{-3} m/s to 149×10^{-3} m/s for apertures ranging from 100 to 500 μ m, which corresponds to hydraulic gradients of 0.005 and above; the higher end of the spectrum found in the subsurface. Although high, such gradients are greater than what is found within the subsurface, the injection of grouts are usually injected under higher hydraulic gradients

to ensure adequate penetration and overcome hydraulic gradients which could be directing groundwater flow to the excavation.

3.3.3 Bacterial Solution

The optical density (OD) of the microbial suspensions was measured using a spectrophotometer (Thermo Scientific Helios Zeta ultraviolet-visible (UV-VIS) model) at a fixed wavelength of 600 nm (OD600). Cuthbert et al., (2013) reported successful sealing of an *in-situ* rock fracture; they used a relatively high OD600 of 1.0. A microbial suspension with an OD600 of 1.0 was used in this study. Table 3.1 presents details of the preparation of the microbial suspensions.

As discussed in Chapter Two, to retain bacteria within the flow-plates, flocculation was induced prior to injection into the fracture flow-plates by mixing with 50mM CaCl₂. The introduction of CaCl₂ leads the positive calcium ions to be attracted to the surface of the bacteria, reducing the double diffuse layer (Derjaguin and Landau, 1941; Verwey and Overbeek, 1948), and therefore reducing the repulsive forces between bacterial cells; they are thus more likely to approach more closely and flocculate (De Schryver et al., 2008).

Table 3.1: Summary of preparation and constituents of injection solutions

<i>Solution</i>	<i>Preparation</i>	<i>Constituents</i>
Microbial suspension	Sporosarcina pasteurii cultured on agar (Brain Heart Infusion with 2% urea), grown overnight in Brain Heart Infusion (with 2% urea). Bacterial separation by centrifuging at 8000 rpm for 5 mins.	Equal volumes of Sporosarcina pasteurii solution + 50 mM CaCl ₂ pH adjust to 6.5. Final Optical Density at 600nm (OD600) = 1.0

Cementation solution	Autoclave CaCl ₂ solution. Sterile injection of 40% urea solution passing a 0.2µm filter.	0.7M CaCl ₂ + 0.5M CO(NH ₂) ₂ pH adjusted to 6.5 using 10% HCl
----------------------	--	---

The addition of CaCl₂, to induce bacterial flocculation prior to injection, allowed for control and observation of the initial floc size distribution. As shown in Figure 3.2, the distributions of the bacterial flocs present in the two microbial suspensions (OD600 = 1.0 and OD600 = 0.25) prior to injection into the flow-plates, were investigated using a microscope (Olympus BX60) under a bright field. Both a 1.0 OD600 and 0.25 OD600 solution were pipetted onto glass slides and heat fixed before gram staining (bacteria become more visible). The formation of an individual large *Sporosarcina pasteurii* floc, a range of other floc sizes and the presence of individual cells in the 1.0 OD600 solution. While single cells were observed in both suspensions, the greatest variation between the two suspensions, is the presence of much larger flocs within the 1.0 OD600 suspension compared to the 0.25OD600 suspension.

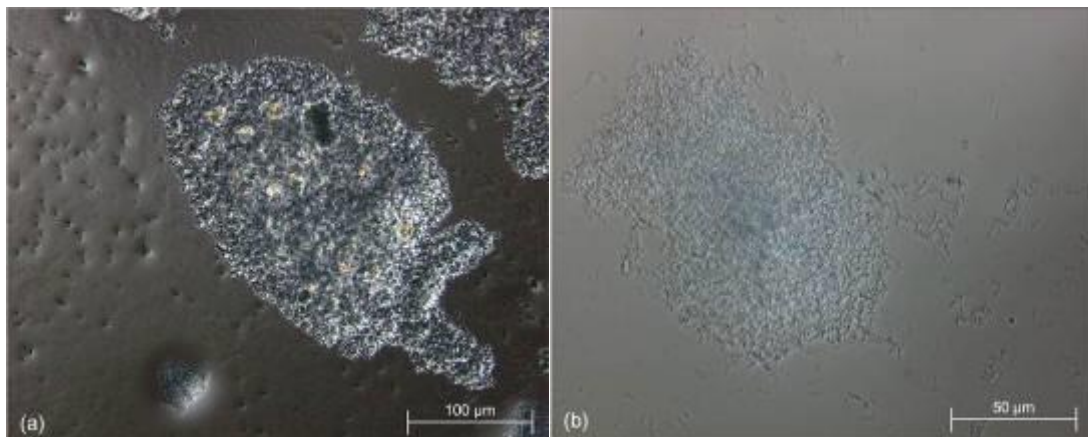


Figure 3.2: Oil immersion Olympus fluorescence microscope images of flocculated bacteria at (a) 1.00OD600 and (b) 0.25 OD600.

3.3.4 Injection Strategy

As discussed in Chapter 2, research has illustrated that *Sporosarcina pasteurii* can become completely encased in calcite, limiting subsequent precipitation (Cuthbert et al., 2012; Tobler et al., 2012). To ensure that precipitation occurs continuously,

repeated cycles of fresh bacterial solution injection followed by the cementing solution were adopted in these experiments.

Prior to each injection cycle, the flow-plates were initially saturated by flushing with water for a minimum of 30 min. The microbial suspension was immediately pumped into the flow-plate after mixing. To prevent precipitation within the tubing a 5ml pulse of sterile water was injected followed by an injection of a 0.7 M CaCl₂ and 0.5M Urea solution, referred to here as the cementation solution (see Table 1). Similar to Whiffin (2007), van Paassen et al (2010) and Cunningham et al (2011), for these experiments, it was desirable to have a high availability of calcium ions and carbonate ions (produced via urea hydrolysis) in the system for calcite precipitation.

Details of the experimental injection strategies are presented in Table 3.2. Two Gilson Minipuls (Model 3) peristaltic pumps were used for pumping the treatment solutions through the flow-plates. Each channel on the peristaltic pumps was connected to an inlet port of an individual fracture in the plates. Each flow-plate experiment was performed with the same flow rate in each individual fracture.

Table 3.2 shows the components of each cycle and the duration of each stage. Equal volumes of microbial suspension (one stage) and then cementation solution (another stage) were used within each injection cycle, in all the experiments. Injection of the microbial suspension was followed by an injection of cementation fluid then a flush injection of sterile DI water, constituting one injection cycle. In section 2.6.2 it was discussed how most experiments have been conducted using static phases which may not be replicable under in-situ conditions. All of the experiments presented in this chapter were carried out under continuous flow conditions; when the cells were not being injected with microbial or cementation solutions (generally overnight when image collection was not feasible), sterile DI water was continuously pumped through the cells at the same flow rate to maintain flowing conditions, to minimize unobserved precipitation and ensure that equal volumes of microbial suspension and cementation fluid were injected per cycle.

Table 3.2: Flow rate, optical density, pumped injection volume, duration and number of injection cycles.

<i>Experiment</i>	<i>Flow-plate</i>	<i>Bacterial OD600</i>	<i>Flow Rate (ml/min)</i>	<i>Bacterial injection:</i>	<i>Cementation fluid injection:</i>	<i>Duration of Stage (min)</i>	<i>No. of cycles</i>
-------------------	-------------------	------------------------	---------------------------	-----------------------------	-------------------------------------	--------------------------------	----------------------

				<i>Volume injected per fracture (ml)</i>	<i>Volume injected per fracture (ml)</i>		
1	1	1.0	1.12	33.6	33.6	30	5
2	1	1.0	4.48	44.8	44.8	10	5
3	2	1.0	1.2	36	36	30	5
4a	2	0.25	1.2	36	36	30	25
4b	2	0.25	0.6	18	18	30	10

3.3.5 SEM Analysis

On completion of Experiment 3 (Table 3.2), the flow-plate was opened and the calcite precipitate was sampled at 12 different locations using sticky carbon tabs (note minimal pressure was used to prevent any damage to the samples). These samples were then analyzed using a Zeiss Sigma field emission scanning electron microscope (SEM) with ionized nitrogen under low vacuum. Using low vacuum conditions meant that the specimens did not need to be coated prior to placing in the SEM. Backscattered (secondary) electron imaging was used to examine the calcite morphology. Energy-dispersive X-ray microanalysis (INCA mapping) was also carried out to determine composition.

3.4 Previous work completed by Msc student

Prior to the beginning of this PhD research, experiments investigating the influence of fracture velocity on MICP were carried out by Laura Gilfillan (an Msc student) between June and August 2011, under the supervision of Dr Grainne El Mountassir and Professor Rebecca Lunn. The research presented in this thesis followed on from this initial study, thus a brief summary of the results from these tests are included here. These experiments were carried out in Flow-plate 1 (Experiments 1

and 2). The author carried out all experiments in Flow-plate 2 (Experiments 3, 4a, 4b) using the methodology described above.

3.5 Influence of Velocity

Figure 3.3 presents the microbially induced calcite precipitation patterns observed in the fractures of Flow-plate 1 after five injection cycles using microbial suspensions with an $OD_{600} = 1.0$ at (a) a constant flow rate of 1.12 ml/min, and (b) a constant flow rate of 4.48 ml/min (Experiments 1 and 2 in Table 2). The widths (w) and aperture (b) of each fracture are noted on the figure, and the velocities indicated are the initial average flow velocities in each individual fracture, v_i prior to any calcite precipitation. The area of each flow-plate presented in the digital photographs in Figure 3.3c and 3.3d, are defined by the dashed rectangle in Figure 3.3b.

In Figure 3.3a, it is evident that similar channel-like patterns of precipitates were created in Fractures 3, 6 and 8, where precipitation has reduced each fracture to a number of smaller tortuous pathways. Fractures 3, 6 and 8, all have the same aperture of 100 μm and exhibited similar precipitation patterns, even at different velocities. The aperture influence can be explained by considering that the microbial flocs have the same vertical distance to travel in fractures of the same aperture before deposition onto the lower fracture surface in the flow-plate, and therefore under creeping flow conditions (Reynold's number < 1), the settling time is equal.

Figure 3.3b shows the same experiment but with an increased flow rate of 4.48 ml/min. In this case, similar channelised flow paths were again observed in Fractures 6 and 8, but channelling was no longer apparent in Fracture 3 at the higher initial fracture velocity of 149×10^{-3} m/s. Furthermore, comparing Fracture 6 from Figure 3.2a and 9b; it is clear, that less calcite precipitate was present on the fracture surfaces at the higher fracture velocity (after five injection cycles), this is despite the fact that for $Q = 4.48$ ml/min, the mass of calcium chloride and urea injection per fracture during each cycle was one third greater than injected at $Q = 1.12$ ml/min (see Table 3.2). At the higher flow rate (Figure 3.2b), wider channels were maintained open compared to the lower flow rate (Figure 3.2a) in which the channels are narrower.

Velocity clearly has an important influence on both the spatial distribution and the eventual mass of calcite that precipitates onto the fracture surfaces.

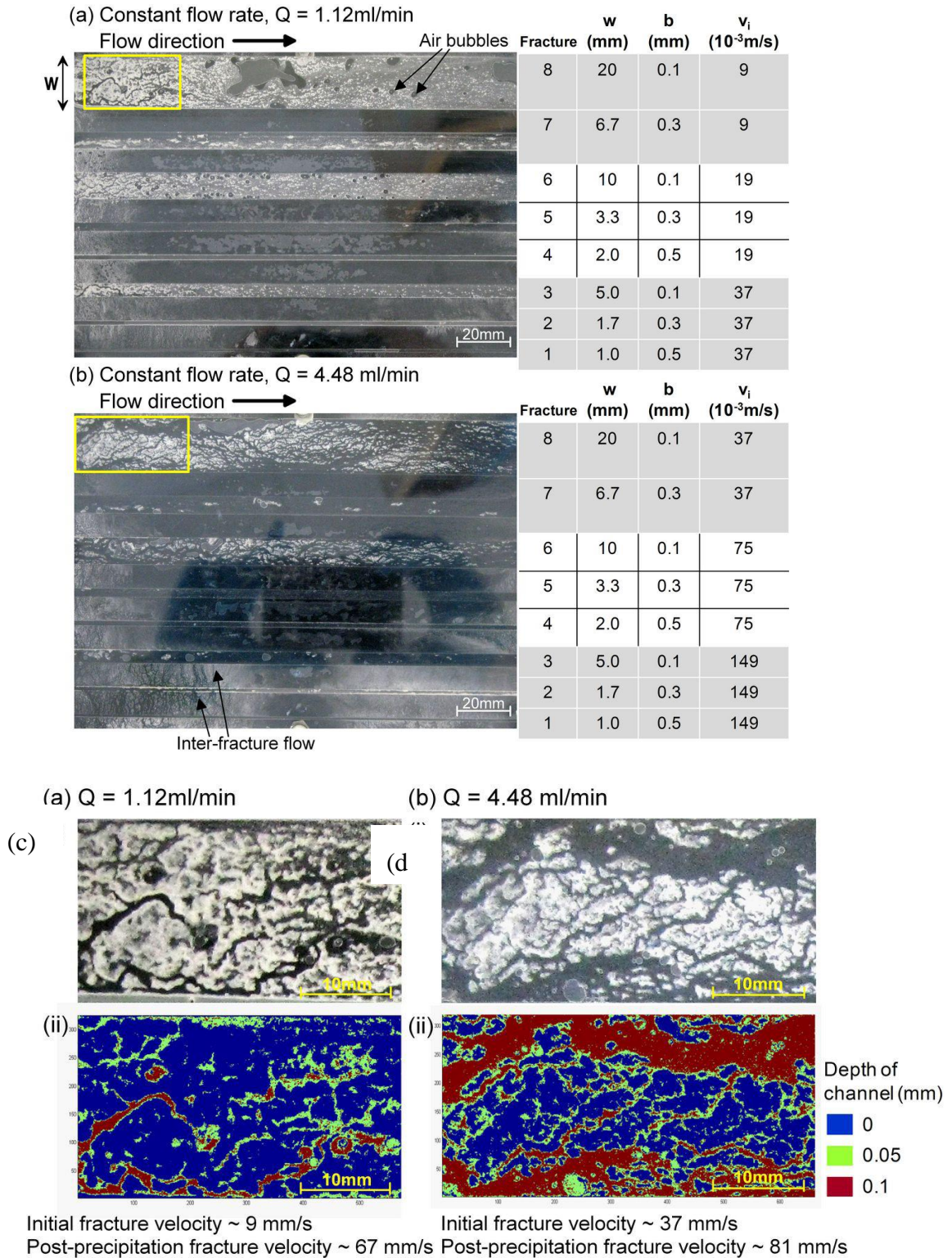


Figure 3.3: Influence of velocity and aperture on calcite precipitation (Flow-plate 1) after five injection cycles at (a) $Q = 1.12 \text{ ml/min}$, (b) $Q = 4.48 \text{ ml/min}$. W is the width of an individual fracture perpendicular to the flow direction and marked in (a), b is the fracture aperture and v_i is the initial average fracture velocity, i.e. prior to precipitation. It should also be noted that the flow-plate was not fully sealed between channels (see b) and across cell flow was observed between fractures; the actual volume of across cell flow was very low, as each fracture was calibrated for the desired flow rate both prior to entering the fracture inlet and at the fracture outlet. Figures (c) and (d) show the development of open faster flowing channels in Fracture 8 after 5 injection cycles at $Q = 1.12 \text{ ml/min}$ and $Q = 4.48 \text{ ml/min}$: (i) Digital photograph of areas in Fracture 8 marked on Figure 3.1, (ii) Digital estimation of depth of calcite precipitation (image analysis conducted using Matlab), where blue indicates that the fracture is fully closed at that location (i.e. aperture = 0), for the red channels the aperture is 0.1mm (fully open) and for the green channels the aperture is 0.05mm

Figures 3.3c and 3.3d show a closer inspection of Fracture 8 post-precipitation at different flow rates for the areas marked with rectangles in Figure 3.3a and b. These detailed images were used to gain an approximate estimate of the magnitude of the velocity in the remaining open channels. Image analysis was carried out using MatLab; using over 500 slices across each image to determine the new cross-sectional area of the fracture post precipitation (A_p).

The average fracture velocity post precipitation (v_p) was then calculated as Q/A_p . Two categorization techniques were used to gauge the sensitivity of the velocity estimates to the technique applied: (i) categorizing each pixel of the image as being either open or closed depending on its grayscale value and (ii) using three categories for the channel: open, half open, or closed depending on its grayscale value (Figures 9cii and dii). Combining the results from both techniques, the velocity in the open channels was estimated to be in the range of 67×10^{-3} m/s to 110×10^{-3} m/s for a flow rate of 1.12 ml/min and in the range of 81×10^{-3} m/s to 112×10^{-3} m/s for a flow rate of 4.48 ml/min.

It is interesting to note that even though the patterns of precipitation vary; the velocity ranges for the open channels were of a similar magnitude. These observations lend support to the hypothesis that, as local velocities increase, shear velocities at fracture surfaces will exceed the actual settling velocity of the microbial floc; then, according to conventional theory on particle entrainment, all flocs will be entrained and deposition will be inhibited (van Rijn, 1984). The results presented in the following section are from the experiments conducted by the author of this thesis.

3.6 Results

3.6.1 Initial Observations

Figure 3.4 illustrates the temporal and spatial evolution of microbially induced calcite precipitation over a number of injection cycles in a single fracture, Fracture 5 of Flow-plate 2 (30mm wide x 300µm aperture). Fracture 5 is focussed on here due to its size (making it easier to visually assess). The calcite can be visually observed since it precipitates as a white mineral. With each injection cycle, more calcite precipitates are located on the fracture surfaces. From examination of the surfaces at the end of each test, it was evident that the precipitates observed in Figure 3.4 were predominantly located on the lower fracture surface, although a thin layer of fine precipitate was present on all fracture surfaces.

In Figure 3.4, it can be observed that more precipitation was located close to the fracture inlets, with less located further along the fractures moving from left to right. Within this system, the white calcite precipitates observed on the fracture surfaces of the flow-plate, may be attributed to (a) calcite crystals which have grown from heterogeneous nucleation on fracture surfaces, (b) microbe-calcite aggregates (i.e., heterogeneous nucleation on cell surfaces), and (c) homogeneous nucleation of calcite crystals in solution (as previously discussed in Chapter 2). Figure 3.4a is an image of Fracture 5 taken 3 min into the cementation injection of Injection Cycle 1 (at $Q = 1.2\text{ml/min}$) and Figure 3.3b is taken at the end of Injection Cycle 1, i.e., after 30 min of injecting cementation fluid. By comparing Figures 3.3a and 3.3b it becomes evident that, during a single cycle, some of the precipitates are deposited and then removed; this type of observation was associated with microbe-calcite aggregates, essentially mineralized flocs.

From visual observation, it is evident that the transport of microbial flocs and calcite precipitates within, and indeed out of the flow-plate, governs the eventual spatial distribution of the calcite precipitates on the fracture surfaces. Calcite precipitates may exit the flow-plate as microbe-calcite aggregates and as calcite crystals which formed in suspension; indeed, a build-up of calcite precipitation was observed in the effluent container during these experiments.

In Figure 3.4, there is clear evidence of channelling and the formation of tortuous, braided pathways within the fracture as calcite is precipitated. Braiding, as

observed here, is a common feature of sedimentation processes (e.g. Leopold and Wolman, 1957). Experiment 3 presented in Figure 3.4 was carried out three times and similar braided patterns of channelling were observed consistently in each case, although the exact location and number of channels differed each time. The formation of channels is consistent with the precipitation patterns observed in Figure 3.3.

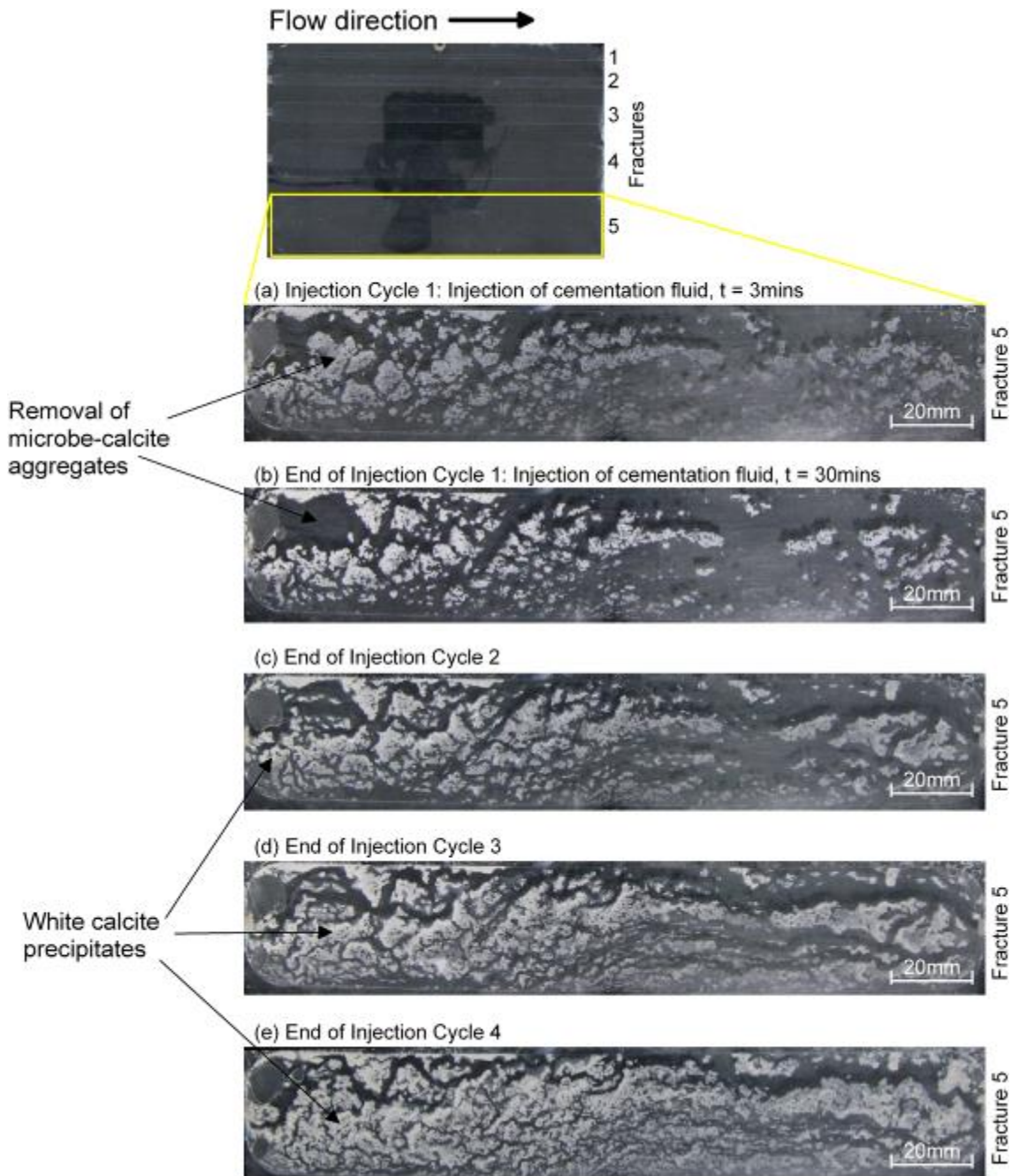


Figure 3.4: Evolution of microbially induced calcite precipitation in Fracture 5 of Flow-plate 2: Digital photographs (a) during the injection of cementation fluid (t=3 mins) in Injection Cycle 1, (b) at the end of Injection Cycle 1 (t=30 mins), (c) at the end of Injection Cycle 2, (d) at the end of Injection Cycle 3, and (e) at the end of Injection Cycle 4.

3.6.2 Bacterial Density

The effect of different floc size distributions on microbially induced calcite precipitation was investigated in Flow-plate 2 where all the fractures had the same aperture of 300 μ m but had different fracture widths. Figure 3.5a presents Flow-plate 2 after five injection cycles had been carried out at a flow rate of 1.2ml/min with an OD₆₀₀=1.0.

The pattern of precipitation observed in Figure 3.5a is strikingly similar in all five of the fractures with lower (initial velocities). There is more precipitate at the fracture inlets, with less located further along the fractures moving from left to right. This is most likely due to a mixture of physical processes, where initially gravitational settlement occurs with the biggest flocs settling out of the flow, then filtration of smaller flocs occurs where the larger flocs and the flow-plate walls are the collectors, in line with classic colloid filtration theory (Yao et al, 1971). There may also be a chemical gradient occurring within the flow-plate due to the presence of larger flocs get access to the cementing solution first.

Figure 3.5b presents Flow-plate 2 after 20 injection cycles have been carried out at an OD₆₀₀ of 0.25. As the bacterial density (OD₆₀₀) was reduced from 1.0 to 0.25, the diameter of the largest flocs in the suspension decreased (as shown in Figure 3.2). Both experiments 3 and 4a (Figure 3.5a and 3.6b) were carried out using approximately the same total numbers of bacteria and equal injection volumes per cycle (see Table 3.2) resulting in the same total availability of calcium ions and urea in each fracture.

Comparing Figure 3.5a and 3.5b, after 4 times as many injection cycles, the mass of precipitate still remained less in the fractures with the lower OD₆₀₀. Furthermore, in Figure 3.5b, the formation of tortuous flow paths is only apparent in the widest fracture shown at the base of the image (Fracture 5) which has the lowest initial flow velocity since it is the widest fracture at the same flow rate as the other fractures. Within the other fractures in Figure 3.5b, the precipitation is more patch-like i.e. at an earlier stage of channel development.

The evidence for lower settling velocities, due to a reduction in the diameter of the largest flocs present in the 0.25OD600 suspension (as measured through oil immersion microscope and photographed in Figure 3.2), is most apparent in Fractures 2, 3 and 4 of Figure 3.5b. The flocs have been transported further before settling out (i.e. precipitation is further downstream compared to that in Figure 3.5a). The experiment confirms the proposition that larger floc sizes give rise to higher settling velocities, which resulted in increased precipitation near the inlet as well as increased total mass of precipitate on the fracture surfaces.

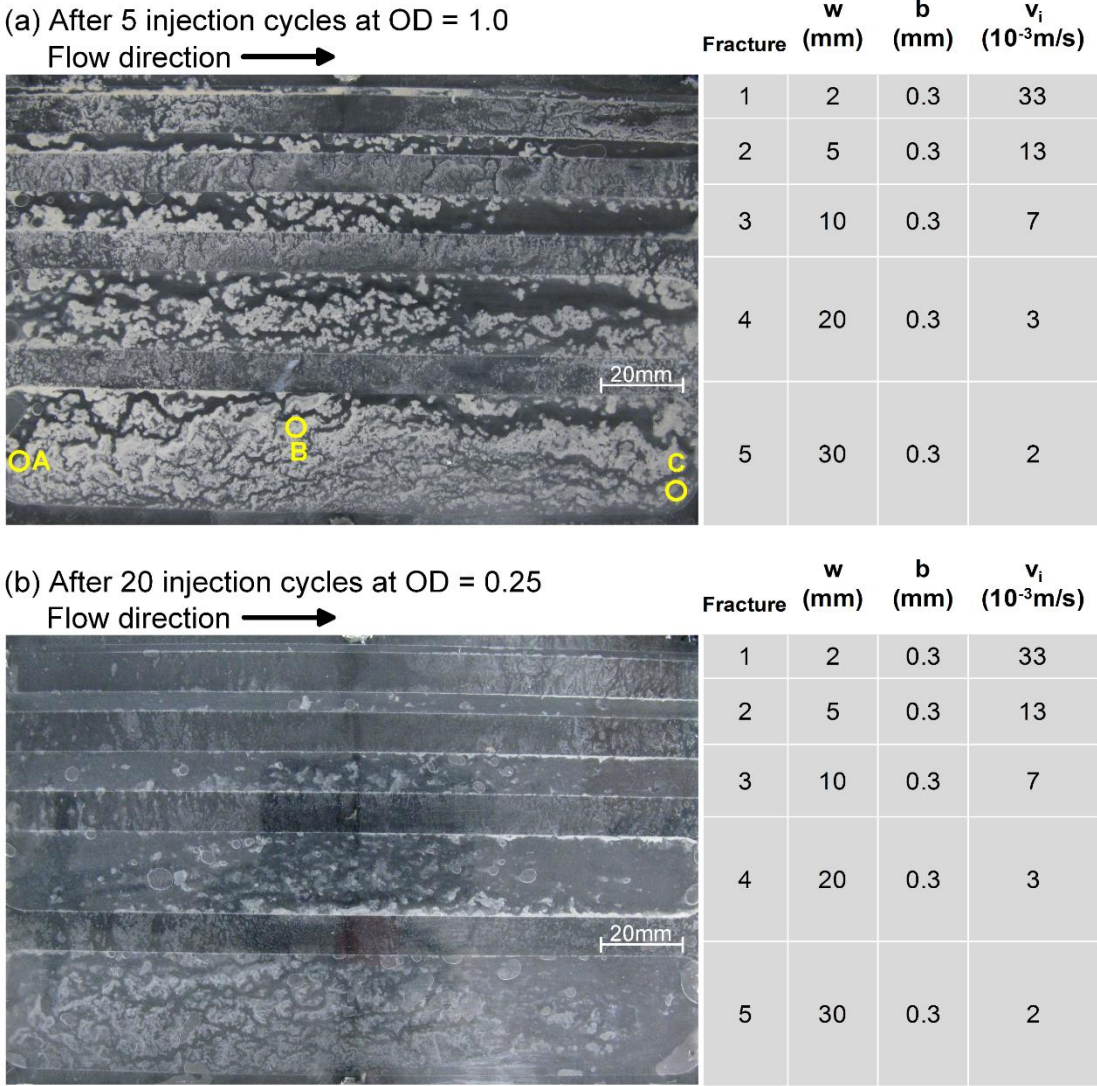


Figure 3.5: Influence of bacterial density on calcite precipitation at $Q=1.2$ ml/min (Flow-plate 2): (a) after five injection cycles at $1.00D_{600}$ and (b) after 20 injection cycles at $0.25OD_{600}$.

3.6.3 Flow Rate Reduction

The results presented in Section 3.4.1 indicate that fracture velocity has important influence on the spatial distribution of calcite precipitation within fractures. It should therefore be possible to fill in a previously stable open channel by dropping the injection flow rate. To test this hypothesis, Experiment 4a was run for 25 injection cycles at an initial flow rate of $Q = 1.2$ ml/min. A comparison of the precipitate at 24 and 25 cycles (Figure 13) shows that, whilst some precipitation was occurring within the mass of precipitates, the open channels themselves had become stable.

In Experiment 4b (Table 3.2), the flow rate was then halved to 0.6 ml/min and an additional 10 injection cycles were carried out (Figure 14). One of the most obvious differences between Figures 14a and 14b, is that Fractures 3 and 4 have developed the braided like patterns of precipitate previously only found in Fracture 5. This is a direct result of the reduced flow rate and hence fracture velocity enabling sedimentation of the smaller bacterial flocs to occur.

By dropping the flow rate and thus the flow velocity, some of the previously open channels in Fracture 5 have started to in-fill (compare Figure 3.7a and Figure 3.7b), which reduced the width of the remaining open channels while other channels became completely blocked with calcite. These results support the hypothesis that it is variations in local velocity that predominantly control the eventual spatial distribution of both the microbial flocs and the microbially induced calcite precipitates on the fracture surfaces. The bacteria act as calcite nucleation surfaces regardless of whether they are in suspension or after deposition onto the fracture surface.

(b) After 24 cycles at $Q = 1.2$ ml/min

(a) After 25 cycles at $Q = 1.2$ ml/min



Fracture	w (mm)	b (mm)	v_i (10^{-3} m/s)
1	2	0.3	33
2	5	0.3	13
3	10	0.3	7
4	20	0.3	3
5	30	0.3	2

Figure 3.6: Comparison of cycles 24 (a) and 25 (b) in experiment 4a. Stable channel formation has occurred.

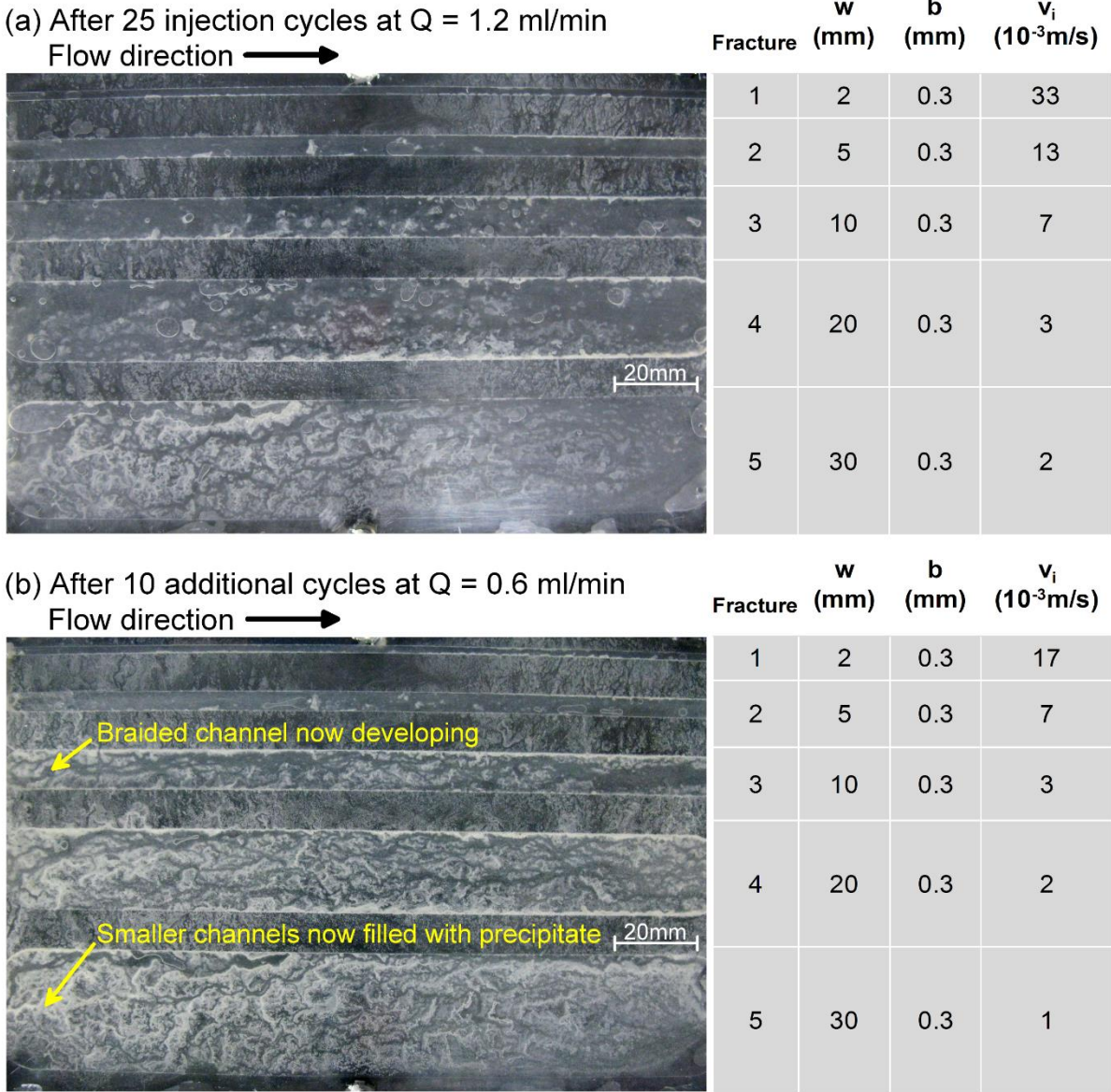


Figure 3.7: The effect of reducing velocity on fracture infilling. Braided channels have developed in three of the fractures and in fracture 5 (the slowest initial flow velocity) previously stable channels have become infilled.

3.6.4 SEM Analysis

To investigate the morphology of the calcite precipitate under different flow conditions within the channel network, specimens were sampled at three locations labelled A, B and C on Figure 3.5. On completion of Experiment 3, the flow-plate was opened and the calcite precipitate was sampled at locations proximal to an open channel but at varying distance from the injection port. Samples were taken by sticky carbon tabs (note minimal pressure was used to prevent any damage to the samples) for SEM analysis.

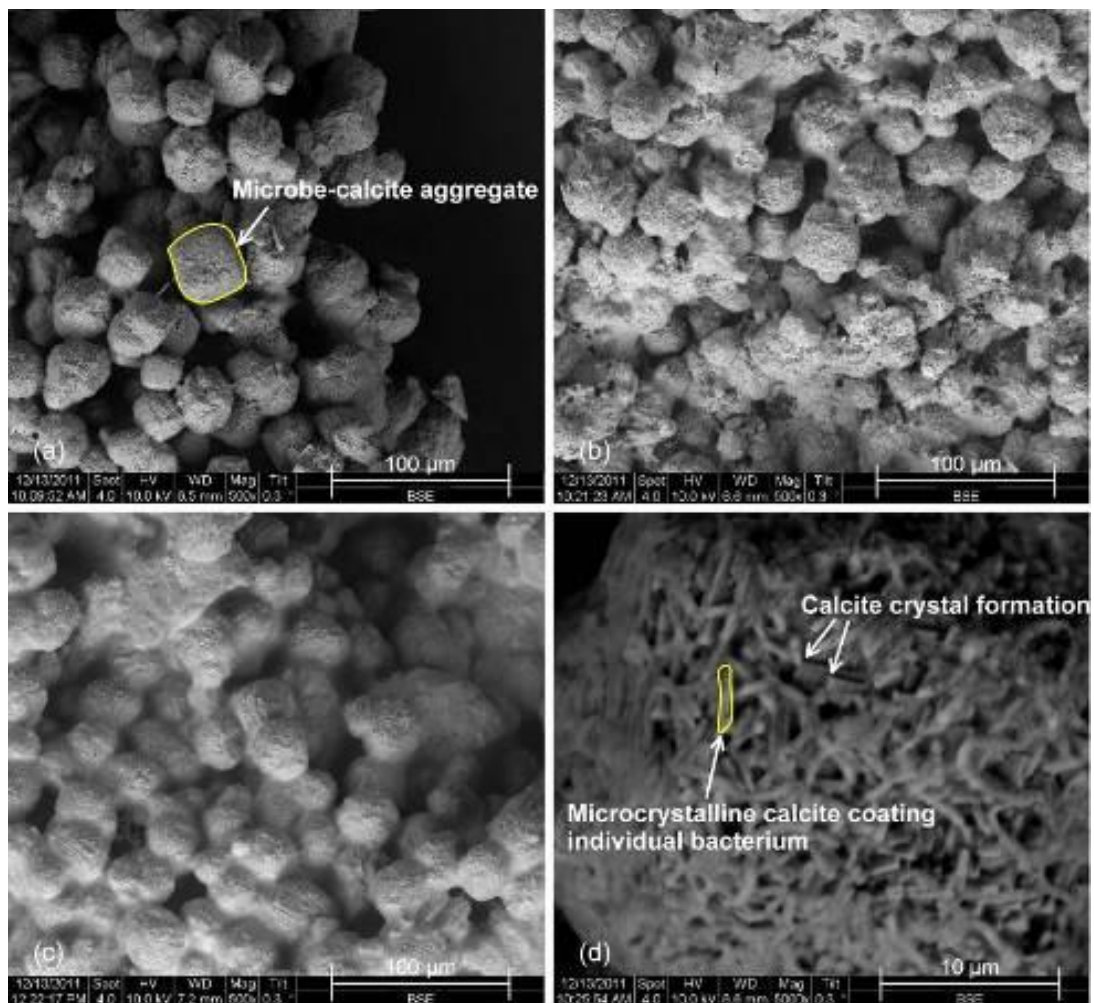


Figure 3.8: SEM images of calcite sampled from fracture 5 in experiment 3. Sample locations are shown in Figure 4a. (a) is proximal to an open channel (where the velocities are higher), (b) is set back slightly from an open channel and (c) is far from an open channel. The microbe-calcite aggregates appear to be highly uniform in size, around 30 - 40 µm. (d) is a higher magnification of Location B showing distinct crystal growth in the form of calcite plates (the beginning of rhombohedrons) are also visible in amongst the mass of calcite coated bacteria.

Figure 3.8 shows images taken from 3 different locations (locations shown in Figure 3.5). As distance increased from the main open channel, there are more bridges and linkages between the microbe-calcite aggregates. This is particularly evident in Figure 3.8c where many of the aggregates appear to be linking together to form a calcite matrix. This suggests that in locations with higher channel velocities (Location A); calcite growth was limited, whereas in the areas of lower channel velocities (Location C) additional crystal growth occurred in the form of bridges between microbe-calcite aggregates.

Figure 3.8d shows a single microbe-calcite aggregate from Location B, at higher magnification. It is evident that calcite has precipitated on the surface of the bacteria, and that calcite encrusted bacteria are rod like and several microns in length. This supports the theory that calcite precipitates nucleate on the surface of the bacterium (e.g., Schultze-Lam et al., 1996; Stocks-Fischer et al., 1999). Distinct crystal growth in the form of calcite plates (the beginning of rhombohedra's) are also visible in Figure 8d among the mass of calcite coated bacteria. The microbe-calcite aggregates appear to be highly uniform in size, around 30–40 μm . This morphology is distinctly different from the SEM images of predominantly rhombohedral calcite crystals reported by other researchers (e.g., Tobler et al., 2012), where experiments include periods of no flow.

3.7 Discussion

For microbially induced calcite precipitation it has been shown that fluid velocity is a key control on the pattern of precipitates observed on the fracture surfaces. These experiments have shown that as calcite precipitates, the fracture aperture distribution is altered and spatially variable patterns of velocity develop which in turn result in increased mass of precipitate in regions of low flow velocities. This greater mass of precipitate, acts to reduce the fracture aperture in those locations, further reinforcing the existence of the channel network. This feedback mechanism between velocity and microbially mediated precipitation, ultimately leads to the maintenance of a small number of self-organized channels that remain open within the fracture-fill if the treatment fluids are injected at a constant flow rate.

Many processes contribute to nucleation and growth of microbially mediated mineral precipitation within fractures. Evidence from the SEM images confirms that in these experiments calcite appears to be predominantly nucleated on the surface of the bacteria. The importance of the bacteria cells as nucleation surfaces is clear if we compare available fracture surface area to cell surface area within one experiment, for example: considering Fracture 8 (the widest fracture) in Flow-plate 1 has a surface area of 7,240 mm², assuming perfectly smooth surfaces. The microbial suspension, with an OD600 = 1.0 corresponds approximately to 3x10⁸ CFU/ml (using the relationship determined for *Sporosarcina pasteurii* by (Parks, 2009)). In Experiment 1 (Table 3.2) a total of 168ml of microbial suspension was injected into Fracture 8 (5 injections of 33.6ml), therefore potentially 5 x10¹⁰ cells could have acted as nucleation surfaces. Assuming *Sporosarcina pasteurii* has a diameter of 0.5µm and a length of 2.5µm (values selected by visual observation of SEM images) this corresponds to a total cell surface area of approximately 216,000mm². Hence, the bacteria clearly provide a much greater surface area for potential nucleation than the fracture surfaces.

Nucleation and growth of calcite occurs while the microbial cells or flocs are still in suspension (and/or after they have been deposited on the lower fracture surface). The experiments presented in this chapter indicate that sedimentation processes dominate the transport of the resulting microbial aggregates (and flocs) within the fractures, with the overwhelming majority of the calcite precipitates located on the lower fracture surface due to gravitational settling of microbe-calcite aggregates.

It has been demonstrated that the rate at which the aggregates settle is controlled by the diameter of the aggregate, with larger flocs settling faster and therefore closer to the injection point in Experiment 3 compared to Experiment 4a. Feedback occurs because once aggregates have settled on the initially smooth fracture surface; they act as obstacles to advective flow resulting in regions of low velocity and a potentially a chemical gradient immediately downstream. These downstream regions promote increased calcite precipitation and crystal growth, and as more and more aggregates settle out of suspension, preferential channels are formed within the fracture. Once the shear velocity at the fracture surfaces exceeds the settling velocity of an individual aggregate, aggregate deposition is inhibited and any deposited aggregates will become mobilized (van Rijn, 1984). The shear velocity required to

keep aggregates in suspension, and hence channels open, will drop with decreasing aggregate size.

Individual bacterial cells are transported to all fracture surfaces by Brownian diffusion (Yao et al., 1971). Their attachment is known to be dependent on the sum of the electrostatic forces acting between the bacterial cell and the surface, including electrical double-layer repulsion (or attraction) and van der Waals forces (DeNovio et al., 2004; Bradford et al., 2006).

Heterogeneous nucleation of calcite on individual cells may be one of the mechanisms contributing to the thin layer of fine calcite observed on all fracture surfaces. It could however also be as a result of heterogeneous nucleation of calcite on the fracture surfaces themselves. Once nucleation has occurred then calcite growth is enhanced at the fracture walls and particularly within the corners of the fractures, as these are low velocity regions, and have correspondingly low shear rates. This results in a very thin layer of calcite precipitating on all the fracture surfaces, alongside slightly greater precipitation in the channel corners. These fine precipitates were observed in the experiments during the early injection cycles and whitening of these fine precipitates did not appear to progress during the experiment. This is consistent with the observations of Holmqvist et al., (2005), who demonstrated that low shear rates (low flow velocities) enhance crystallization by improving transport to crystal surfaces whereas higher shear rates (higher flow velocities) considerably reduce growth rates and ultimately prevent crystal growth, due to particles being sheared off from the crystal surface and by preventing incorporation of particles in the fluid phase into the crystal structure.

Throughout all the artificial fracture experiments conducted, it was repeatedly observed that less calcite precipitation occurred during the first injection cycle than in subsequent cycles. One potential explanation for this is the initially pristine condition of the smooth-walled fracture, which may affect the sedimentation process. Once calcite precipitation is initialized, increased surface roughness enhances the boundary layer effect, increasing drag near the surface and reducing the advective velocity. This will promote floc settling. In addition, the activation energy required for nucleation is typically greater than for crystal growth (e.g. Rodriguez-Blanco et al., 2011), thus growth proceeds more rapidly once calcium carbonate nuclei have already formed in the system. There may also be an influence of the negative surface charge on the

pristine polycarbonate sheet, which may repel to some extent the deposition of individual bacteria and flocs and reduce attachment due to electrostatic forces. This is consistent with the results of Schultz et al. (2011) and Tobler et al. (2012) who also noted that calcite precipitation increases once calcite is present on a material surface.

An observation in the experiments carried out with the 1.0 OD600 microbial suspension, (characterized by a floc size), was that the mass of precipitation was always greater closest to the injection point and decreased along the length of the fracture. Several mechanisms combine to promote this. First, the larger floc sizes result in more rapid sedimentation, closer to the inlet. Second, once flocs have settled and calcite has precipitated, the fracture aperture is reduced resulting in a straining of the flocs and individual microbes. Finally, whilst early in the precipitation process straining occurs, once stable narrow channels have been formed the increased channel velocity was observed to exert sufficient force to break down the large flocs and further straining was inhibited.

Immobilization of particles closer to the inlet is predicted in classical filtration theory (CFT) models (e.g. Yao et al, 1971). However, more recently experimental studies (Tufenkji and Elimelech, 2004; Gargiulo et al., 2007) have demonstrated that microbial filtration is significantly greater closer to the inlet than that predicted by CFT due to the more complex nature of microbe-surface interactions. In addition, the greater mass of precipitates located closer to the injection point may also be due to depletion of the reactants' concentrations further downstream, as observed by Hilgers and Urai, (2002). However; this is thought to occur only when flow velocities are sufficiently small (Noll et al., 2006) and thus is unlikely to be the main reason for the variation observed with length along the fractures in this study.

By controlling the flow rate and ultimately velocity within the fracture, it is possible to achieve a better distribution of calcite precipitate. This is desirable from a grouting perspective. Remaining open channels are formed because of having a constant flow rate. In practice, it will be necessary to step down the flow rate in stages to improve the fill.

3.8 Conclusions

To seal fine aperture rock fractures, we have to engineer microbially induced calcite precipitation under different physical conditions. When using MICP for porous strata, the bacteria are trapped at pore throats (Tobler et al, 2012). Thus to improve distribution throughout the test section, the aim is to minimize bacterial flocking. However; when it is to be used within fractures the aim is to not only create bacterial flocs but to also control their size which can help to control their distribution.

This chapters shows that we can control the distribution of calcite by understanding that calcite precipitation begins with nucleation upon bacterial cell surfaces, and that transport of flocculated bacteria to fracture surfaces, is governed by sedimentation. The microbial flocs settle out at a velocity that is dependent on individual floc size and density. This settling velocity competes with the bed shear velocity, inhibiting deposition via entrainment. As precipitation progresses the flow becomes more channelled within the fracture, enhancing precipitation in regions of low flow and inhibiting it in the remaining high velocity channels.

4. IMPROVING THE UNIFORMITY OF MICP DISTRIBUTION IN ROCK FRACTURES

4.1 Introduction

Chapter 3 showed that during MICP in rock fractures which have flowing conditions, the bacterial cell surfaces act as nucleation sites for the precipitation of calcium carbonate. Due to a feedback mechanism between precipitation and fluid velocity, the transport of flocculated bacteria to fracture surfaces is inhibited by the bed shear velocity. As precipitation progressed the flow became more channelled within the fracture, enhancing calcium carbonate precipitation in regions of low flow and inhibiting it in the remaining high velocity channels. This resulted in a dendritic-like preferential flow producing a small number of self-organising channels that remained stable resulting in a fracture aperture that does not seal in the presence of constant flow rate conditions.

To use MICP for field scale grouting operations, it is important to develop an injection strategy that promotes a homogeneous distribution of calcium carbonate precipitate in fractures and avoid the development of preferential flow through higher porosity pathways. This chapter focuses on improving the distribution of microbially induced carbonate precipitation (MICP). As discussed in Chapter 2, most research into MICP has included the use of static periods to create a biofilm which helps to improve the distribution of calcium carbonate. However; under real conditions it is unlikely that there will be no flow within an open fracture in the phreatic zone. Thus, it is necessary to evenly distribute the bacteria within the fracture under flowing conditions

This chapter presents results from a series of batch experiments which were carried out to investigate how the concentration of nutrients impacts calcium carbonate precipitation. The batch test results were then used to inform the injection strategy used for the subsequent flow cell experiment. The flow cell experiment was carried out to evaluate the achievable hydraulic conductivity reduction and distribution of calcium carbonate precipitation resulting from the revised injection strategy developed in this chapter.

The research presented in this chapter has been published in *Water Resources Research*: El Minto, J., MacLachlan E., Mountassir G., and Lunn R.J. (2016). Rock fracture grouting with microbially induced carbonate precipitation: ROCK FRACTURE GROUTING WITH MICP. *Water Resources Research* Vol 52, No. 10 <http://dx.doi.org/10.1002/2013WR013578>).

4.2 Materials and Methods

4.2.1 Bacterial and Cementing Solutions

The components of a MICP injection fluid are a ureolytic bacterium (*Sporosarcina pasteurii*) a source of calcium (calcium chloride) and urea (an energy source for the bacteria). *Sporosarcina pasteurii* was initially grown (strain ATCC 11850), on Brain Heart Infusion (BHI) agar with urea (20g/L). A single colony was then transferred using aseptic technique to liquid BHI with urea (20g/L) and grown overnight at ~30°C. The bacteria were centrifuged from the growth medium (at 8,000 rpm for 8 mins) and diluted with sterile tap water until the required optical density (OD) was achieved. Optical density measurements were taken using a UV-VIS spectrophotometer at 600nm.

As per other researchers, to ensure that the cementing solution does not become a limiting factor a final concentration of 77.7 g/L CaCl₂ and 30 g/L of Urea is utilised within the cementing solution (Dejong, 2006; Whiffin, 2007, van Paassen et al, 2010; Cunningham et al, 2011; Tobler et al, 2012). Anhydrous CaCl₂ is dissolved in nano-pure water and then sterilized by autoclaving. Once cool, a sterile urea solution (sterilized by syringe filtering) is added to the sterile calcium chloride solution under aseptic conditions. This cementing solution has a final concentration of 0.7M CaCl₂ (77.7g/l), 0.5M urea (30g/l). pH was measured using a Mettler Toledo Seven Multi pH / Conductivity meter and adjusted to 6.5 with 40% Hydrochloric Acid.

Prior to each injection cycle, the flow-plates were initially saturated by flushing with water for a minimum of 30 min. A staged injection was then utilised where; the microbial suspension was immediately pumped into the flow-plate after mixing. To prevent precipitation within the tubing a 5ml pulse of sterile water was injected followed by an injection of the cementation solution (see Table 1) (Whiffin, 2007, Cunningham et al 2011; Tobler et al, 2012

4.2.2 Determination of cation concentrations

Ammonium and Calcium concentrations were determined using Ion Chromatographic (IC) analysis for both batch tests and flow cell experiments. Samples were taken on a scheduled basis, filtered and stored at -80°C to prevent degradation of any ammonium present until the end of the experiments. The samples were defrosted to room temperature and volumes of either 50µl (for ammonium cations) or 20µl (for calcium cations) of each sample was topped up to 10ml with nano-pure water. The different dilutions used for each cation is due to the high concentration of calcium ions that could be present which could exceed the sensitivity of the instrument.

4.2.3 Scanning Electron Microscopy

Samples from both the batch tests and the flow cell experiment were analyzed using a Hitachi SU-66000 Field Emission Scanning Electric Microscope (FE-SEM). Backscattered (secondary) electron imaging at 10kV was used to examine the precipitate morphology. Energy-dispersive X-ray microanalysis (INCA mapping) was also carried out for elemental analysis. Note minimal pressure was used to prevent any damage to the samples. Sampled precipitates were placed upon sticky carbon tape and were gold coated prior to imaging.

4.2.4 Laser Scanner

The dolerite base of the flow-plate before and after the experiment was scanned by a scanCONTROL 2700 Micro-Epsilon scanner allowing measurement of the initial dolerite surface elevation and the elevation post precipitation. This gives us the thickness and spatial variation of any precipitate. Each scan series covered a length of 110mm thus five scans of the dolerite base were taken to cover the 394mm length which gave sufficient overlap to allow alignment of the scans into a single image. The scanControl 2700 scanner produced datasets of the dolerite base topography with an x,y resolution of 200µm and an elevation (z) resolution of 5µm

4.3 Batch Tests

Three batch tests were set up in triplicate to examine how time, the ratio of bacteria to cementing solution affected both the rate and mass calcium carbonate produced (Table 4.1). Table 4.1 details the components of each batch test (which was performed in triplicate). Ammonium concentrations were measured over the first 48 hours then once again at the end at 96 hours. At the end of 96 hours, the batch tests were air-dried and samples taken for SEM analysis.

Table 4.1: Batch test setup, examining the impact of different ratios of bacterial volume to cementing solution volume and calcium carbonate morphology.

<i>Batch Test</i>	<i>Test Details (Final Concentration)</i>	<i>(Final OD600: Ratios)</i>	<i>Final OD600 Concentration</i>
1	10ml of 0.5 OD600 (diluted with sterile tap water) : 390ml of 0.7M CaCl ₂ /0.5MUrea	1:39	0.0125 : 0.6825/0.4875
2	100ml of 0.5 OD600 : 300ml of 0.7M CaCl ₂ /0.5MUrea	1:3	0.125 : 0.525/0.375
3	390ml of 0.5 OD600 (diluted with deionised water) : 390ml of 0.7M CaCl ₂ /0.5MUrea	1:1	0.25 : 0.35/0.25

4.3.1 Batch Test Results, which Informed Flow-plate Set-up

Figure 4.1 presents the amount of ammonium produced in batch tests using the different ratio of bacteria to cementing solution.

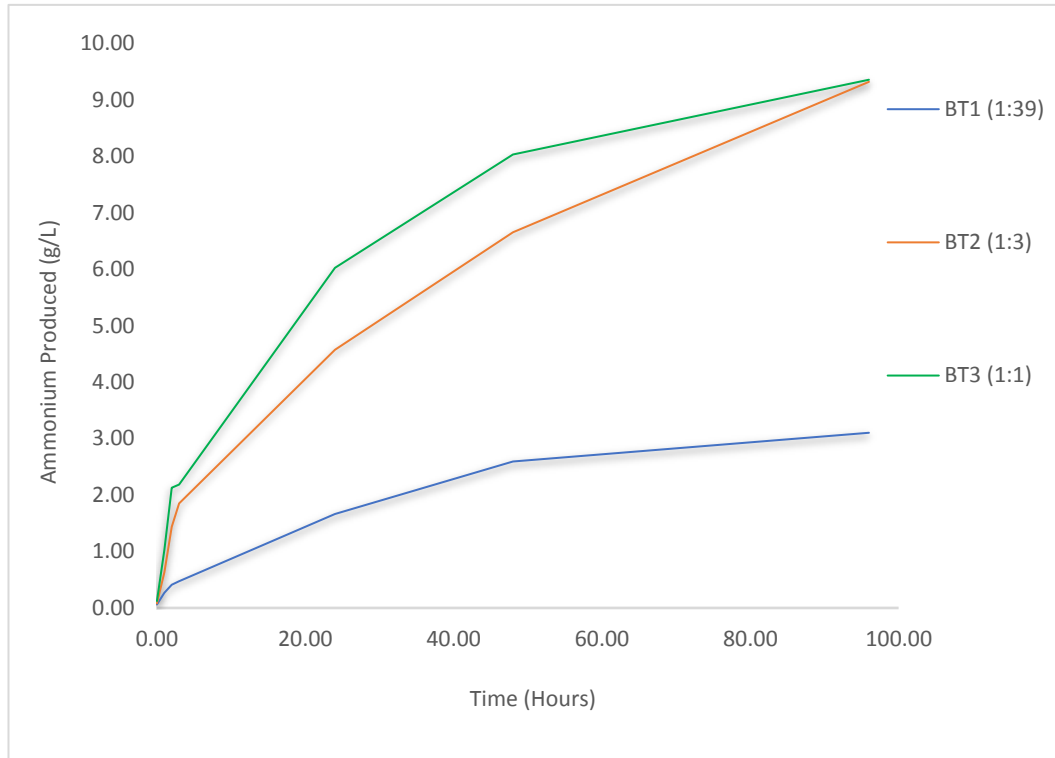


Figure 4.1: Plot of the average cumulate ammonium concentration produced by each triplicate batch test over 96 hours.

Figure 4.1 shows concentration of ammonium over time for each ratio as an average for each set of triplicates. Ammonium production is greater in the first 3 hours as indicated by the steep curves. After 3 hours, production slows and by 24 hours they have all reached approximately half of their total ammonium production in a quarter of the total test time (96 hours). As expected, the greater the volume of 1 OD_{600} bacteria the greater the rate and total amount of ammonium produced this is due to their being more of the enzyme urease thus more urea hydrolysis. It is also noticeable that ammonium production levels out. This could be due to nutrient limitation. For every 1 mole of urea hydrolysed, 2 moles of ammonium are produced, thus for the volume and concentration of cementing solution used the maximum amount of ammonium that can be produced is 32.79g/L of ammonium. The maximum amount of ammonium actually produced was 11.15g/L for the 1:1 ratio.

The results above would indicate that all the urea had not yet been utilized thus although nutrient limitation could still be occurring it was not due to the concentration or volume of cementing solution. Cuthbert et al (2012) whilst using static conditions found that encapsulation by calcium carbonate prevented the bacteria from accessing nutrients thus limiting ureolysis. If this encasement occurs too quickly then the bacteria are unable to access nutrients that are present.

This process of calcium carbonate encapsulation would explain why ammonium production falls off. The mechanism that causes this is related to the pH of the solutions. It is the rise in pH that triggers the precipitation of calcium carbonate, because there are equal volumes of bacteria in the 1:1 batch test, the pH rise is quicker and higher as shown in Figure 4.2 below, thus the bacteria become encapsulated within calcium carbonate quicker too. pH does not increase to the optimum for this bacterium (~Ph 9) due to the rapid precipitation of calcium carbonate which produces an excess of protons (Equation 7)..

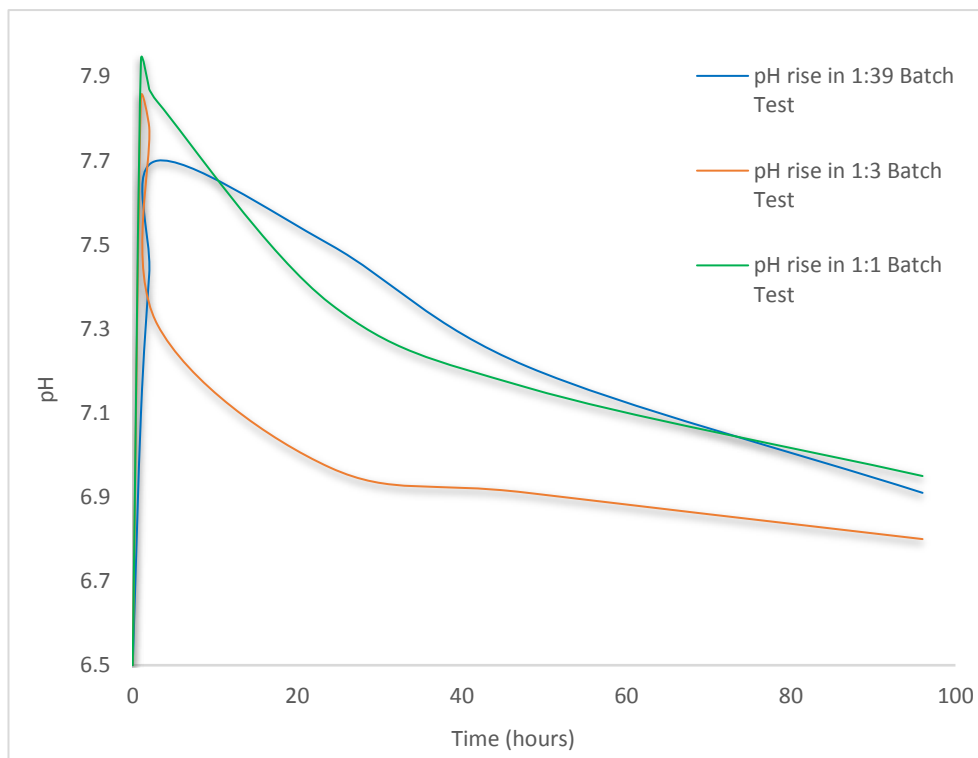


Figure 4.2: Plot of the pH produced by each triplicate batch test over 96 hours.

Growing the bacteria will be the costliest part of a microbial grout thus maximizing calcium carbonate production (and concomitantly ammonium production) per bacterial volume is essential. Figure 4.3 shows the efficiency of calcium carbonate production by plotting the amount of calcium carbonate produced against the bacterial and cementing solution volume as a percentage in grams per litre.

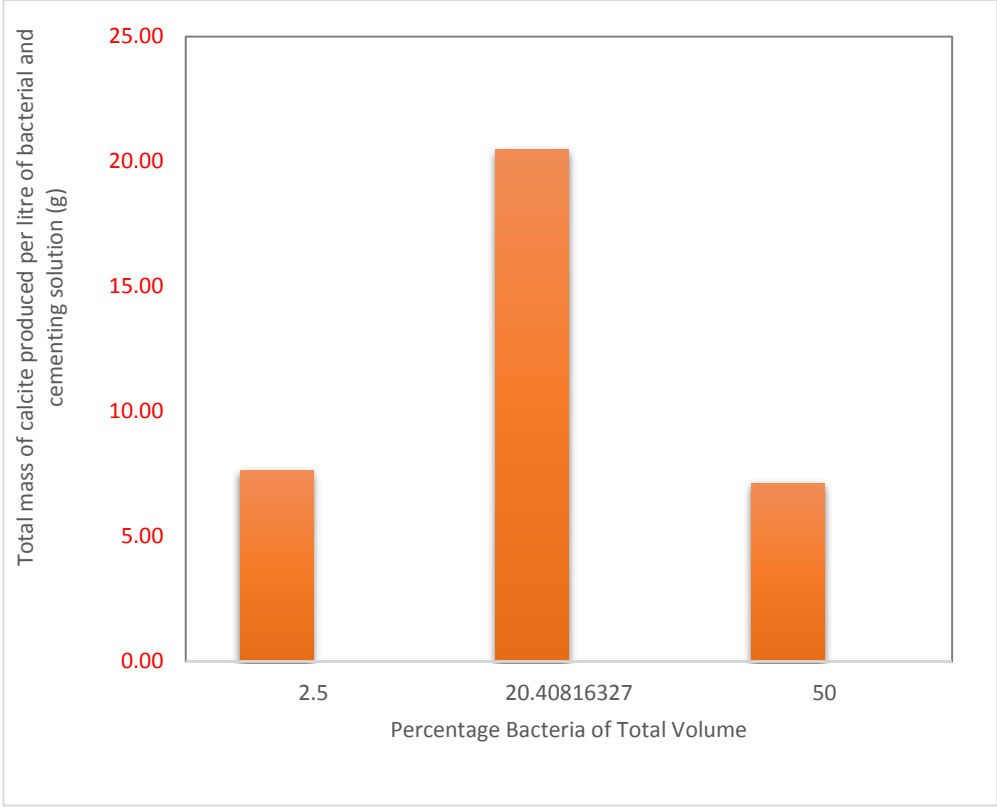


Figure 4.3: Plot of calcium carbonate mass produced against the percentage of bacteria of total volume.

Figure 4.3 clearly shows that a twenty percent bacterial of the total cementing volume gives the greatest amount of calcium carbonate precipitate.

4.4 Flow-plate Experiment

Following on from the batch tests which were used to identify potential ratios/combinations of bacteria and cementing solution, a new flow-plate was created which utilised 1 large simulated fracture, 10 times longer and 4 times wider than the largest channel of flow-plate 2 (as used in Chapter 3). A dolerite flow-plate base was chosen as igneous rocks will be the most typical rock type within a nuclear repository. Dolerite also contains less reactive minerals than a lot of rock types thus removing any impact on MICP that could occur due to dissolution of minerals.

4.4.1: Flow-plate 3 Setup

Flow-plate 3 was composed of a polycarbonate top plate and a dolerite base. Dolerite was chosen as a base due to its similarity to the high strength crystalline rocks that Finland and Sweden plan to use as the host rock of the geological waste repositories (SKB, 2014). A polycarbonate top plate enabled visual observation of microbially induced calcium carbonate precipitation on the fracture surfaces over time (Figure 4.4) without disturbing the precipitation.

Flow-plate 3 comprised a single fracture of length 394mm and width 118mm. The fracture was created by embedding a rubber seal into the polycarbonate top-plate. The base-plate and top-plate were attached to each other via ten bolts which when tightened compressed the rubber seals creating a small fracture aperture and a watertight seal. There were five injection ports equidistantly spaced along the short side of the flow-plate. Figure 4.4 shows a schematic of the experimental setup. Calcium carbonate precipitation within the fractures was monitored over time using a Canon Powershot G9 camera. The flow-plate was in the horizontal position with the digital camera mounted above, at a distance of 800 mm, allowing the full fracture to be photographed at a resolution of 12.1 megapixels. Reflection from the upper polycarbonate surface was minimized using a Hoya 58 mm circular polarizing filter. Digital photographs were taken every 120 seconds during each injection cycle.

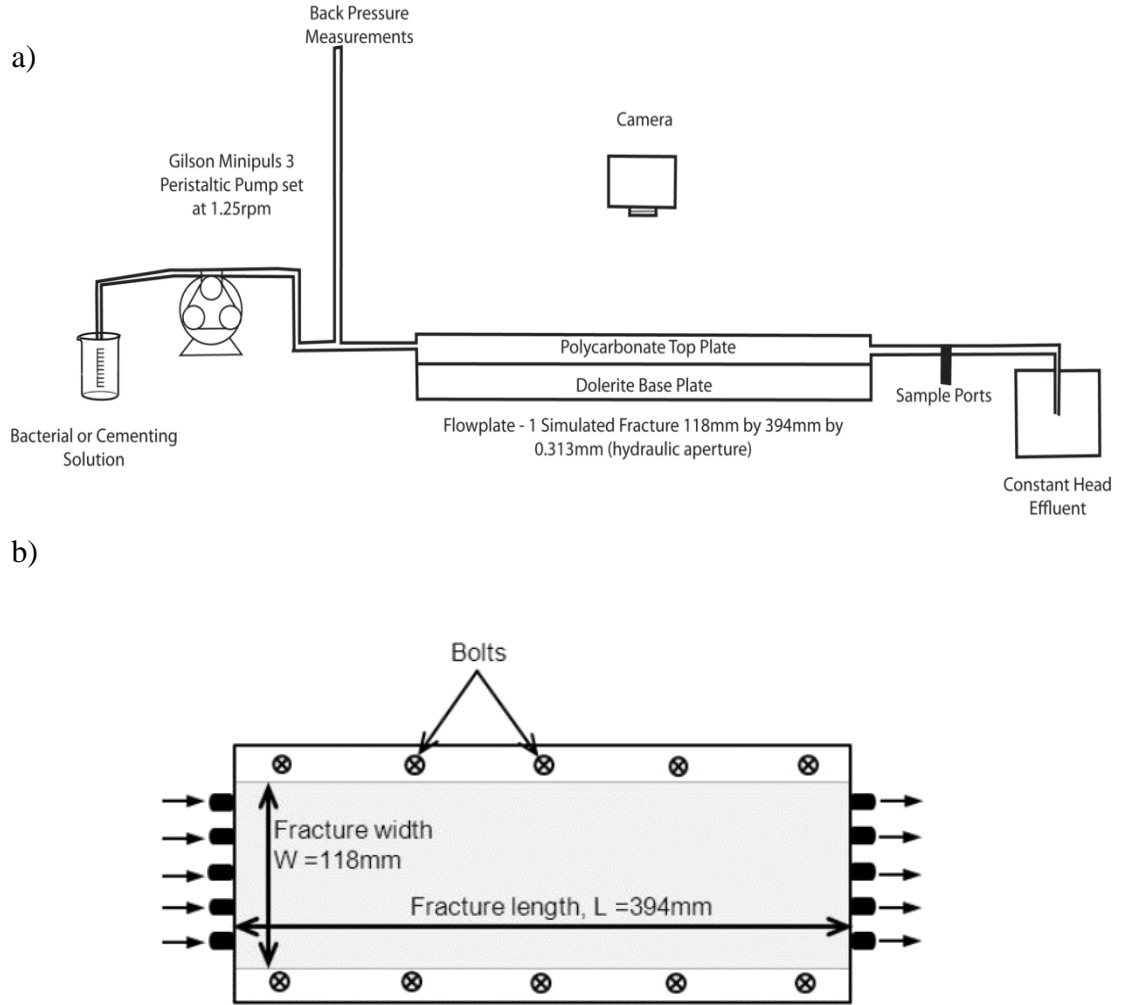


Figure 4.4: a) Schematic diagram of the flow-plate 3 set-up and b) plan view of the flow-plate.

4.4.2 Hydraulic aperture and fracture velocity

Due to the fracture aperture being created by the compression of rubber seals, and the dolerite surface being uneven, the aperture was unknown. Thus; the initial hydraulic aperture (Equation 15) was calculated from the equation below.

$$Q = \frac{W}{L} \frac{r g}{12 m} b_h^3 D h \quad (\text{Equation 15})$$

Q is the volumetric flow rate, W is the width of the fracture (m), L is the length of the fracture (m), ρ is the relative density (kg/m^3), g is the acceleration due to gravity (m/s^2),

μ is the dynamic viscosity of the fluid, Δh is the hydraulic head loss between the piezometers and the constant head boundary at the flow-plate outlet. The hydraulic aperture calculated using Equation 2 was $228\mu\text{m}$.

In order to verify the flow regime in the fracture prior to any calcium carbonate precipitation, fluorescein dye was injected at 1.56 ml/min and photographed every ten seconds. As can be seen from Figure 4.5, flow within the plate is laminar. The five distinct flow lines at the entrance of the plate (flow is from left to right) correspond to the five inlet ports of the fracture flow-plate (Figure 4.4 b).

$t=1\text{ minute (60 seconds)}$



$t=6\text{ minutes (360 seconds)}$



$t=9\text{ minutes (540 seconds)}$

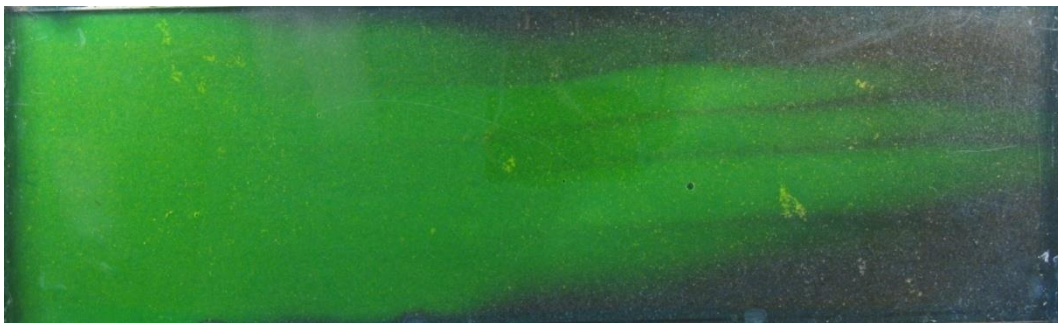


Figure 4.5: Photographs of flow paths (as indicated by the fluorescein dye) at 1, 6 and 9 minutes.

Due to aperture variation and boundary effects within the fracture, it is evident from Figure 4.5 that velocities were faster in the centre of the fracture than at the edges. Based on the breakthrough time determined from the image analysis, the velocity in the centre of the fracture is 0.55mm/s and the velocity at the edges of the plate is 0.2mm/s.

4.4.3 Injection Strategy for Flow-plate 3

In Chapter 3, it was evident that flocculation of the bacteria (by mixing with a solution of 50mM CaCl₂ as per van Paassen (2010)) contributed to sedimentation of the bacteria and straining which resulted in a reduction in the distance bacteria penetrated into the fractures, a build-up of precipitate at the inlet (as illustrated in Chapter 3). In order to improve the spatial distribution of calcium carbonate in fractures, in the following flow-through experiment (Flow-plate 3), no salts were added to the bacterial suspension in order to minimise bacterial floc size. Furthermore; a lower optical density of 0.5 OD₆₀₀ was used compared to 1.0 OD₆₀₀ in Chapter 3.

Preliminary experiments indicated that channelling did not occur to the same extent using this new bacterial suspension. The results shown in Figure 4.6 indicate that under flowing conditions with the flow velocities we have set up for the flow-plate 3 (0.2 mm/s to 0.55 mm/s), bacteria should stay within the fracture and precipitate should be more evenly distributed.

As discussed in Chapter 3, when bacteria, calcium chloride and urea are mixed together prior to injection, the injection ports clog very quickly. To promote precipitation with the fracture, a staged injection (Whiffin, 2007; Cunningham, 2011, Cuthbert et al, 2013) comprising of the cycles presented in Table 4.2 was followed.

Table 4.2: Injection strategy for the Flow-plate, consisting of a bacteria stage, a water pulse to clear the tubing, the cementing solution stage and final water pulse before the following cycle. The fracture volume is the total volume injected per stage divided by the initial fracture liquid volume. * after three hours, the effluent was recirculated to create a closed system that could be left running overnight without cessation of flow.

<i>Cycle Stage</i>	<i>Q (ml/min)</i>	<i>Time</i>	<i>Fracture Volumes (-)</i>	<i>Concentration</i>
Bacteria	1.56	3 hours	26	0.5 OD600
Water Pulse	1.56	5 minutes	0.74	-
Cementing Solution	1.56	21 hours *	186	0.7M urea, 0.5M CaCl ₂ , pH 6.5
Water Pulse	1.56	5 minutes	0.74	-

The above cycles were repeated until the back pressure had risen to >1400 mm (13.7 kPa). Nine cycles were completed in total.

4.5 Flow-plate 3 Results and Discussion

Figure 4.6 below shows images of calcium carbonate precipitation within the simulated fracture at the end of injection cycles 0 (a), 3 (b), 6 (c) and 9 (d). By the end of cycle 3, calcium carbonate is clearly visible throughout the entire fracture in a similar distribution to that of the Fluorescein dye rather than the ‘braided river’ pattern found in Chapter 3. By the end of Cycle 6 this pattern is beginning to fade and by the end of Cycle 9 the pattern has dissipated further allowing the full fracture to be coated with precipitate.

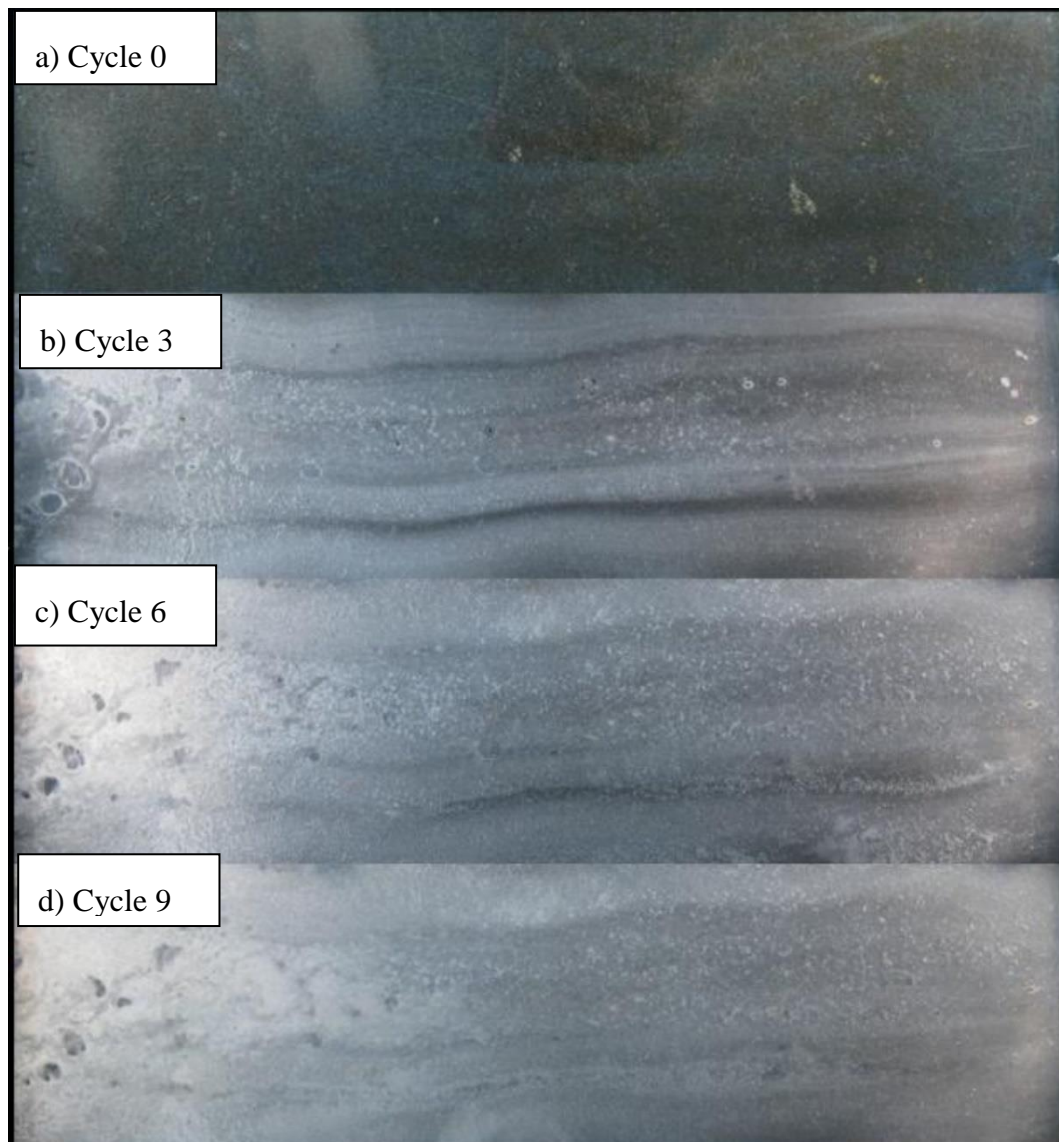


Figure 4.6: Photographs of the full flow-plate surface. Calcium carbonate can clearly be seen coating the entire fracture surface.

The change in the pattern of precipitate could be down to a decrease in injection rate. Up until cycle 6, the reduction in transmissivity due to precipitation within the fracture was low (as shown in Figure 4.7). By the end of Cycle 6, one of the injection ports had become blocked with precipitate thus reducing the inflow from 1.56ml/min to 1.25 ml/min. Then halfway through Cycle 8 (after the microbial injection stage) a second injection port became blocked with precipitate further reducing the flow to 0.94 ml/min for the rest of Cycle 8 and for Cycle 9.

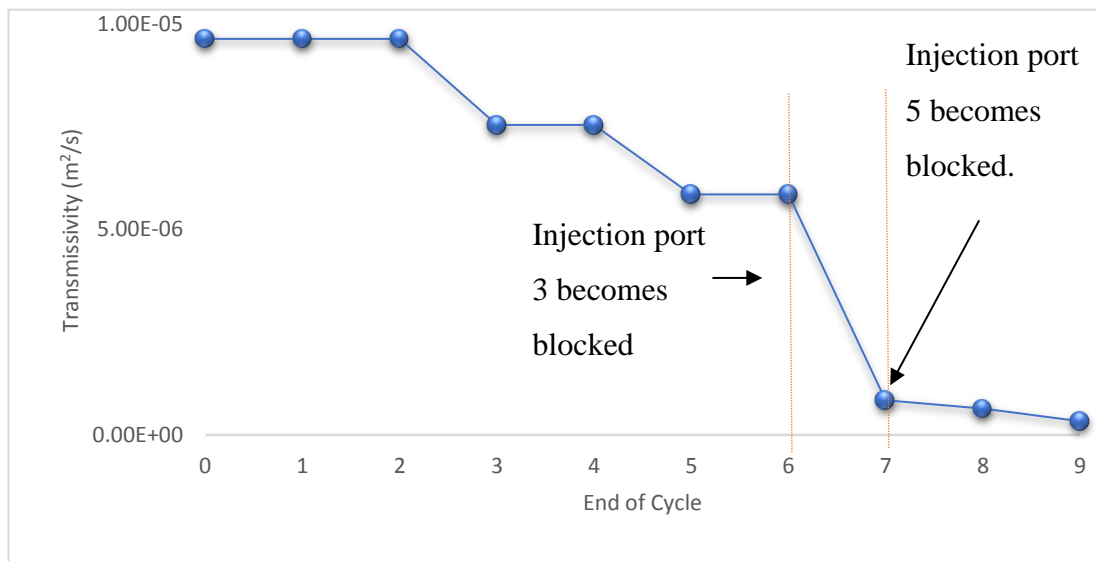


Figure 4.7: Plot of the changes in fracture transmissivity at the end of each cycle. Each cycle was composed of four stages (see Table 4.2) and each cycle lasted a day. Transmissivity was calculated from pressure drop readings taken across the low-plate at the end of each 2 hour injection cycle accounting for the reduction in flow-rate which occurred when injection ports became blocked (as indicated by the dashed red lines).

Figure 4.7 shows clearly that the largest reduction in transmissivity is found one full cycle after the reduction in flow rate when injection port 3 becomes blocked. Transmissivity reduces from $9.65 \times 10^{-5} \text{ m}^2/\text{s}$ before any precipitation to $3.72 \times 10^{-8} \text{ m}^2/\text{s}$ at the end of cycle 9. This is three orders of magnitude or a 99.6% reduction in the transmissivity of the fracture. This experiment was terminated after cycle 9 due to the pressure head exceeding the height of the piezometer tubing.

The final mass of calcium carbonate was determined via a weight change after acid digestion. The total mass of precipitate was 21.51g of which 18.85 grams was attached to the dolerite base of the flow-plate and 2.66 grams attached to the polycarbonate upper surface of the flow-plate. After samples were removed from the flow-plate, the attachment of the calcium carbonate was assessed by gently then

vigorously rinsing the dolerite plate with tap water. Gentle rinsing removed 1.66 grams of the 18.85 grams (8.8%). Vigorous rinsing did not remove any further calcium carbonate indicating a strong attachment to the dolerite base.

4.5.1 Chemical Analysis of Effluent

In Figure 4.8 below, the effluent breakthrough profile for the bacterial stage of each stage is plotted against the number of fracture volumes injected. The number of fracture volumes is used rather than time, due to the injection ports becoming blocked as the number of cycles progressed which resulted in fewer fracture volumes injected per hour. In Figure 4.8, the breakthrough curves show that there is a reduction in the peak OD600 after the first four cycles indicating that greater numbers of bacteria are being retained within the fracture. The peak OD600 also occurs earlier and their duration is shorter; suggesting that fluid velocity within the fracture is increasing as the cross-sectional area of the fracture reduces due to the precipitation of calcium carbonate within the fracture.

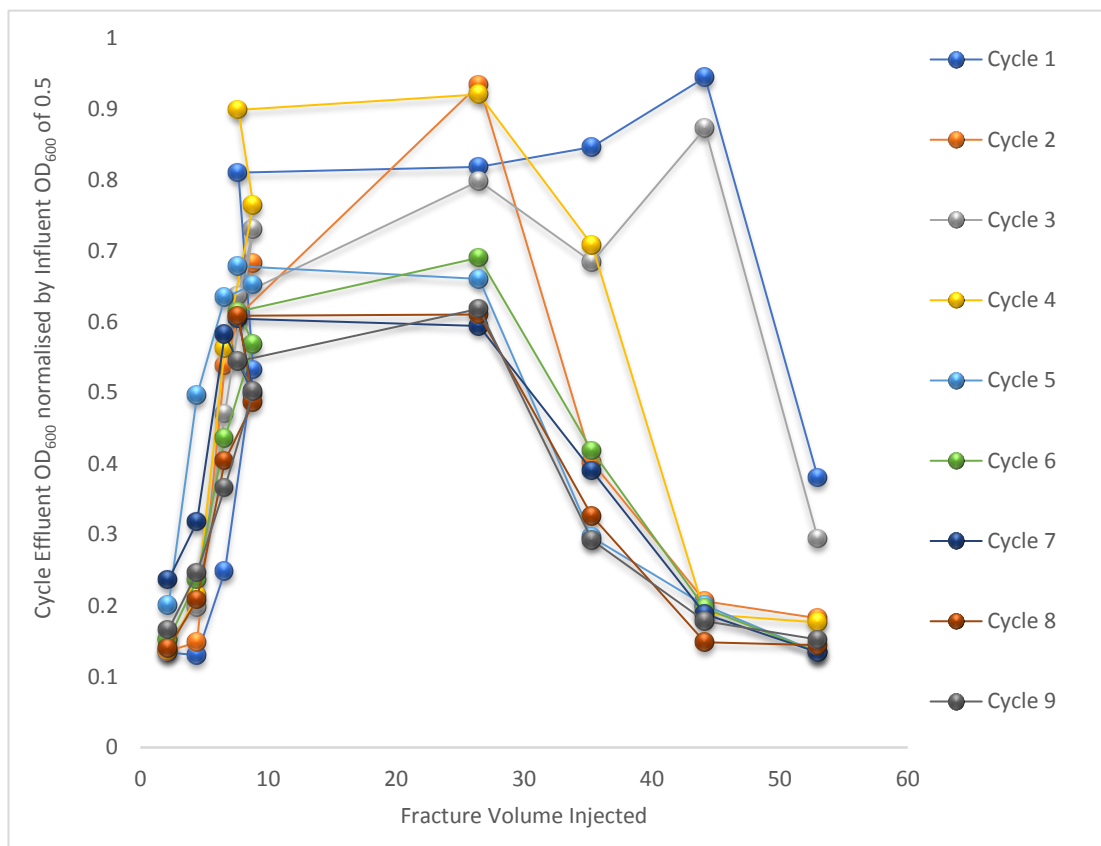


Figure 4.8: Bacterial breakthrough curves for each cycle throughout the three hours of bacterial injection per cycle. Bacterial concentration is normalised by the original concentration of 0.5 OD600 thus a value of 1 is equal to full breakthrough and no retention of bacteria within the fracture.

Figure 4.9 below, shows how the concentration of ammonium (a) and calcium (b) within the effluent, changes during the first three hours of the cementing stage of each cycle.

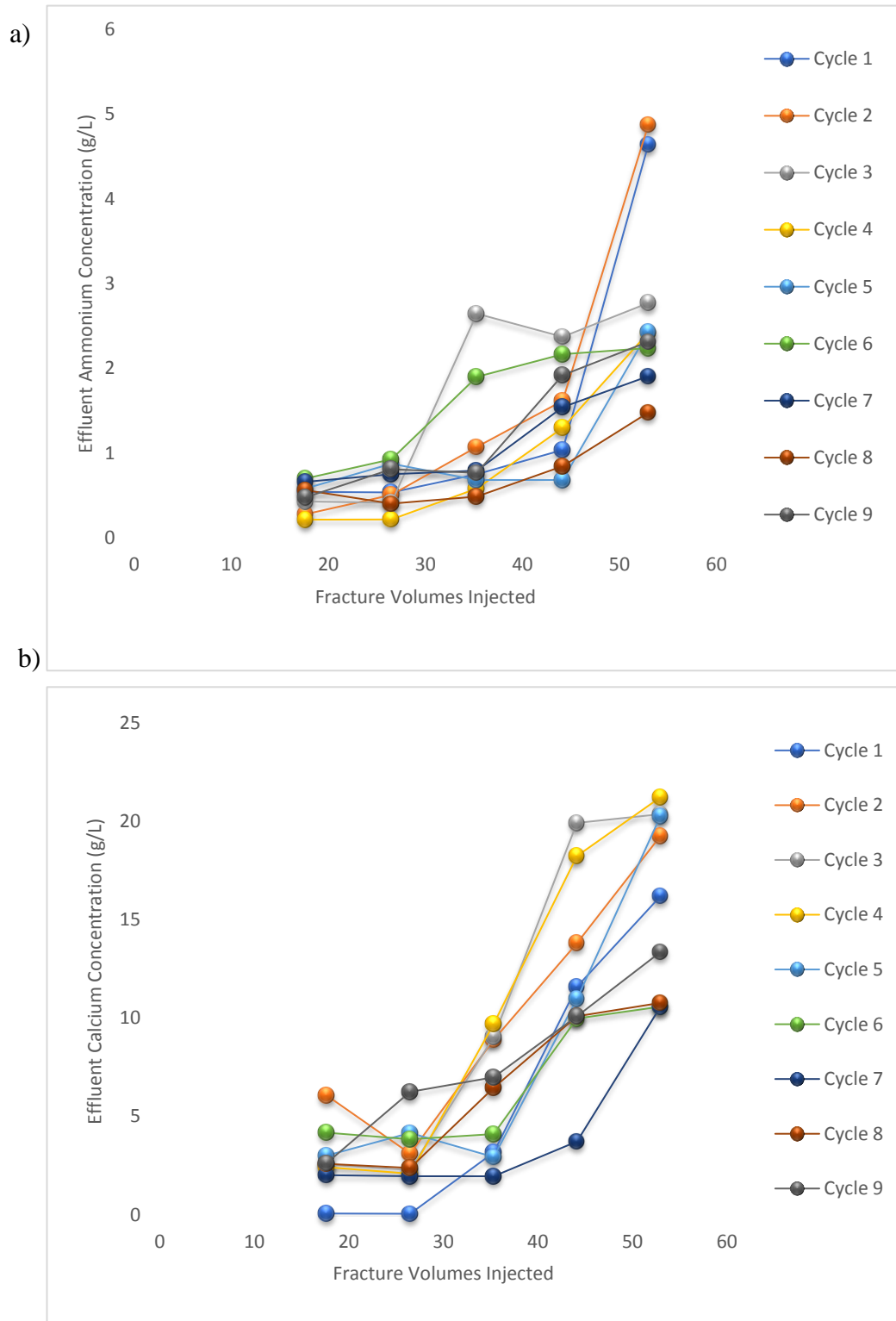


Figure 4.9: Changes in ammonium and calcium concentration of the flow-plate effluent. The x-axis measures fracture liquid volume injected which is n-based on the initial measurement of hydraulic aperture.

Figure 4.9 a) and b) show breakthrough curves for calcium and ammonium effluent concentrations over the first three hours (the non-recirculating portion) of the 21 hour cementing injection. The ammonium concentration increases as urea hydrolysis progresses. Although the calcium concentration also increases it never reaches the influent concentration of 28.05 g/l, showing that calcium is being retained within the fracture. To estimate the final percentage of urea that is hydrolysed and the percentage of calcium that has precipitated out, a final measurement of calcium and ammonium concentration in the effluent at the end of each cycle (after 18 hours of cementing fluid recirculation) was made. These results are presented in Table 4.3.

Table 4.3: urea hydrolysis and calcium utilisation calculated from the reduction in re-circulated cementing fluid at the end of each cycle. urea hydrolysis calculated from the ammonium produced over the cycle divided by the maximum possible amount of ammonium that could be produced had all of the urea present had been hydrolysed.

Cycle	<i>Recirculated Cementing Solution:</i>	
	Percentage Calcium Precipitated	Percentage Urea Hydrolysed
1	3%	26%
2	4%	27%
3	23%	15%
4	22%	13%
5	25%	13%
6	54%	12%
7	51%	11%
8	51%	8%
9	52%	11%

During the first two cycles, calcium utilisation is low at three and four percent. This is consistent with the low retention of bacteria as found in Figure 4.8 and the clean fracture surface, both of which are potential nucleation sites for the precipitation of calcium carbonate (El Mountassir et al, 2014). Once calcium carbonate has begun to precipitate out onto the fracture surface, the percentage of calcium utilised over cycles three to five increases. After cycle 5 when there is reduction in flow rate calcium utilisation increases further to around 50%. Comparing

calcium utilisation to urea hydrolysis during the recirculating portion of each cycle, it can be seen that the increase in calcium utilisation is not due to an increase in urea hydrolysis. It is likely to be due to crystal growth of precipitated within the fracture plate in addition to precipitation.

4.5.2 Fracture Topography

To examine the distribution of calcium carbonate within the flow-plate, laser scans using were taken before and after precipitation. Although it would have been preferable to scan the plate as a whole entity, due to the size of the flow-plate it was necessary to take 5 scans of the flow-plate. These scans show the changes in topography created by precipitation and can be used to estimate the thickness of the precipitate along the fracture.

Laser scans before precipitation showed that the surface elevation was normally distributed with a mean of zero and a standard deviation of 57 μm and a range of 235 μm over 2.5 standard deviations (99% of measurements). After calcium carbonate precipitation, the range in surface elevation was 1440 mm, greatly exceeding the calculated hydraulic aperture of 228 μm , indicating that calcium carbonate precipitation and crystal growth caused bowing of the upper polycarbonate plate.

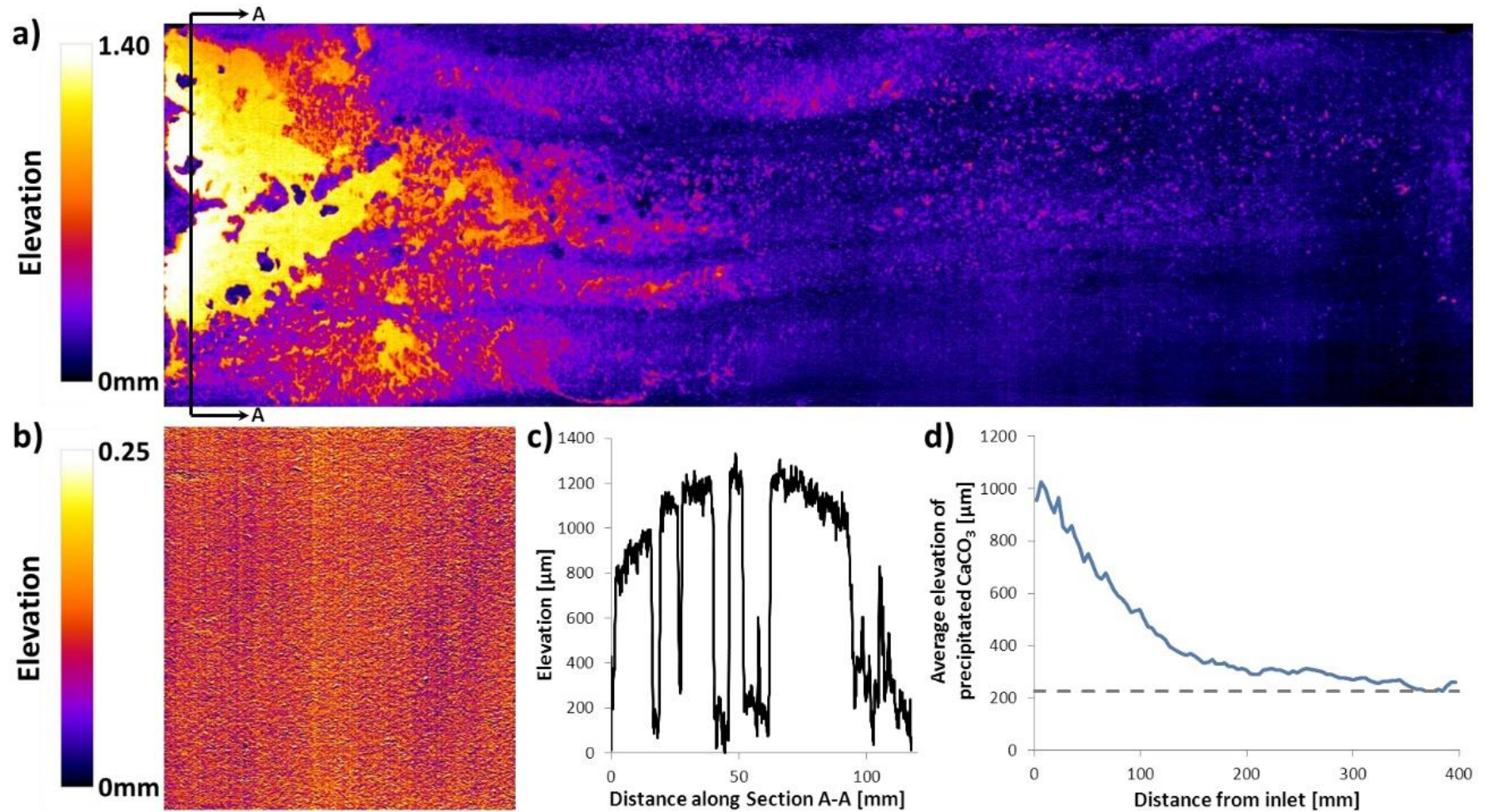


Figure 4.10: a) change in elevation due to calcium carbonate precipitation relative to the dolerite base, b) variation in the elevation of the clean dolerite base, c) variation in the elevation of calcium carbonate precipitate along the line A-A, and d) average elevation of calcium calcium carbonate precipitate measured of 4mm thick bands from inlet to outlet.

Laser scans of the polycarbonate upper surface could not be made as the reflection from, and the transmission through the clear polycarbonate disrupted laser measurement. Due to this, the spatial distribution of the precipitate attached to the upper polycarbonate surface could not be measured (12% of the total calcium carbonate precipitated). However, a visual inspection showed the presence of an even coating of precipitate over the entire polycarbonate surface.

Figure 4.10a shows laser scans of the distribution of calcium carbonate precipitate at the end of the experiment. Figure 4.10b shows laser scans of the base plate before the experiment. A dramatic change in topography is seen both across the five injection ports and throughout the length of the fracture. Close to the injection ports, the precipitate has completely filled the fracture. After removal of the top plate, the precipitate was found to be better attached to the base plate than the top plate and at points was smooth and flat.

A transverse line (A – A) across the fracture (Figure 4.10c), shows a variable topographic height within the dolerite base plate between 0.8 and 1.4mm and a domed shape to the precipitate created by increasing pressure and/or crystal growth deforming the semi-flexible polycarbonate. Figure 4.10d, shows the distribution of calcium carbonate from inlet to outlet. The distribution was calculated by dividing the image into a series of 4mm long bands and averaged over the fracture width. The resulting graph shows that there is greater precipitation within the first 150mm of the fracture after-which there is more constant distribution.

4.5.3 SEM Analysis

Samples for SEM analysis were taken from the flow-plate with as little force as possible to prevent any damage to the samples, placed upon sticky carbon tape and coated with gold. Figure 4.11 shows the base-plate with precipitate after removal of the top plate, the locations where the samples for SEM analysis were taken and the SEM images of the samples taken from a thick patch and an even patch of precipitate.

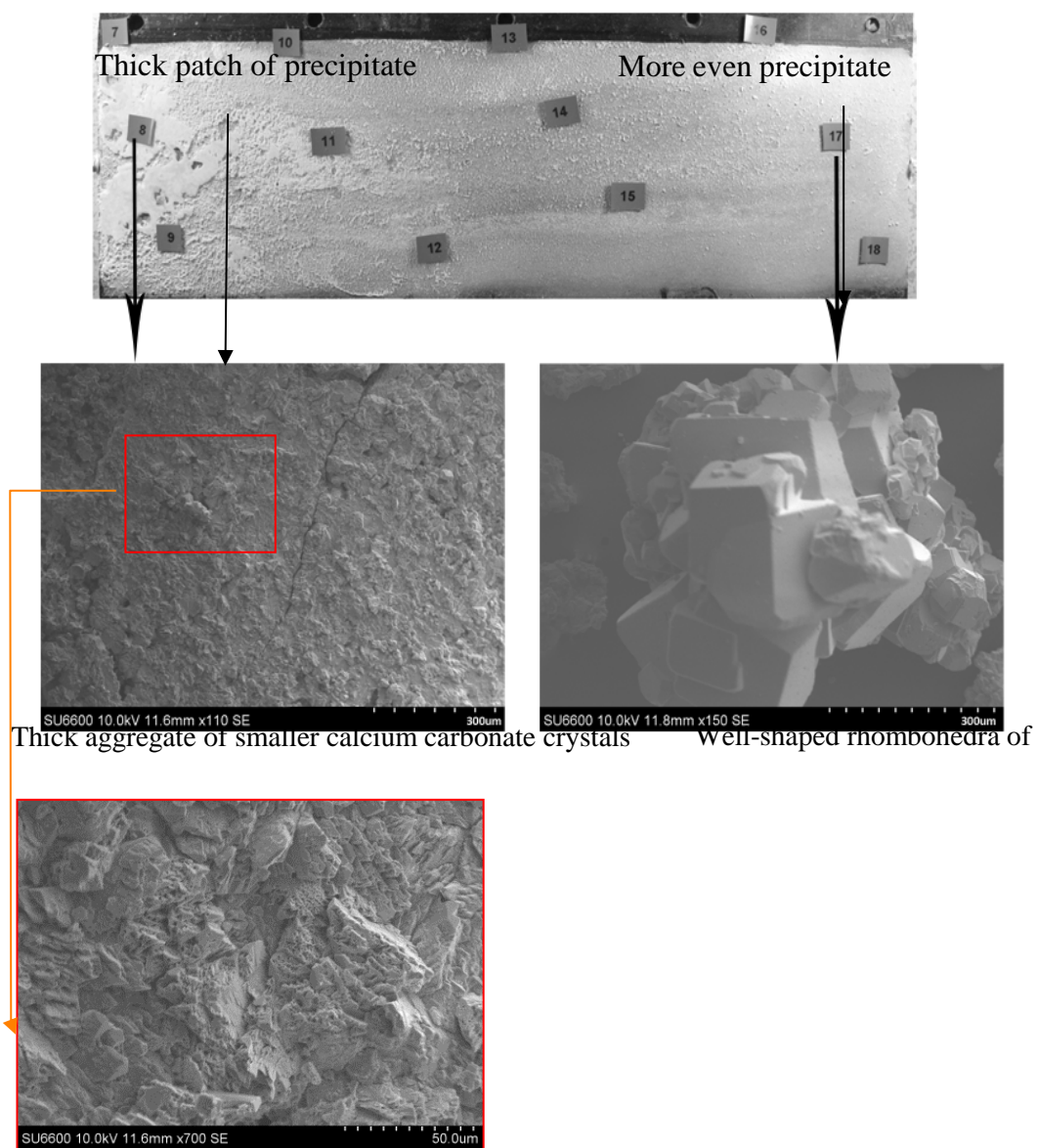


Figure 4.11: SEM analysis of samples taken from base plate in the middle of the precipitate at a point close to the inlet (location 8) where there is a large thick patch of precipitate, and a point close to the outlet (location 17) where the precipitate is smoother. The red bordered image is a close-up view of location 8.

The SEM images presented in Figure 4.11 show that there is a clear difference in the morphology of the precipitate found at the inlet and at the outlet. Solid mats of calcite were more common close to the inlet whilst distinct well-shaped rhombohedral calcite crystals were more common at the outlet. Cuthbert et al (2012) proposed that these differences in morphology is due to the rate of crystal growth, that higher numbers of bacteria produce higher concentrations of ammonium (and concomitant rise in pH) which in turn leads to high rates of nucleation which consequently reduces the rate of crystal growth thus crystal size.

4.5.4 Discussion and Conclusion

The batch tests showed that higher concentrations of bacteria produced more calcium carbonate, but that lower concentrations resulted in more efficient use of the injection fluids. Bacterial ureolysis continued for 96 hours in most batch tests; however, 50% of the urea hydrolysis occurred during the first 24 hours. From these results, to make the most efficient use of the bacteria, the cementing solution should be injected for around 24 hours per bacterial cycle. The choice of injection solution concentrations and ratios will depend upon the relative costs of bacterial and cementing solution as well as the cost of labour and plant. For example; it may be more economical to precipitate calcium carbonate as quickly as possible instead of making the most efficient use of the bacteria and cementing solutions.

In the fracture experiment, transmissivity was reduced by 99.6%, with both bacterial retention and calcium consumption increasing with each subsequent cycle. The precipitated calcium carbonate was attached to both the top and the bottom of the fracture and bridged the gap between the two fracture surfaces potentially increasing the strength of an MICP sealed rock mass. Due to the flexible nature of the upper polycarbonate plate, bowing of the upper plate occurred due to crystal growth. Within a natural fracture bowing would not occur and an even greater reduction in transmissivity would be possible.

Overhead photographs of the flow-plate (Figure 4.6) show that initially the precipitation/distribution of calcium carbonate followed the flow paths made visible by the Cycle 0 tracer. Over the 9 cycles, these flow paths changed resulting in a more even distribution of calcium carbonate as shown in Figures 4.10 and 4.11. Despite the

constantly flowing conditions, the formation of stable open channels observed by El Mountassir et al (2014) in a similar flow-plate experiment were absent.

In this study, bacteria were not flocculated prior to injection (in contrast to Chapter 3) and the fracture average fluid velocity and the average fluid velocity was considerably lower in this experiment (0.55mm/s vs 2 to 33 mm/s), thus bacterial attachment to the fracture surface was not inhibited. Similarly to other researchers (Ferris et al, 1992; Whiffin et al, 2007; van Passen, 2010; Cunningham et al, 2011) a gradient in precipitation was found. Although further research is required to improve the distribution, the more even distribution further down the flow-plate (away from the inlet) in this experiment shows that MICP has the potential to uniformly seal rock fractures. Furthermore, the reported inhibition of bacterial attachment to the rock surface when velocities are high (as shown in Chapter 3) raises the possibility that fluid velocity can be used as a method of controlling where within in a fracture calcium carbonate is initially precipitated thus could be used to minimize bacterial attachment close to the injection point.

It took 9 cycles thus 9 days to seal the flow-plate. By the introduction of a filler that can also act as a nucleation site for calcium carbonate precipitation may be a way of reducing the time it takes for the sealing of a fracture. One such potential filler is colloidal silica. Ions produced by the bacteria could be used to gel Colloidal Silica and at the same time, the colloidal silica could act as a potential nucleation surface due to it also have a negative surface charge. The nanometre size colloidal silica could allow for a better penetration, distribution and enhanced calcium carbonate precipitation, this is investigated in Chapter 5. The following chapter presents a review of colloidal silica and its uses in grouting contexts to date.

5. THE DEVELOPMENT OF A COMBINED BACTERIAL CALCITE AND SILICA GROUT.

5

5.1 Introduction to Colloidal Silica Grout

Over the last two decades, the interest in colloidal silica as a new chemical grout has grown due to its durability, chemical and biological inertness (Moridis, 1993). Colloidal silica is a mono-disperse stable suspension of amorphous silica with a particle size that can range from 5 – 100 nm. All colloids have a large surface area, this along with the low viscosity of colloidal silica, means it has a similar wetting ability to that of water. An authoritative work on silica chemistry was produced by Iler (1979), describing the theory regarding colloid silica and its gel states. Stable suspensions of colloidal silica are generally of pH between 8 and 10. Within this range the silica particles are ionised thus have negatively charged surfaces.

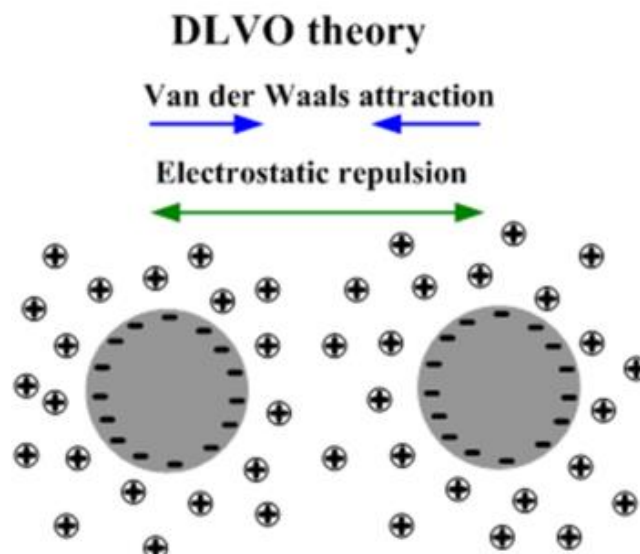


Figure 5.1: Van der Waals attraction is the results of forces between molecules in each colloidal particle. One molecule of the colloid has a van der Waals attraction to each molecule in the other colloid. In a regime where there is repulsion, there is an energy preventing further attraction. We can decrease the energy barrier by increasing the ionic strength or changing the pH.

The interaction of the charged surfaces of colloidal silica particles can be described according to DVLO theory (Derjaguin and Landau, 1941; Verwey and Overbeek 1948) Figure 5.3). Electro-static double-layer repulsion between particles due to surface charges is countered by attractive Van der Waals forces, creating an overall stable suspension. When the ionic strength of the liquid is increased by adding

a salt such as sodium chloride, calcium chloride or ammonium chloride; the inter-particle repulsive forces will decrease and Van der Waals attractive forces will dominate. The silica particles will aggregate, with siloxane (Si-O-Si) bonds forming between silica particles, this destabilises the silica suspension leading to gelation (Figure 5.4). When gelation begins, a ‘skeleton’ of silica particles form and water present is trapped inside the skeleton. As further formation of siloxane bonds occurs a high porosity gel is formed, that has a very low hydraulic permeability.

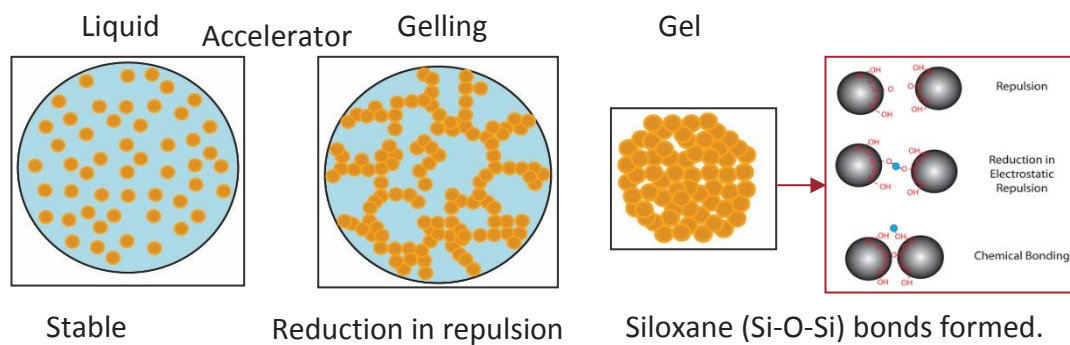


Figure 5.2: Cartoon of how colloidal silica can be gelled using counter-ions.

The gel time of colloidal silica is dependent upon the silica solid content, the size or surface area of the silica particles, the pH, the charge on the particles, and the salt concentration. Gel time increases as the silica solids content is decreased, as the size of the silica particles increases (thus surface area decreases), and as the ionic strength (salt concentration) decreases. pH has an interesting effect upon gel time where the minimum gel times tend to occur between pH 5 and 6. Substantially higher gel times can be achieved if the pH is either above or below this range (Iller, 1979; Gallagher and Mitchell, 2002).

5.2 Colloidal Silica as a Grout for Imparting Strength

Persoff et al, (1998) found that the unconfined compressive strength of treated samples after seven days increased with increasing concentration of colloidal silica as shown in Figure 5.4.

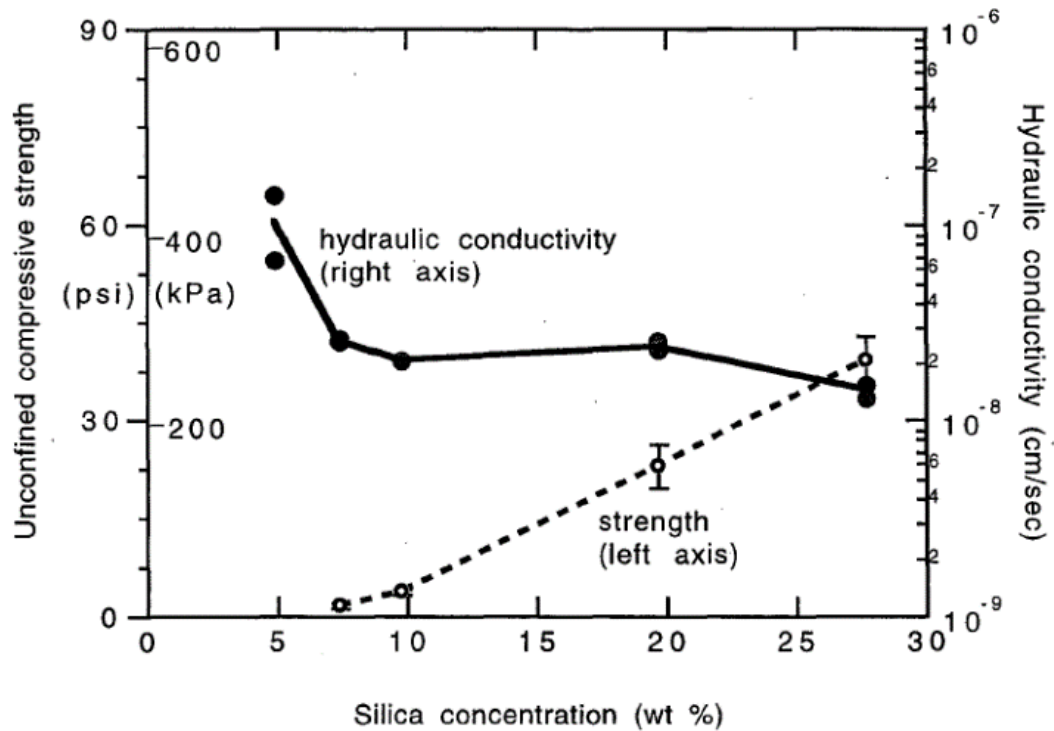
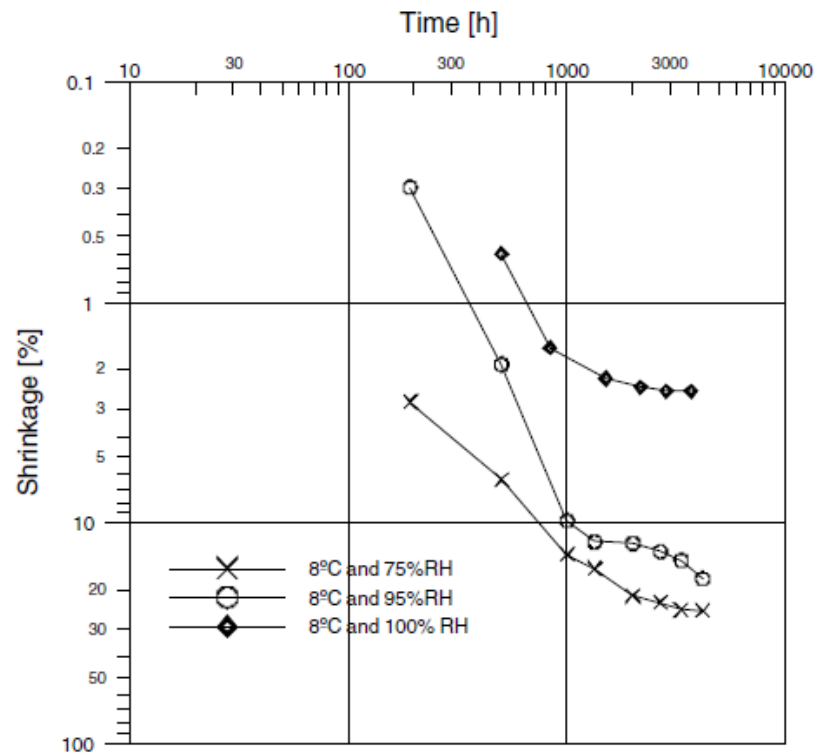


Figure 5.3: As the % weight colloidal silica increase from 5% to 27.5% there is a linear increase in the unconfined compressive strength (Persoff et al, 1998).

The strength continued to increase in samples immersed in water over the course of a year. A sample with 20 % colloidal silica had strength of about 670 kPa at 349 days.

Axelsson (2006) went further and examined how strength changed with humidity rather than looking at immersed samples only (Figure 5.5). He found that the increase in strength was directly related to the relative humidity of the environment that the sample was placed in and that the relative humidity directly affected syneresis and associated shrinkage of the sample.

5.4 a)



5.4b)

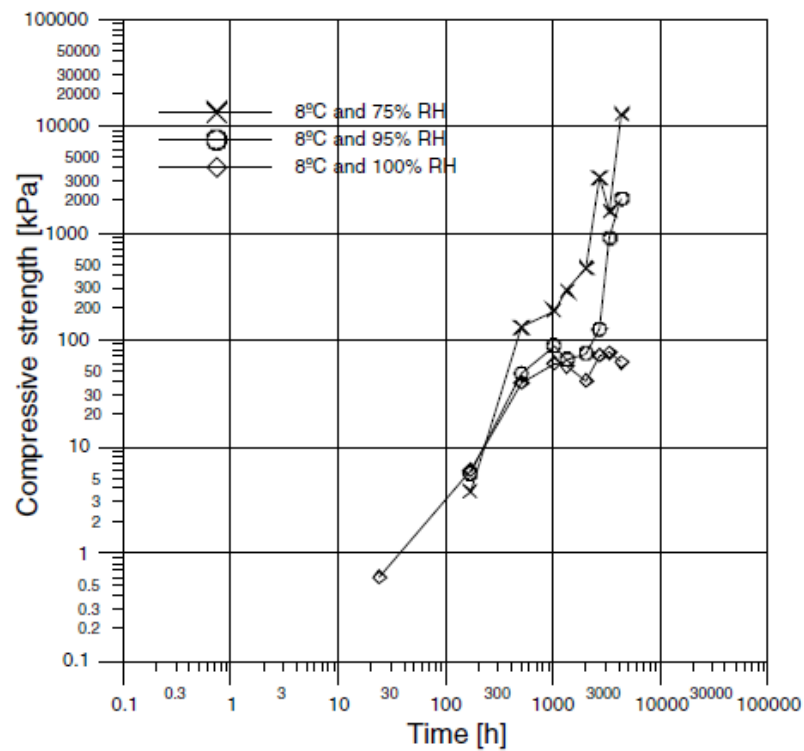


Figure 5.4: shows the change in volume (shrinkage) over six months, When the colloidal silica is in a 100% relative humidity the shrinkage is the smallest whilst the lowest humidity (75%) had the highest shrinkage. In Figure 5.5b) with a relative humidity of 75%, the rate in the strength increase of strength occurs sooner than in the 95% relative humidity; specimens kept at 100% relative humidity there was very little change in the strength.

The lowest humidity resulted in the fastest increase in strength, but there was a reduction in volume due to the expulsion of water. This is due to a continued increase in the building of siloxane bonds. This may be of concern when grouting within unsaturated zones as open pathways for flow may develop, however it would also be possible to periodically grout the area repeatedly reducing the aperture of these pathways.

Butron et al (2008) examined the mechanical behaviour of colloidal silica as a rock grout. A series of 8:1 ratio of (35% weight colloidal silica and 0.029M sodium chloride solution) mixes were gelled in plastic moulds, stored in temperatures between 8 and 60°C, and either immersed in deionised water or kept at a relative humidity of 100%, 95% or 75%. These samples were then tested over five months for shear strength. Within a day after gelling, the shear strength of all the samples reached 10 kPa. The shear strength of the samples continues to increase with time at a rate that was dependent upon its storage environment. After 47 days, samples stored at 20°C and at a relative humidity of either 100% or 75% showed the greatest strength increase of >60kPa, whilst samples immersed in deionised water regardless of temperature reached a strength of 20kPa. Odometer testing of immersed samples showed that when there is confinement of the grouts, colloidal silica behaves ductilely and thus would be able to withstand loading and unloading cycles.

The strength of a colloidal silica grout in a saturated zone may seem low compared to chemical grouts such as sodium silicate which has a minimum strength of 248 kPa after six months (Karol, 1983) and cementitious grouts such as Rheocem 650 (a Portland cement) whose strength is 1.0 MPa after twenty-eight days (Garshol, 2003). However; this grout has other benefits such as a low viscosity, a controllable gel time and a lack of toxicity that mean it may be preferable for use in some environments, such as for the sealing of tunnels or the sealing of small aperture fractures at a geological disposal of nuclear waste, where a reduction in hydraulic conductivity at a low pH is a requirement.

Colloidal silica has been proposed as a passive remediation grout to reduce the liquefaction potential of non-cohesive soils in active earthquake zones through permeation grouting. (Gallagher and Mitchell, 2002). Loose sands were packed into either water, or a 10% weight colloidal silica solution, or a 20% weight colloidal silica solution and allowed to cure before conducting cyclic triaxial tests. It was found that

untreated sands deformed very quickly, whilst colloidal silica grouted samples did not. The higher the percentage colloidal silica used the greater the resistance to deformation.

Gallagher and Finsterle (2004) used a box model to investigate how well colloidal silica penetrated sand. 1.5 pore volumes of a 5% by weight colloidal silica solution was permeated into a box model through 5 injection wells over 10 hours. After this the grouted sand was cured for two weeks before being dissected and tested for unconfined compressive strength (UCS), the maximum strength reported was 61 kPa. This may seem quite weak when compared to other grouts, but it is sufficient to reduce liquefaction potential.

Gallagher et al (2007), followed up on previous work by using centrifuge in-flight shaking to investigate the effect of colloidal silica treatment on the liquefaction and deformation resistance of loose sand. Loose sand was saturated with colloidal silica grout and subjected to two shaking events. The treated soil did not liquefy during either shaking event. Gallagher and Lin (2010) then evaluated colloidal silica transport mechanisms to determine if an adequate concentration could be delivered to a soil, before gelation began. They grouted fifteen 0.9 m column tests packed sand or graded silty sand to identify the variables that influence stabilizer transport through porous media. It was found that colloidal silica could be successfully delivered in an adequate concentration to mitigate liquefaction potential.

Transport occurred mainly via advection with some limited hydrodynamic dispersion. The main variables influencing stabilizer transport were found to be the viscosity of the colloidal silica stabilizer, the hydraulic gradient, and the hydraulic conductivity of the liquefiable soil.

5.3 Colloidal Silica as a Grout to Reduce Hydraulic Conductivity

As shown above although colloidal silica can be used to densify soils, thus reducing their susceptibility to liquefaction, the increase in the strength of the soils is minimal compared to other chemical and cementitious grouts. The great advantage of colloidal silica is its low viscosity, which means it is able to permeate small pore/aperture space and, hence, that it could be effective in reducing the hydraulic conductivity.

5.3.1 Reduction in the Hydraulic Conductivity of Soils

Colloidal silica has been investigated for subsurface contaminant barriers, where its initial low viscosity means that it can be easily injected into porous media, producing an impervious barrier after gelation. Of particular importance for the emplacement of such barriers, is good control of the colloidal silica viscosity.

Noll et al (1992), researchers at Du Pont (a chemical research and environmental remediation company) were the first to promote colloidal silica as a grout to reduce the permeability of contaminated soils. A 5% weight colloidal silica solution with a pH of 7 and 0.2M sodium chloride as the accelerator was mixed giving a gel time of 16 hours. This was then injected into a sandbox over 14 hours. The hydraulic conductivity of the sand had been reduced by four orders of magnitude from $3 * 10^{-4}$ m/s to $6 * 10^{-8}$ m/s. It was noted, however, that gelling had begun earlier than the predicted 14 hours and that the injection wells became clogged after 14 hours. This was attributed to a lag between mixing and application, and an error in the calculation of gel times. However; their research did not take into account the impact that the sand may have had on the gelation of colloidal silica.

Persoff et al. (1994) performed experiments using soils which contained significant concentrations of exchangeable calcium ions and the effect that they had on colloidal silica with different cation accelerators. It was found that chemical interactions between the calcium cations and the colloidal silica grout caused rapid, uncontrolled gelation of the grout. This is because the presence of divalent cations, decreases the gel time of colloidal silica; they increase the ionic strength and collapse the double layer. Persoff et al. (1994) suggest that to prevent premature gelation, pre-

flushing with a sodium chloride solution or a dilute colloidal silica solution should be a precursor to the actual grout injection, to displace the divalent cations.

Moridis et al, (1996) used a sodium chloride pre-flush before using colloidal silica to grout heterogeneous, unsaturated deposits of coarse sands, gravel and some silt. Initial tests showed that the presence of the sand rapidly decreased the gel time of the colloidal silica. By pre-flushing the sand with a sodium chloride solution there was then no change in colloidal silica gel time and that with improved penetration, the hydraulic conductivity of this coarse sand reduced from 10^{-3} m/s to 10^{-6} m/s. The above research shows that soil-specific interactions can dramatically affect colloidal silica gel time/rate, which in turn affects how well the grout is able to penetrate in the subsurface.

5.3.2 Colloidal Silica as a Grout for the Reduction of Hydraulic Conductivity of Fractured Rock

Limitations in the penetrability of cementitious grouts, has led researchers to look at colloidal silica as a grout for fine aperture fractures in rock (Butron et al, 2010). Funehag and Axelsson (2003) conducted a field study in a Swedish gneiss with a few narrow fractures. A 40% weight colloidal silica with a 10% sodium chloride solution, in a ratio of 5:1, was able penetrate fractures with apertures as low as $40\mu\text{m}$ with a 100% sealing efficiency.

Funehag (2004) performed a field trial in the Hallandsås tunnels which are formed in Precambrian gneiss. A series of boreholes were drilled for hydraulic characterisation and then grouting with colloidal silica in an 8:1 ratio with sodium chloride. The median hydraulic conductivity was $3 * 10^{-6}$ m/s, with an inflow of 70 l/min. Grouting with a cementitious grout resulted in a reduction in hydraulic conductivity to $5 * 10^{-8}$ m/s with an inflow of 2 l/min, however, when colloidal silica grout was used instead of the cementitious grout, the hydraulic conductivity was even lower at $1.1 * 10^{-9}$ m/s with an inflow of 0.2 l/min. Hence, colloidal silica can be a more efficient grout than cement, for reducing inflow into tunnels.

In a field trial where a grouting programme was conducted in the Törnskog tunnel, North of Stockholm by Funehag and Gustafson (2008). They demonstrated that colloidal silica could be used to penetrate fractures with apertures as low as 14

μm , reducing the total rock hydraulic conductivity for a 100m length of tunnel by one order of magnitude to 3×10^{-9} m/s around the tunnel, (below the required tunnel stipulation of 3.2×10^{-7} m²/s).

Eriksson and Lindstrom (2008), used colloidal silica as a grout in their testing of a new mega-packer at the Äspö Hard Rock Laboratory. The requirement was to reduce inflow to 0.1 l/min or below. Before grouting, the inflow varied between locations from 0.148 and 2.4 l/min, with fracture apertures varying between 27 and 124 μm . After grouting, the inflow was reduced to between 0.004 and 0.025 l/min at these same locations.

Butron et al (2010), was also able to reduce inflow to very low levels when using a colloidal silica grout to seal the roof of an 85m section of the Nygård tunnel in Western Sweden. The transmissivity of the rock mass before grouting was 6.2×10^{-6} m²/s; post colloidal silica grouting the transmissivity was reduced to below the measurement limit of 1.8×10^{-8} m²/s and dripping was minimised to 0.06 l/min which was well below the permitted inflow of between 4 and 9 l/min. The research discussed here shows that colloidal silica is very effective at reducing the hydraulic conductivity of fractures.

5.4 Penetration of Colloidal Silica

Colloidal silica is an evolutive Newtonian fluid where viscosity slowly then rapidly increases over time, rather than a pure Newtonian fluid (where viscosity remains constant until setting) as found with other chemical grouts or a Bingham fluid (where viscosity rises continually) such as cementitious particulate grouts. The rise in viscosity is the gel point where the gel phase is half of the total grout volume (Iler, 1979).

Kim and Corapioglu (2002) developed a numerical model to examine the gelling of colloidal silica with different concentrations of sodium chloride within porous media. They found that an impermeable gel formed at twice the gel point time for all concentrations, and that as you reduce the concentration of sodium chloride there is a greater risk of migration and a reduction in the ability to seal spore space.

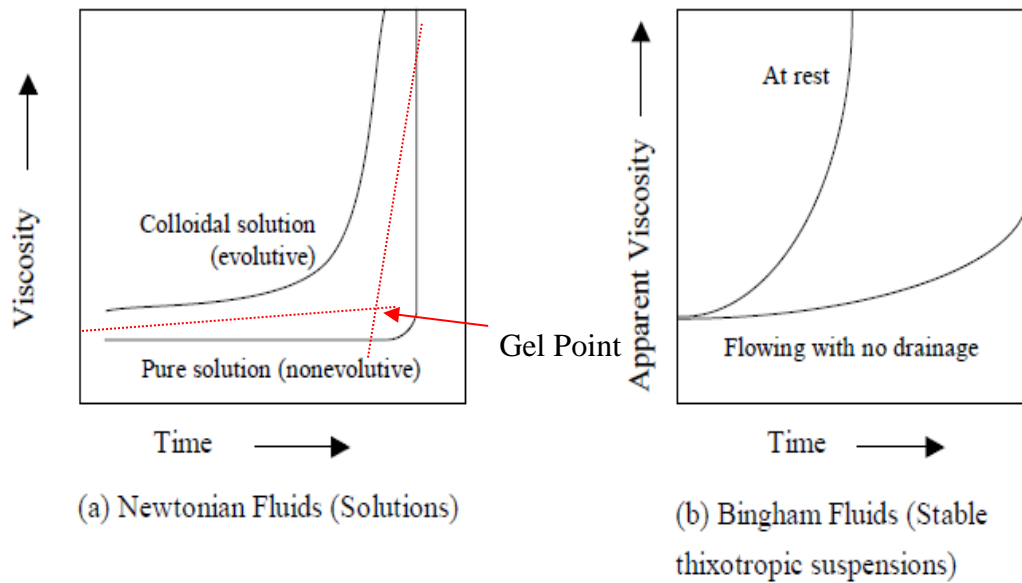


Figure 5.5: Newtonian fluid grouts have a rapid setting (gelling) rate whilst 3b) Bingham fluid grouts have a slow setting (gel) rate which begins immediately. Colloidal silica is in between these two grouts where initially the viscosity remains low (similar to chemical grouts) and then as gelling begins the viscosity increase is more akin to cementitious Bingham grouts (after Mongilardi and Tornaghi, 1986; Bruce et al, 1993). Note the red data for the ‘gel point’ (Kim and Corapcioglu, 2002).

Eriksson and Lindstrom (2008) during their work with the mega-packer at Äspö Hard Rock Laboratory, found that the smaller the aperture the lower the sealing effect, this is due to it being easier for the grout to penetrate larger aperture fractures. They recommended the pumping pressure or grouting time to be increased in smaller aperture fractures. A higher pumping pressure was also recommended to prevent dilution of the colloidal silica grout by groundwater, as the quicker the fracture is filled, the less time there is for the groundwater to dilute or erode the grout front.

The majority of researchers (including the above) use sodium chloride as an accelerator and we can see from Figure 5.5 that the gelling curve that has a lower rate of gelation than traditional chemical grouts. This lower rate of viscosity increase can result in poor placement of the grout and reduce its effectiveness at decreasing hydraulic conductivity. Also because it does not remain at a consistently low viscosity like chemical grouts with a rapid rate of gelation, it requires a higher pumping pressure to penetrate smaller apertures, this increase in pumping pressures may result in enlargement and propagation of the very fracture you are trying to seal (Gothall and Stille, 2009). So, is it possible to make an evolutive Newtonian solution such as colloidal silica behave more like a non-evolutive Newtonian chemical grout?

5.5 Choice of Accelerators for the Gelling of Colloidal Silica

The most important factor, after pH, in the gelling of a colloidal silica solution is the accelerator. Noll et al (1992), stated that sodium chloride is the preferred accelerator as firm resonating gels were produced consistently whilst ammonium of an equivalent ionic strength caused the pH to rapidly decrease causing the silica particles to agglomerate and settle. Calcium had little effect in the acid pH range, but decreased the gel time rapidly in the basic pH range.

Trompette and Clifton (2004) further investigated the influence of accelerator on the gel time and strength of gelled colloidal silica. Comparing sodium and ammonium ions (both monovalent ions), they found that the gel time for ammonium ions was half that of sodium ions and that the strength of gelled silica networks is greater in the presence of ammonium ions.

Schantz Zackrisson et al. (2008) used small angle x-ray scattering to investigate the gelation of colloidal silica where the accelerator was direct addition of ammonium hydrogen carbonate (NH_4HCO_3) salt or the NH_4HCO_3 was produced by the urease-catalysed hydrolysis of urea (non-ionic). The urease enzyme was obtained from Jack-beans. Although the direct addition of NH_4HCO_3 salt caused irreversible aggregation and gelation to occur more quickly at lower ionic strengths, it also resulted in a non-uniform distribution of ions during aggregation. The NH_4HCO_3 produced by urease-catalysed hydrolysis of urea, caused gelation to occur at higher ionic strengths and produced a more uniform distribution of ions during aggregation by raising the ionic strength gradually.

The above research shows that changing the accelerator can have a dramatic effect on gel time and can affect the strength of the gel once gelation is complete. There has been no work on the gel curves produced by the different accelerators which is fundamental to engineering a colloidal silica grout to gel like more traditional chemical grouts.

5.6 Is it Possible to use Colloidal Silica as a Filler during MICP?

The aim in this Chapter is to investigate whether the addition of a small amount of colloidal silica to the cementing solution during the MICP process might make it more efficient. It is postulated that the addition of the colloidal silica as a filler material might reduce the time taken to achieve a given permeability as well as enabling the technique to be applied to fractures with a larger aperture.

Colloidal silica is an aqueous suspension of negatively charged, nm sized spherical silica particles with a density and viscosity similar to that of water. Tobler, et al (2012) showed that the addition of colloidal silica nanoparticles to MICP during grouting of uniform sand, could produce an increased permeability reduction. MICP tests were conducted with and without a small volume of colloidal silica added to the cementing solution. A reduction in permeability was seen of 90% when using MICP alone and 95% when MICP was used in conjunction with colloidal silica. In addition, the rate of permeability decrease was more rapid when colloidal silica was added to the MICP process.

5.6.1 Methods and Materials

To explore whether the approach of Tobler et al (2012) might be equally effective within fractures, as opposed to soils, a fracture-filling experiment was conducted using the same fracture plate as that described in Chapter 4. The injection strategy was the same as that used in Chapter 4, but with the addition of 25ml of colloidal silica per 1 litre of cementing solution. The concentration of colloidal silica used was determined by the results of 5 batch tests. The aim was to keep the colloidal silica as a low viscosity solution allowing the particles to act as a filler and due to their negative surface charge potentially act as sites for calcite precipitation thus increasing the amount of calcite precipitated. Table 5.1 below shows the composition and results of these batch tests.

The batch test that contained 25ml/L (40% colloidal silica concentration within the 25ml) of colloidal silica produced the greatest mass of calcite, the equivalent of 32.25g of calcite per litre of bacteria/cementing/colloidal silica solution. Any greater a concentration of colloidal silica resulted in less calcite being produced.

5.6.2 Results

5.6.2.1 Differences in Precipitation

Table 5.1: Composition of batch tests and mass of calcite produced by each individual test, cs = colloidal silica.

<i>Sample</i>	<i>Concentrations</i>	<i>Start pH</i>	<i>End pH</i>	<i>Gelled?</i>	<i>Mass of calcite (g)</i>	<i>Ave Mass of calcite (g)</i>
1a	10ml of 2OD + 30 ml	6.31	6.897	no	1.18	1.13
1b	0.7M CaCl ₂ /urea with	6.31	6.910	no	1.18	
1c	10ml/l cs	6.31	6.873	no	1.04	
2a	10ml of 2OD + 30 ml	6.53	7.076	no	1.28	1.29
2b	0.7M CaCl ₂ /urea with	6.53	7.081	no	1.3	
2c	25ml/l cs	6.53	7.097	no	1.29	
3a	10ml of 2OD + 30 ml	6.55	7.169	no	1.1	1.03
3b	0.7M CaCl ₂ /urea with	6.55	7.199	no	1.07	
3c	50ml/l cs	6.55	7.232	no	0.93	
4a	10ml of 2OD + 30 ml	6.53	7.124	no	0.86	0.93
4b	0.7M CaCl ₂ /urea with	6.53	7.130	no	0.95	
4c	100ml/l cs	6.53	7.157	no	0.97	
5a	10ml of 2OD + 30 ml	6.5	6.846	no	1.07	1.08
5b	0.7M CaCl ₂ /urea	6.5	6.848	no	1.08	
5c		6.5	6.918	no	1.09	

Figure 5.6 compares the results of grouting with MICP only (reproduced from Chapter 4 in Fig 5.2a) with the MICP with colloidal silica added (Figure 5.6b). For the MICP only flow-plate, 9 cycles were completed before the back-pressure rise was sufficient to inhibit further injection. The MICP with colloidal silica flow-plate only required 8 cycles to achieve the same back-pressure rise. Visible within the MICP

only flow-plate is an even distribution of calcite precipitate. Upon opening the plate, calcite precipitate was found to be firmly adhered to both the top and bottom surfaces.

a) MICP in the fracture after 8 cycles



b) MICP + Colloidal Silica in the fracture after 8 cycles



Figure 5.6: Comparison between MICP (a) and MICP with Colloidal Silica (b). Calcite can be distinguished from colloidal silica by colour, the grey white colour is calcite whilst the blue white colour is colloidal silica.

In Figure 5.6b, there are preferential flow-paths which are blue/white in colour with some grey/white patches. What appears on visual inspection to be solid fill was found to be mobile if you pressed down upon the Perspex top. Upon opening of the flow-plate, it was found that very little of the back pressure rise during the experiment was due to solid well-attached calcite precipitate. Under a gentle water rinse, the majority of grout within the fracture plates flowed away.

Table 5.2: Comparison of grout weights between MICP and MICP with 25ml per litre of cementing solution.

	<i>NFP1</i>		<i>NFP2</i>	
	Dolerite	Perspex	Dolerite	Perspex
After treatment	3790.76g	1115.80	3722.76	1116.94
After wash	3789.10g	1115.12	3721.41	1116.17
After acid wash	3771.91g	1113.14	3718.86	1115.23
Total grout mass	18.85g	2.66g	3.9g	1.71g
Total mass of grout	21.51g		5.61g	

After opening and rinsing (to remove any reactants and stop the MICP process), the flow-plate was left to air dry for 24 hours. Table 5.2 shows the difference in weight between the MICP after 9 cycles and the MICP + colloidal silica after 8 cycles. A clear difference in the mass of grout retained within the fracture can be seen with MICP showing by far the greatest weight increase. During the 8 grouting cycles with MICP + colloidal silica there appeared to be pieces of calcite travelling through the open channels i.e. precipitation seemed to be occurring in suspension. This would indicate that for some reason, the calcite is unable to attach to the fracture surface. To further understand this phenomenon, samples were taken from the fracture for SEM analysis as per the method used in Chapter 4.

5.6.2.2 Sampling and SEM Analysis of NFP2

Figure 5.7 shows the sampling locations and SEM images of the MICP + colloidal silica grout within the fracture. Initial batch tests indicated that the 25ml/l concentration of colloidal silica was too dilute for the colloidal silica to form a gel. Despite this, at the two sampling locations selected, there appears to be a complex mixture of silica-coated calcite crystals and rhombohedral crystals of calcite, embedded within a colloidal silica matrix. Although INCA maps could not be clearly produced due to the complexity and small scale of the interaction between the calcite and colloidal silica. Elemental analysis did confirm the presence of colloidal silica coating calcite. SEM analysis is unable to determine whether the gelation of the colloidal silica occurred first, however, it seems likely that since both reactants (the calcium ions for the colloidal silica and the urea for bacterial ureolysis) are present the colloidal silica gelation and the calcite precipitation occurred at the same time. This is then likely to have been followed by continued growth of the calcite crystals and the addition of silica particles to the silica matrix.

5.6.3 Discussion and Conclusion

When this grout was used in fine sands as in Tobler et al (2012), the colloidal silica was thought to reduce permeability at the pore throats, thus retaining greater numbers of bacteria and, hence, increasing the associated calcite production within in the system. In this fracture plate experiment, however; the fracture aperture is too large to retain the colloidal silica within the system via filtration, unless the aperture has been reduced via calcite precipitation.

From the observations of the previously mentioned colour changes at the end of each cycle (off-white for calcite and blue-white for colloidal silica), it is clear that calcite precipitation within the MICP with colloidal silica is delayed or attachment is inhibited. This, in conjunction with the observations of mobile calcite crystals would tend to suggest that the colloidal silica particles in suspension, are acting as nucleation sites for the calcite crystals, thus decreasing the mass of calcite precipitation on the fracture surfaces. This experiment demonstrates that adding a small amount of colloidal silica nanoparticles to the cementing solution, when applying MICP to seal fractures, does not improve the grout efficiency. In fact, the grouting process is significantly less effective.

Granular looking colloidal silica coating vaterite (calcium carbonate)

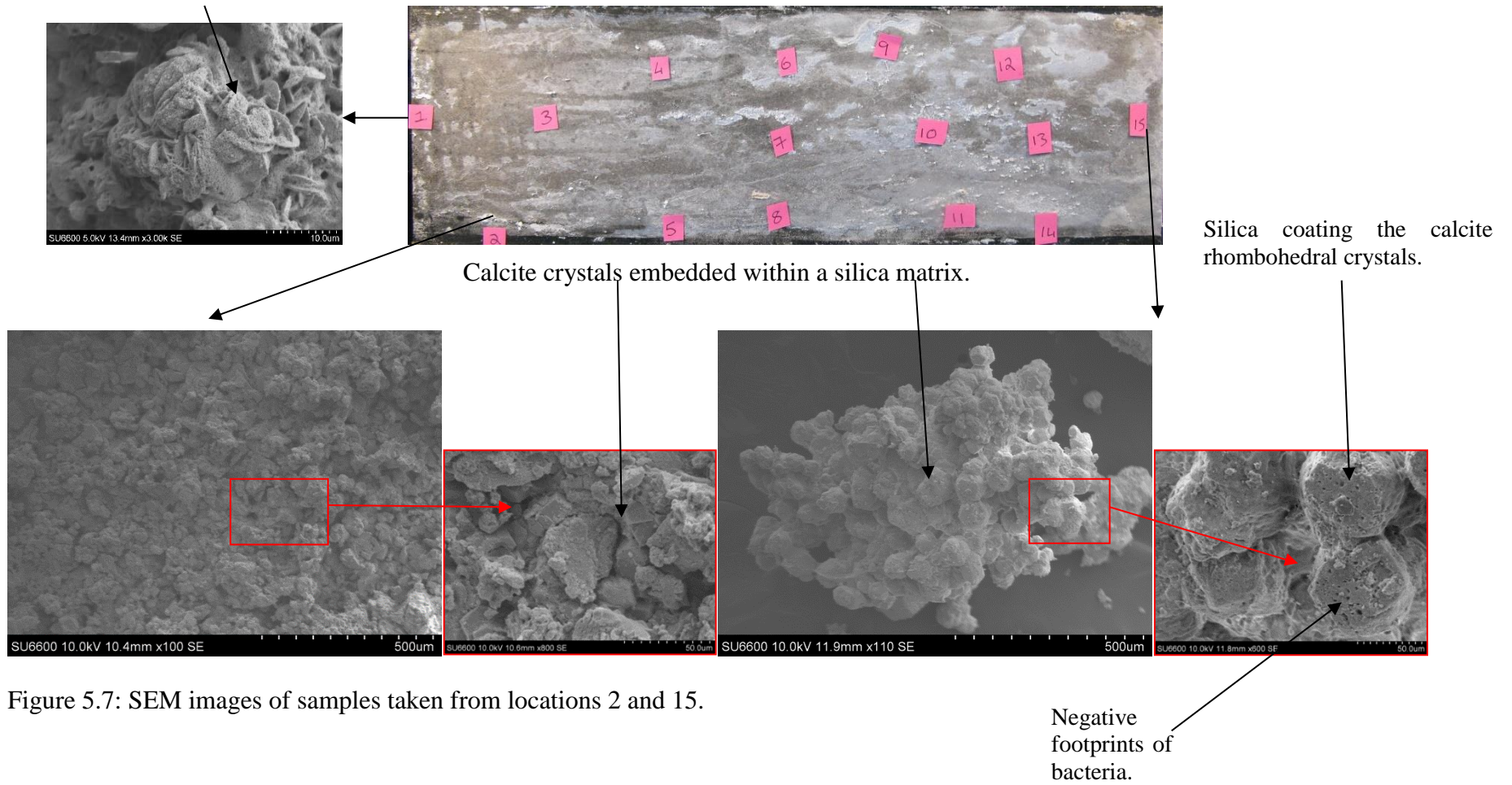


Figure 5.7: SEM images of samples taken from locations 2 and 15.

Although this method of combining colloidal silica nanoparticles with MICP was not effective, there may still be other avenues of research that will prove successful for this combined grout. In my MSc thesis, a 10ml per litre dilution of colloidal silica was mixed with an equal volume of 1.2OD600 bacteria and pushed through a coarse-grained granite filled flow cell followed by the cementing solution. MICP only resulted in a decrease in hydraulic conductivity by one order of magnitude by the end of 3 cycles, whereas the MICP + colloidal silica mixture resulted in a decrease in hydraulic conductivity by two orders of magnitude. This success may not be down to the difference in pore throat size.

In the application within my MSc thesis, the bacteria were injected with the growth broth which contained urea. Thus, they were able to produce some ammonium, which may have acted to gel the colloidal silica and hold the bacteria in place, prior to the application of the cementing solution. Thus, increasing the number of bacteria retained within the system that were able to produce calcite precipitate. This hypothesis was evidenced by the MICP + 1% colloidal silica mix resulting in 1.31g of calcite and 0.32g of colloidal silica being produced per cycle, in comparison to a control sample using only MICP only which produced 1.0g of calcite per cycle. The remainder of this Chapter focusses on development of a combined grout in which the principal component of the grout is the colloidal silica, as opposed to the MICP.

5.7 Varying the Accelerator for Colloidal Silica Grouting

As discussed colloidal silica has already had many of its properties examined for use as a fine aperture fracture grout. Studies show that colloidal silica has significant potential for ground barrier formation, however, there are still questions over the effect of different saline solutions on the gel strength, gel time and gel rate of the grout (Trompette and Meireles, 2003; Trompette and Clifton, 2004). Further, Schantz Zackrisson et al (2008) demonstrate production of an aggregation gradient upon addition of the saline solution, which raises questions about grout homogeneity.

In the remainder of this Chapter, the effects of differing common saline accelerators on grout gelling and performance are explored. These results are also compared with those obtained when colloidal silica is gelled using bacteria to produce the ammonium ions *in situ*, via urea hydrolysis. The ureolytic bacterium, *Sporosarcina pasteurii*, used in the MICP grouting process in Chapter 4 is used to gel the colloidal silica. The research presented in the remainder of this Chapter is described within MacLachlan E., El Mountassir, G., and Lunn, L. (2013). Use of Bacterial Ureolysis for improved gelation of colloidal silica in rock grouting. Geotechnique Letters.

5.7.1 Materials and Methods

The colloidal silica used in this study is MP320, produced by Meyco (BASF), which has been developed for injection into fine rock fractures as well as for the consolidation of loose sediments. MEYCO MP 320 is a colloidal silica suspension which is destabilised by the additions of an accelerator, with no solvent or toxic components. Sodium chloride (1.7M NaCl) is the standard accelerator that is sold in conjunction with Meyco MP320 colloidal silica. The colloidal silica suspension is a whitish/clear liquid, and at 20°C has a dynamic viscosity of around 10 cP (water at 20°C has a viscosity of ~1cP), a density of 1.3 g/cm³, a pH of 9.5 to 9.8 and a SiO₂ concentration of 40 ± 1 % (BASF, 2009b).

A number of different accelerators were investigated in this batch test study, (i) sodium chloride (NaCl), (ii) ammonium chloride (NH₄Cl), (iii) calcium chloride (CaCl₂) and (iv), bacterially-induced ammonium ions (NH₄⁺). These were investigated at a number of different concentrations and combinations. Colloidal silica was mixed with each accelerator in a ratio of 5:1. Table 1 shows the composition of each grout

and the accelerator molarity of each grout after mixing. For the purposes of our experiments, molarities were chosen to produce gel times of up to 3 hours.

Bacterial ureolysis relies on the chosen bacteria containing the enzyme urease. *Sporosarcina pasteurii* (strain ATCC 11850) provide the bacterial urease for these experiments. *Sporosarcina pasteurii* was initially grown on solid Brain Heart Infusion (BHI) agar with urea (20g/L). A single colony was then transferred using aseptic technique to liquid BHI with urea (20g/L) and grown overnight at ~25°C. The bacteria were centrifuged from the growth medium (at 8,000 rpm for 4 mins) and diluted with sterile tap water until the required optical density (OD) was achieved. The optical density of the bacterial solution is essentially a measure of the ability of light to pass through a solution. It is commonly used as a method of ensuring that similar numbers of bacteria are present in prepared solutions. The more transparent the solution the lower the OD and the lower the bacterial concentration. The optical density was measured using a UV-VIS spectrophotometer.

For each batch test, the colloidal silica to accelerator ratio was 5:1. Where bacterial ureolysis was used as an accelerator, equal volumes of bacteria to urea (or urea/saline solutions) were used with a final OD of 0.33, and a final molarity of urea of 0.145M after mixing with colloidal silica. The urea (or urea/saline solutions) and bacteria were mixed together immediately before adding to the colloidal silica (Table 5.3).

Table 5.3: The final optical densities of bacteria and how they were achieved. The bacterially-induced ammonium ions was achieved by mixing 20ml of required bacterial suspension and 20ml of 1.74M Urea together and then mixing with 200ml of colloidal silica. To achieve optical densities >1, larger volumes of lower concentration suspensions were centrifuged, and the supernatant re-suspended in smaller volumes of sterile water.

<i>Initial OD₆₀₀</i>	<i>Volume of Urea (1.74 M)</i>	<i>Volume of colloidal silica</i>	<i>Final D₆₀₀</i>
20ml of 4 OD ₆₀₀	20 ml	200 ml	0.33
20ml of 8 OD ₆₀₀	20 ml	200 ml	0.67

Dynamic viscosity measurements were taken using a Brookfield Digital Viscometer (LVT DVII model) in accordance with ASTM D4016-93. ASTM D4016-93 recommends that you rotate through different spindles to give a greater range of viscosity measurements; however, this method was unsuitable for this study as it

caused a disturbance to the gelling of the silica. Instead only one spindle was used; the appropriate spindle (Spindle 3) was selected such that the gel point was well within its range. For these viscosity batch tests, 200ml of colloidal silica to 40ml of accelerator was used; double these volumes was used for shear strength testing. Samples were mixed together and shaken gently for 30 seconds then placed in a water bath at 20°C and viscosity measurements were recorded every two minutes.

The viscosity of the colloidal silica increases as gelation occurs; measurements were recorded until the maximum viscosity for Spindle 3 at 30 rpm was reached (4010 cP). At 4010 cP, the silica showed jelly-like movement but did not flow when tilted 90° to the horizontal. The gel point is commonly defined as the intersection of the tangents to the two straight line portions of the viscosity-time plots (Summers et al., 1988) (see Figure 5.8); the time taken to reach this point is referred to here as the gel time.

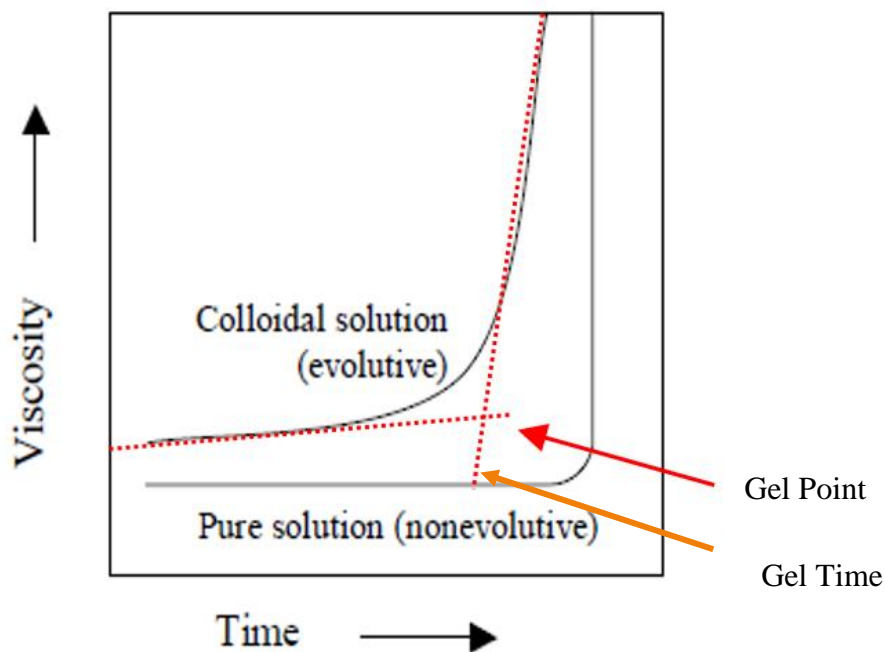


Figure 5.8: Graph showing the Gel point and the gel time of a colloidal solution.

The rate of gelation for each grout was determined by calculating the average gradient (i.e. the average of the gradients between each subsequent pair of data points after the gel point) of each curve after reaching the gel point. For each viscosity batch test, the viscosity-time plots were determined for three specimens and the gel time and rate of gelation listed in Table 5.4 is the average of the triplicate.

Shear strength tests were carried out using a Wykeham Farrance laboratory vane apparatus in accordance with BS1377-7:1990. A vane with a height to diameter ratio of 2:1 was used, where the height of the vane was 25.12 mm and the spring used had a spring calibration factor of 5.55 Nmm/°. Samples were mixed gently together for 30 seconds before being poured into the testing vessel and covered with two layers of parafilm to prevent evaporation. The grouts gelled in their testing vessels and were then allowed to develop for a period of (i) 24 hrs and (ii) 7 days at a constant temperature of 20°C. Unlike cementitious grouts, colloidal silica gel does not rely upon hydration to develop strength over time (curing) but rather hardens as water diffuses out of the silica gel network, i.e. syneresis, (Brinker and Scherer, 1990; Daniel, 2009). When grouting in dry porous rock, this could be advantageous as the rock mass tends to absorb water from the grout. This suggests that colloidal silica could successfully be used to grout fractures that are wet and dry. The extent of water diffusion will be dependent on the relative humidity of the local environment (Axelsson, 2006).

The shear strength of the different colloidal silica and accelerator combinations investigated was calculated as follows:

$$\tau_v = \frac{M}{\pi D^2 \left(\frac{H}{2} + \frac{D}{6} \right)} * 1000 \quad \text{(Equation 16)}$$

where τ_v is the shear strength (kPa), M is the angular rotation (°) of the vane multiplied by the spring calibration factor (Nmm/°), H= vane height (mm) and D=vane diameter (mm). Table 1 lists the gel time, rate of gelation and shear strength after 24 hrs and 7 days for each of the grout compositions tested.

The ureolysis rate constant, k_{urea} was calculated for aqueous solutions from using experimental measurements of ammonium concentration over time ($[NH_4^+]_t$), where $[urea]_0$ is the initial urea concentration (Tobler et al., 2011):

$$\left[NH_4^+ \right]_t = 2[urea]_0 (1 - e^{-k_{urea}t}) \quad \text{(Equation 17)}$$

Ammonium concentrations were determined using the colorimetric Nessler method as described in Tobler et al., (2011). This method could not be used to

determine the ammonium concentration in colloidal silica, due to its opalescence. However, since the hydrolysis of urea produces ionic products from a non-ionic substrate it is possible to measure conductivity (Whiffin, 2004; DeMuyne et al, 2011). For both aqueous bacterial suspensions the linear relationship between conductivity and ammonium was derived (R^2 values of 0.95 and 0.98) enabling ammonium concentration within the colloidal silica to be estimated using conductivity measurements and hence calculation of k_{urea} .

XRD (x-ray diffraction) of samples was performed using a Bruker D8 HRXRD, set up with either Gobel mirror or TWIN dual optics and the LYNXEYE detector. Samples of gelled colloidal silica were ground to a very fine powder (passing through a 45 μ m sieve) and placed within the sample holder. Start and Stop angles were 20 to 60 degrees with increments of 0.01. Peaks were analysed using diffract suite. For each crystal phase, a good match was determined where the relative intensities and positions of 3 strongest lines and minor lines (the greater the number of lines that match the better) of unknown and standard pattern from database coincide.

5.7.2 Results

5.7.2.1 The effect of varying the accelerator concentration

Previous research has shown that the gelation properties of colloidal silica can be controlled by varying the type and concentration of the accelerator (e.g. Funehag and Axelsson, 2003). To examine the effect that different concentrations of the same accelerator can have, three experiments were performed (each in triplicate), using undilute colloidal silica with sodium chloride as the accelerator, varying the applied accelerator final mass from 0.26M to 0.36 M as shown in Table 5.4.

Table 5.4: The gel time for different sodium chloride concentration colloidal silica grouts.

<i>Accelerator</i>	<i>Final molarity (M) of accelerator(s)*</i>	<i>Gel time (mins)</i>
NaCl	0.36	17
NaCl	0.29	38
NaCl	0.26	120

Figure 5.9 shows the resulting viscosity measurements over time. As the concentration of NaCl accelerator decreases from 0.36M to 0.26M, the gel time increases from 17 to 120 minutes, with a corresponding decrease in the rate of gelation from 322 to 241 mPa.s/min. Also evident from Figure 5.9, is that at lower concentrations, the onset of gelation is more gradual.

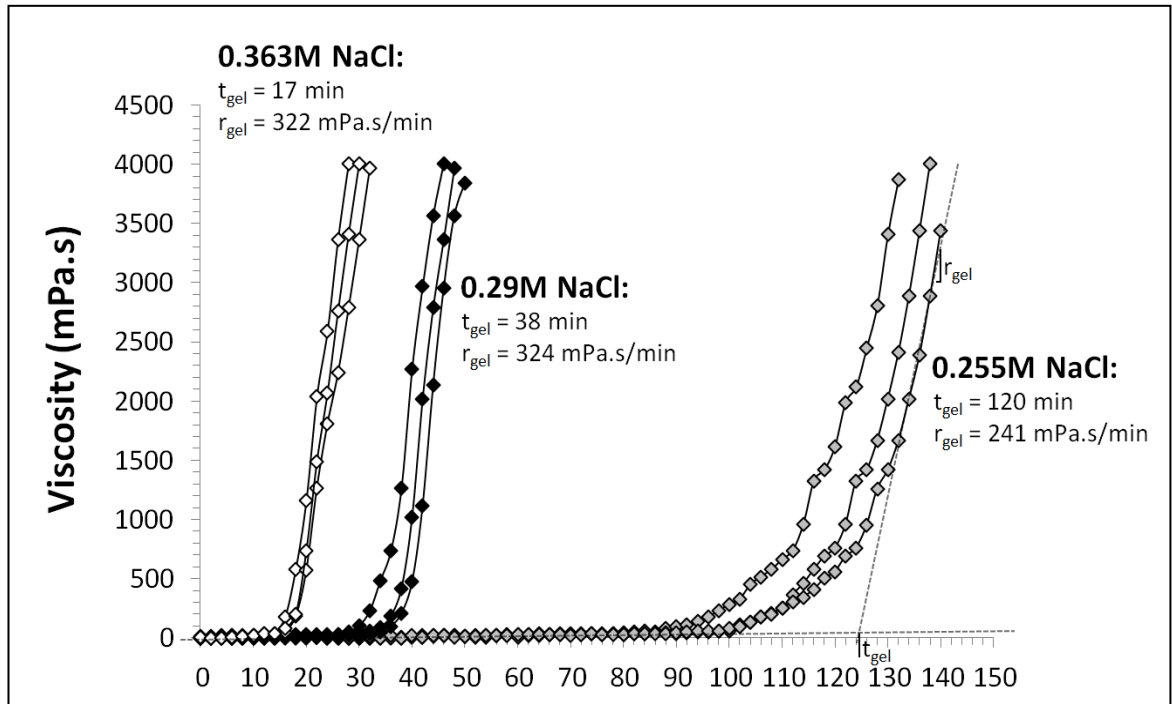


Figure 5.9: Viscosity-time curves for the gelation of silica sol destabilised using sodium chloride accelerators. For each concentration, the experiment was performed in triplicate. Gel time (t_{gel}) is defined as the intercept of the extrapolations from the two straight line portions of the viscosity-times curves (Summers et al., 1988) and the rate of gelation (r_{gel}) as the slope of the curve as marked on the figure. Values of t_{gel} and r_{gel} reported are averages of each triplicate.

From the results in section 5.7.2.1, 0.29M NaCl was selected as a baseline for comparison with other of accelerators due to the gel time of 38 minutes which is long enough to take measurements but also give a good rate of gelation. 0.29M NaCl, is termed Grout A in Table 5.5 and in Figure 5.10 below. A series of 7 experiments were conducted (each in triplicate) that varied the type and concentration of the accelerator applied to gel the colloidal silica grout. Table 5.5 summarises presents the mean result for each of the triplicates, in terms of their gel time, gel rate, shear strength after 24 hours and shear strength after 7 days. The corresponding viscosity profiles over time are shown in Figure 5.10.

In the following sections, these results are discussed in detail by considering each accelerator variable (concentration, valency, atomic mass, in-situ production) in isolation.

Table 5.5: Composition and concentration of different accelerators tested and corresponding colloidal silica grout properties.

<i>Series</i>	<i>Accelerator</i>	<i>Final molarity (M) of accelerator(s) *</i>	<i>Gel time (mins)</i>	<i>Rate of gelation (mPa.s/min)</i>	<i>Shear strength after 24hrs[#] (kPa)</i>	<i>Shear strength after 7 days[~] (kPa)</i>	
A	NaCl	0.29	37	324	28	51	
B	CaCl ₂	0.033	29	625	28	76	
C	NH ₄ Cl	0.29	4	1451	30	79	
D	NH ₄ Cl	0.21	23	1468	24	66	
E	NH ₄ Cl	0.16	141	192	24	39	
F	0.33 Bacterially-induced NH ₄ ⁺	Max. NH ₄ ⁺	0.29	155	546	21	50
G	Bacterially-induced NH ₄ ⁺ + CaCl ₂	Max. NH ₄ ⁺ + 0.029 CaCl ₂	0.29	171	150	29	50

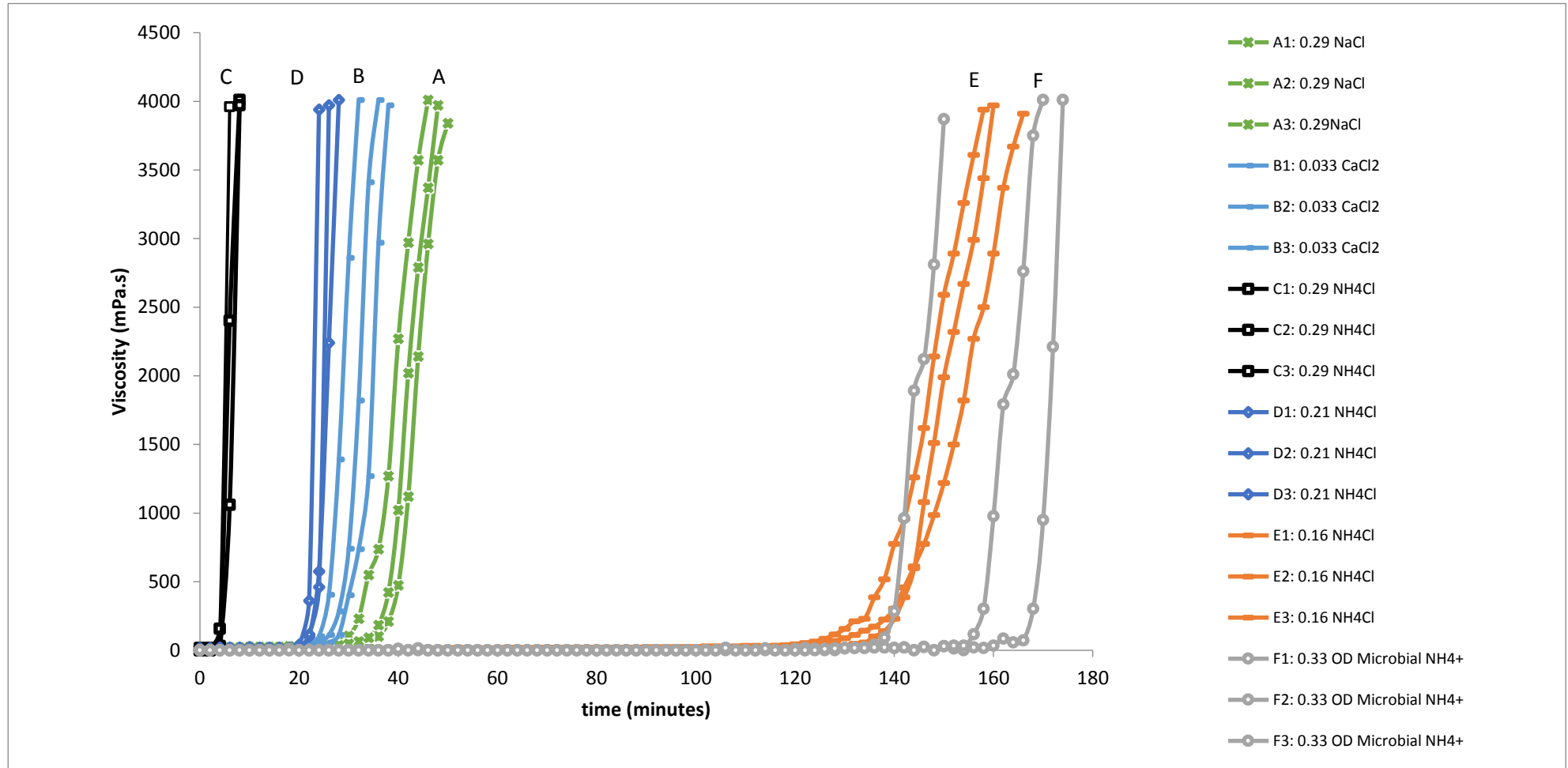


Figure 5.10: Viscosity-time curves for the gelation of silica sol destabilised using different accelerators. Table 5.4 summarises the properties of each grout.

5.7.2.2 Comparison between monovalent and divalent ions

To investigate the effect of colloidal silica gelation due to the addition of cations with a differing valency, the colloidal silica was gelled using calcium chloride as the accelerator. The baseline grout (Grout A) has a molarity of 0.29M NaCl. At the same concentration (0.29M) of CaCl₂ the colloidal silica gelled immediately on mixing and, as a consequence, viscosity changes could not be captured. At one tenth of the concentration, 0.029M, the colloidal silica took over 7 hours to gel and was outside the time limits for set for the experiment. In the end, a concentration of 0.033 M CaCl₂ was selected and Figure 5.9 compares the gel time curves of Grout A (0.29M NaCl) with Grout B (0.033M CaCl₂). It is evident that the gel time was shorter for Grout B (29 mins) than for Grout A (38mins) even though the ion concentration was almost one order of magnitude lower for the calcium chloride gelled grout. The rate of gelation (Table 5.5) was also higher for Grout B (625 mPa.s/min) than Grout A (324 mPa.s/min) suggesting that once gelation begins, it proceeds at a faster rate in the presence of Ca²⁺ ions than in the presence of Na⁺ ions.

The large difference in salt concentration required to obtain similar gel times for Grouts A (0.29M NaCl) and B (0.033M CaCl₂) is due to the divalent calcium ion being more effective at compressing the double diffuse layer around the silica particle, (Savarmand, 2003). The negative charge of the colloidal silica particle is balanced by counter-ions that cluster around the surface of the particle and surround it in a diffuse cloud. The negatively charged surface of the silica particle and the distributed charge in the adjacent phase is termed the double diffuse layer (Figure 5.11). As the calcium ions have a stronger charge than the sodium ions, fewer ions are needed to balance out the negative surface charge of the silica particle. Therefore, for a solution at the same concentration, increasing the cation valency leads to a decrease in the surface potential and also a reduction in the thickness of the double diffuse layer, thereby reducing electrostatic repulsion between particles.

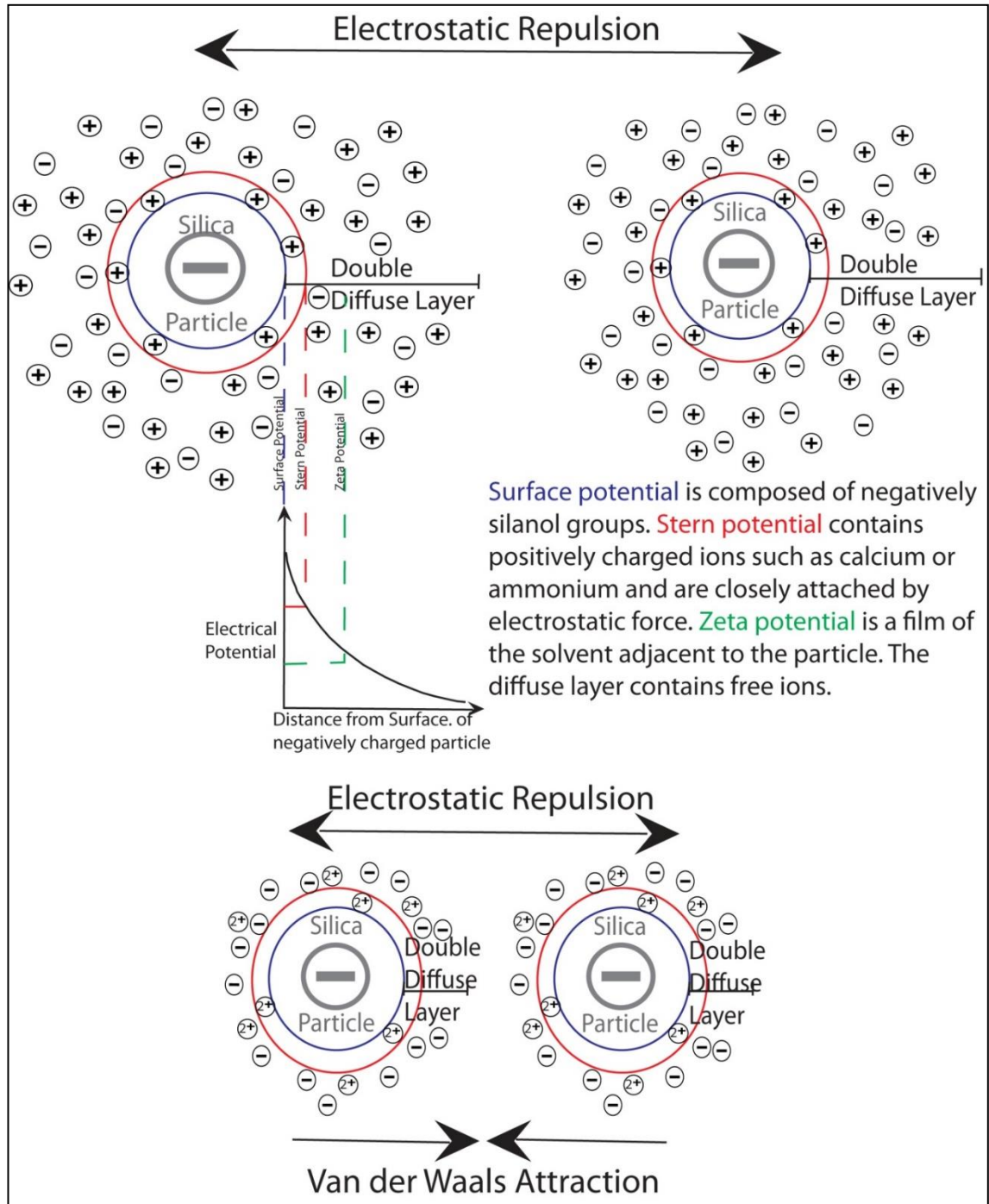


Figure 5.11: illustrates the double diffuse layer of counterions around a negatively charged silica particles in an electrolyte of monovalent cations, and the reduction in the thickness of the diffuse layer and the reduction in electrostatic repulsion between particles in an electrolyte of divalent cations at the same concentration.

By contrast, ion valency seems to have little impact on the shear strength of the grout; after 24 hrs both Grout A and B have a shear strength of 28 kPa (Table 5.5). Although after 7 days Grout B exhibited a higher shear strength (76 kPa) compared to that of Grout A (51 kPa).

5.7.2.3 Comparison between differing monovalent ions

Figure 5.12 compares gelation of the colloidal silica for two differing monovalent accelerators; ammonium chloride (Grout C) and the baseline grout, sodium chloride (Grout A). Grout C (0.29M NH₄Cl) gelled much quicker than Grout A (0.29M NaCl) for the same molar concentration of accelerator added, with a gel time of 4 mins compared to 38 mins.

Additionally, the rate of gelation was much higher for the ammonium chloride-induced gelation (Grout C) at 1451 mPa.s/min compared to 324 mPa.s/min for Grout A; thus once gelation had begun the colloidal silica grout with ammonium chloride reached a higher viscosity much quicker. After 24 hrs both grouts had a similar undrained shear strength (cohesion), however after 7 days, Grout C (0.29M NH₄Cl) exhibited a greater shear strength of 79 kPa compared to 51 kPa for Grout A (0.29M NaCl) (Table 5.5).

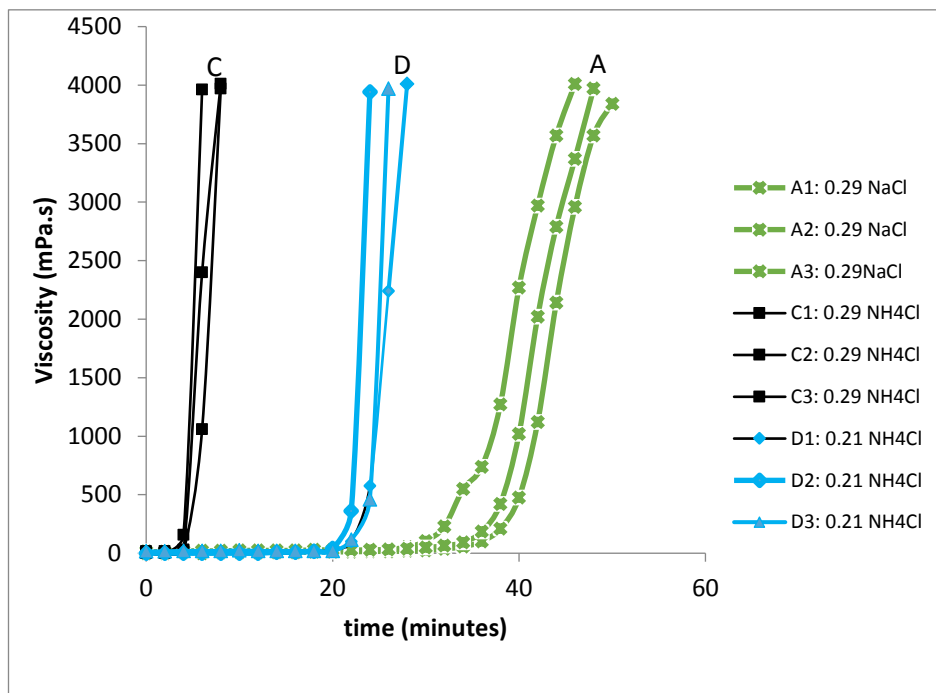


Figure 5.12: Viscosity-time curves for the gelation of silica sol destabilised using different accelerators. Table 5.5 summarises the properties of each grout marked on this figure.

Also plotted on Figure 5.12 are the results for an ammonium chloride concentration of 0.21M (Grout D). As expected, a decrease in the concentration of ammonium chloride from 0.29M (Grout C) to 0.21M (Grout D) increases the gel time from 4 mins to 23 mins respectively.

The observed differences in the gel time curves and shear strengths between the two monovalent ions (Na^+ and NH_4^+) can be explained by considering the way in which these ions interact with the structure of water and their ionic radius (Figure 5.13). When cations are present in water, water molecules become ordered around the cation in a sphere due to the electronegative oxygen atom, forming a hydration sphere (Figure 5.13).

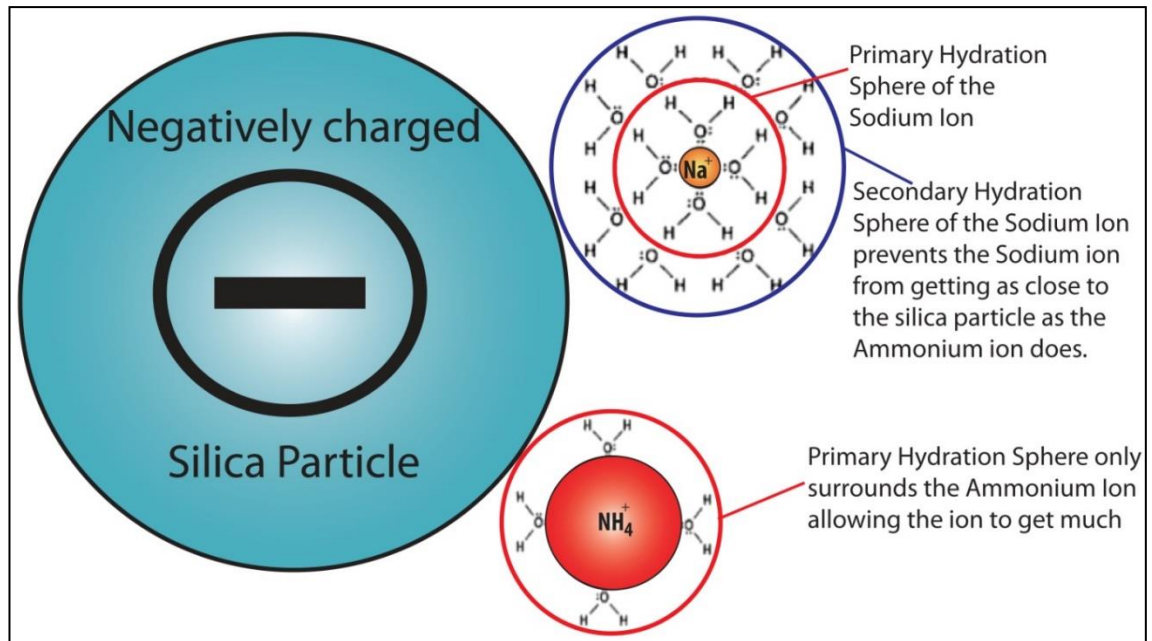


Figure 5.13: Influence of ion specificity on hydration spheres surrounding monovalent ions.

Small ions with high charge density like Na^+ exhibit stronger interactions with water molecules than exists between water molecules, and therefore are referred to as kosmotropic ions, as they are capable of breaking hydrogen bonds between different water molecules (Trompette and Meireles, 2003). Large ions with low charge density, like NH_4^+ exhibit weaker interactions with water than exists between water molecules and therefore have little impact on the hydrogen bonding of surrounding water and are called chaotropic ions (Trompette and Meireles, 2003). As a result, ammonium ions have smaller hydration spheres due to their smaller impact on the surrounding hydrogen bonds between water molecules (Berry and Rice, 2000).

At a pH between 7 and 11, as in this investigation, ammonium ions, which are poorly hydrated (small hydration sphere) are preferentially adsorbed onto silica because within this pH range silica has a low degree of hydration and the adsorption follows the concept that "like adsorbs like" (Trompette and Meirles, 2003). This is due

to the absence of neutral hydroxyl (-OH) groups (to form hydrogen bonds) at a pH over 7 (Trompette and Meireles, 2003). In addition to this, the smaller hydration sphere is adsorbed closer to the silica particle surface (Figure 5.13) creating a stronger attractive force, which can explain the higher shear strength observed in the gels destabilised using ammonium ions.

5.7.2.4 Bacterially-induced ammonium ions compared with direct addition of ammonium chloride

In order to investigate the effect of bacterially-induced cations on colloidal silica gelation, Grout C (0.29M NH₄Cl) referred to here as the direct addition of ammonium is compared with Grout F. In Grout F, bacterial ureolysis was used to produce ammonium ions with a maximum possible production of 0.29M NH₄⁺ (the same as Grout C), controlled by the urea concentration. From Figure 5.14, it is clear that the grout destabilised by bacterially-induced ammonium ions only (Grout F) had a much longer gel time (155mins) and a lower rate of gelation than Grout C (gel time of 4mins). Furthermore Grout F exhibits a lower shear strength than Grout C both after 24 hrs and after 7 days (Table 5.5).

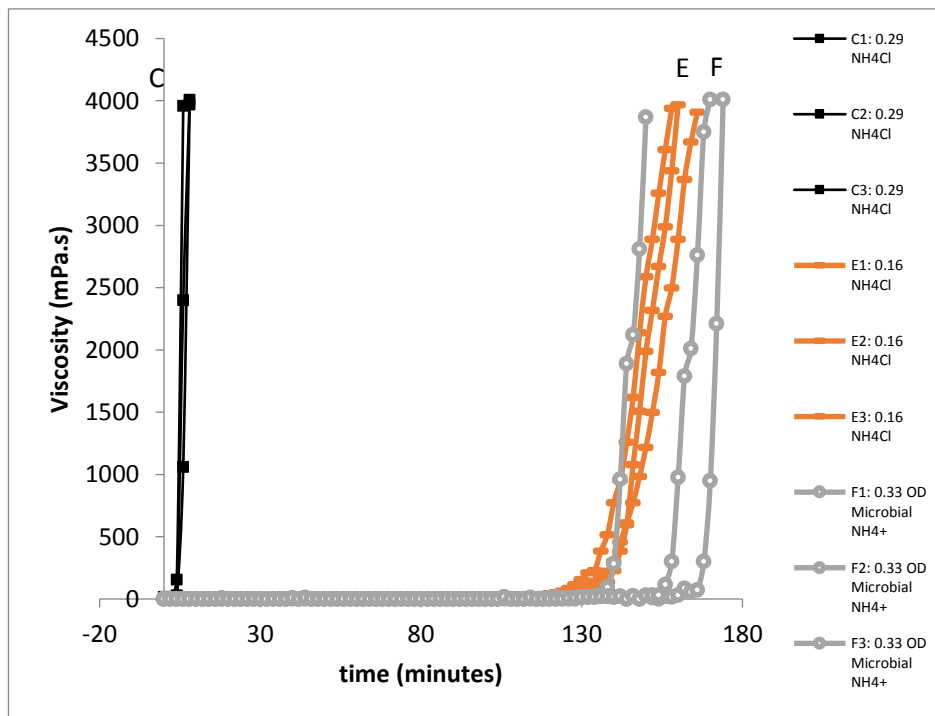


Figure 5.14: Viscosity-time curves for the gelation of silica sol destabilised using different accelerators. Table 5.5 summarises the properties of each grout.

The longer gel time and lower gel rate observed for Grout F is likely due to the ureolysis rate; it takes longer to produce enough ammonium ions to reach the gel point, which limits the rate of gelation, producing a gentler increase in viscosity. The lower shear strengths (cohesion) observed for Grout F may be a consequence of the bacterial cells within the gel forming ‘weak’ points within the grout structure, or they may be due to the mass of ammonium produced through ureolysis being much less than the maximum possible value - resulting in fewer siloxane bonds being formed after the 7-day period.

Interestingly, when you compare the direct addition of NH_4Cl versus the addition of NH_4Cl via in-situ bacterial production, for a grout mix that has a similar gel time, the shear properties the bacterially-produced grout is no longer weaker. Figure 5.14 also shows the results for Grout E – 0.16M NH_4Cl . When Grout E is compared to Grout F, both of which have a gel time of 141 and 151 minutes respectively, Grout F has a rate of gelation that is 2.8 times higher than that of Grout E (546 mPa.s/min compared to 192 mPa.s/min, Table 5.5) and demonstrates a 25% higher 7-day shear strength than Grout E.

5.7.2.5 The effect of bacteria concentration on the gelation of Colloidal silica

Figure 5.15 compares the viscosity evolution of silica sol destabilised using two different bacterial densities, equivalent to 0.67OD_{600} and 0.33OD_{600} . It is evident that for the grout with the higher number of bacteria (0.67OD_{600}), the gel time is much shorter and the rate of gelation is higher than that for 0.33OD_{600} grout. This can be explained by considering the production of ammonium ions, which is dependent on bacterial density (OD_{600}) (Figure 5.15).

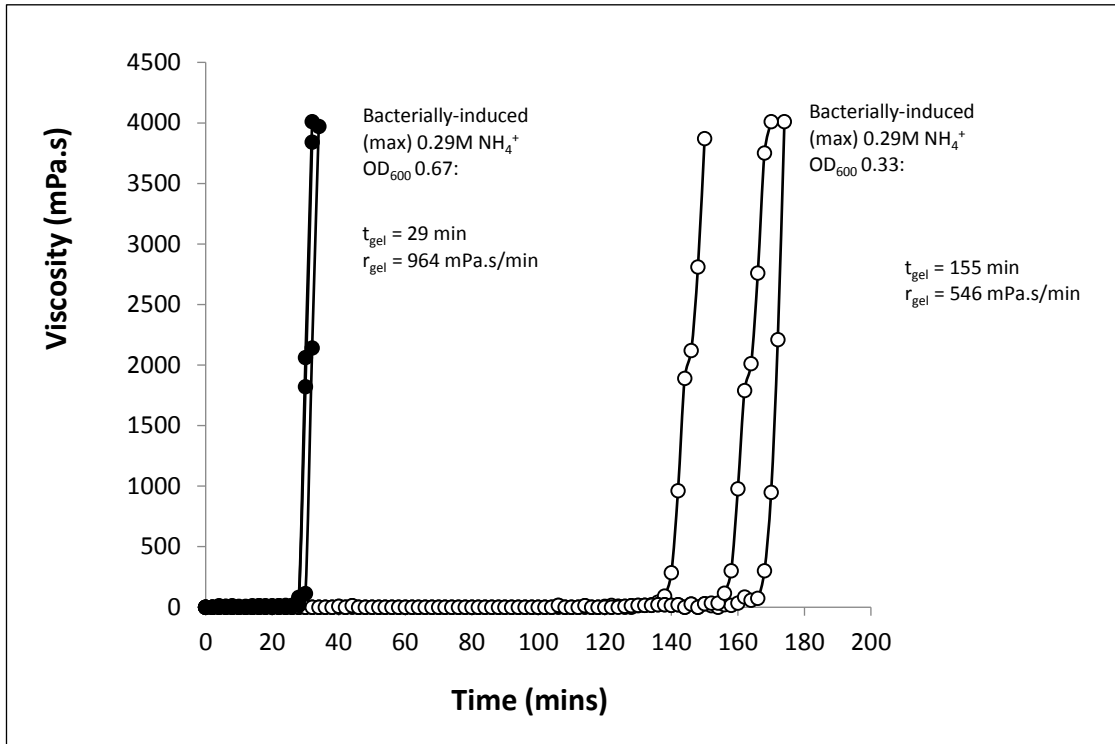


Figure 5.15: Viscosity-time curves for in situ destabilisation via bacterial ureolysis at two different bacterial densities: 0.33OD600 and 0.67OD600. Experiments were performed in triplicate.

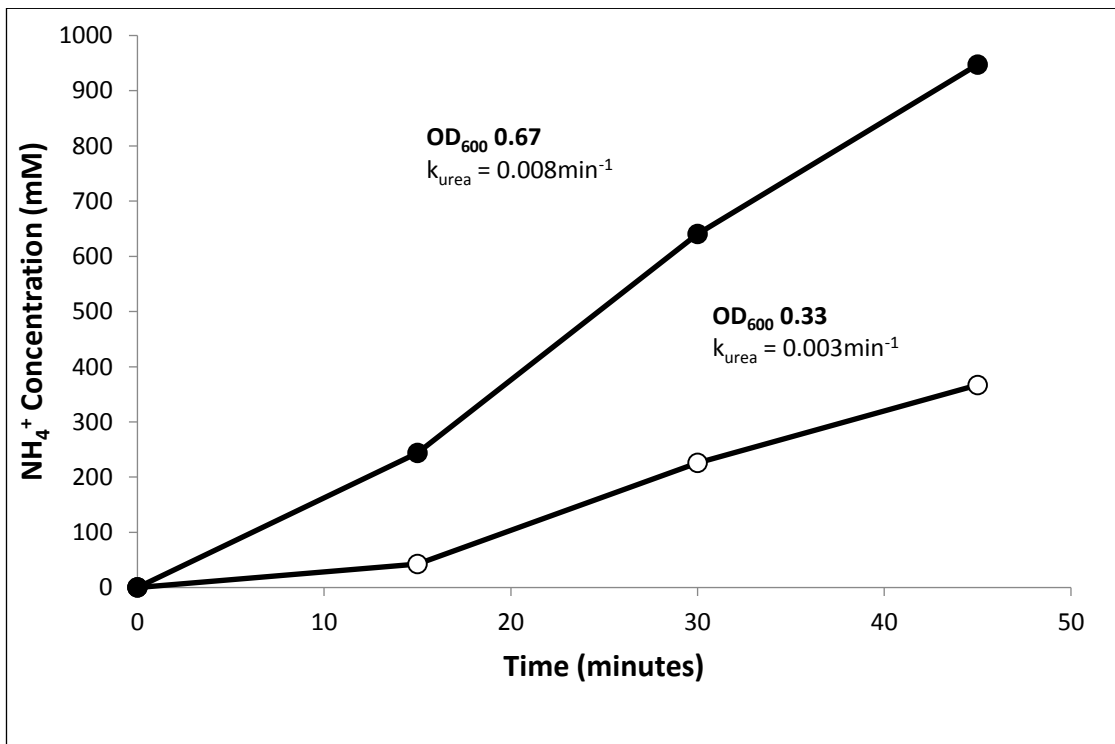
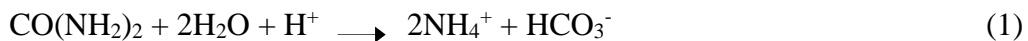


Figure 5.16: Ammonium production and k_{urea} in silica sol at two different equivalent bacterial densities: 0.33OD600 and 0.67OD600. Initial urea concentration used for determination of k_{urea} was 1.5M. Closed and open circles are ammonium concentrations estimated from conductivity measurements.

Figure 5.16 shows that ammonium ions are produced before gelling begins in both bacterial grouts. However; 0.67OD₆₀₀ has a higher ureolysis rate (0.008 min⁻¹) and thus produces ~ 600mM of ammonium within the first thirty minutes whilst 0.33OD₆₀₀ produces <400mM at 45 minutes. This indicates that there is a critical ion concentration for gelation to begin and that this is reached much sooner in higher bacterial densities (0.67OD₆₀₀) due to its higher ureolysis rate constant k_{urea} .

5.7.2.6 Bacterially-induced ammonium ions with and without the direct addition of calcium chloride.

During the hydrolysis of urea, *S. pasteurii* produces not only ammonium ions (NH₄⁺) but also bicarbonate ions (HCO₃⁻), discharging both ion species to its proximal environment. If calcium ions are present then calcium carbonate (CaCO₃) may be precipitated in a high pH environment (pH ~ 9) if the critical saturation state of calcite is exceeded (Ferris et al., 1996; Ferris et al., 2003; Mitchell and Ferris, 2006):



To investigate the influence of calcium carbonate production on the gelation and shear strength of a silica grout, Grout G contained 0.029M of calcium chloride (which on its own has a gel time >7 hrs thus should not interfere with gelling of the colloidal silica over a two hour period) with the bacteria, and sufficient urea to produce a maximum of 0.29M NH₄⁺ ions.

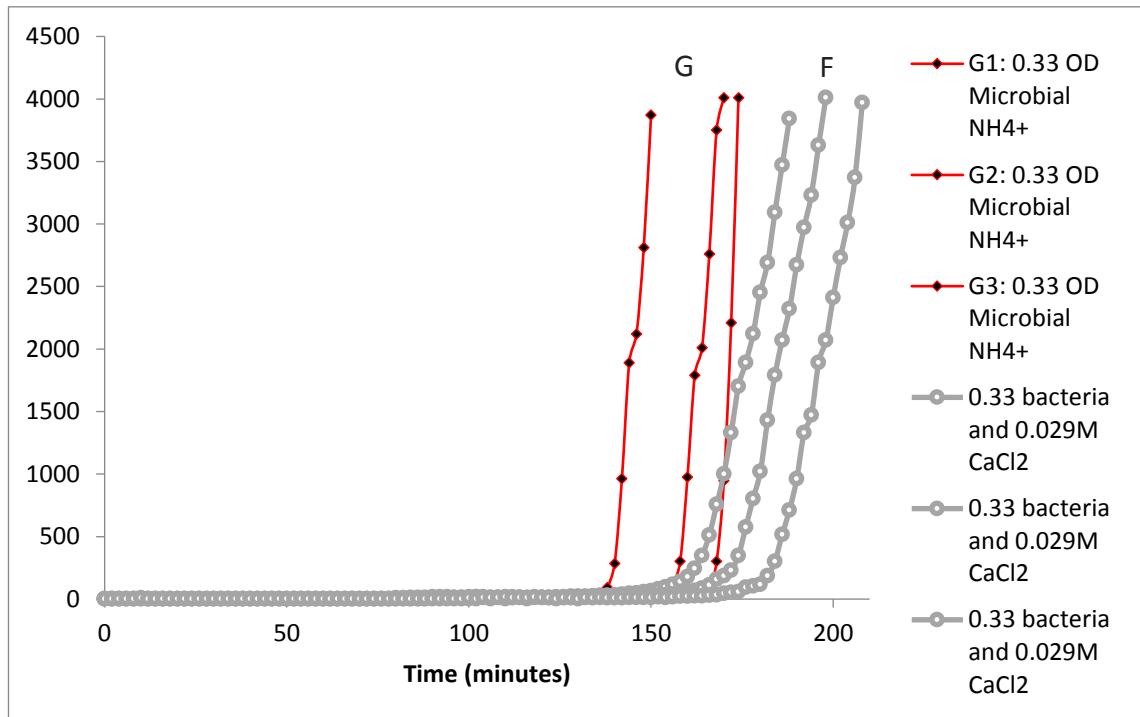


Figure 5.17: Comparison between grouts F(bacteria only) and G (bacteria and calcium chloride). Note that the Gel rate for bacteria only is greater than the gel rate for the same concentration of bacteria but with the added calcium ions.

Figure 5.17 compares the viscosity curves of Grout G (with the addition of CaCl) with Grout F, which was destabilised by bacterially-induced ammonium ions only. It is evident that the gel time for Grout G (171 mins) was longer than for Grout F (155 mins). The rate of gelation of Grout G (with 0.029M CaCl₂) was also lower than that obtained for Grout F at 150 cP/min, compared to 478 cP/min. A comparison of the shear strengths of these grouts shows that after 24 hrs, the initial shear strength of Grout G is slightly higher than that of Grout F but after 7 days Grouts F and G both exhibited the same shear strength of 50 kPa.

The longer gel time and the lower rate of gelation observed for Grout G in the presence of calcium chloride appear to suggest that the presence of calcium ions has slowed the gelation process when compared to Grout F, where only bacterial ureolysis was the accelerator. This is likely to be due to a reduction in the amount of ammonia being produced within the network, as a result of the bacterial cells acting as a nucleation surface for the calcite crystals (Fortin et al., 1997; Fujita et al., 2004).

Recent studies on bacterially-induced calcite precipitation have shown that *S. pasteurii* cells can become encapsulated in calcite, therefore limiting ureolysis and subsequent production of ammonium ions (Cuthbert et al., 2012; Tobler et al., 2012).

The shear strength of Grout G after 7 days also indicates that the calcium ions have not been free to participate in the gelation process but have been precipitated as calcium carbonate, as the cohesion of the grout is the same as that destabilised using bacterial ureolysis only.

The formation of calcium carbonate in Grout G was confirmed by X-ray diffraction analysis. Initially, the samples were to be analysed with a Goebel mirror set up. Grout G was analysed using this method, Figure 5.18 shows the curve produced by the amorphous silica and the very clear peaks of Calcite.

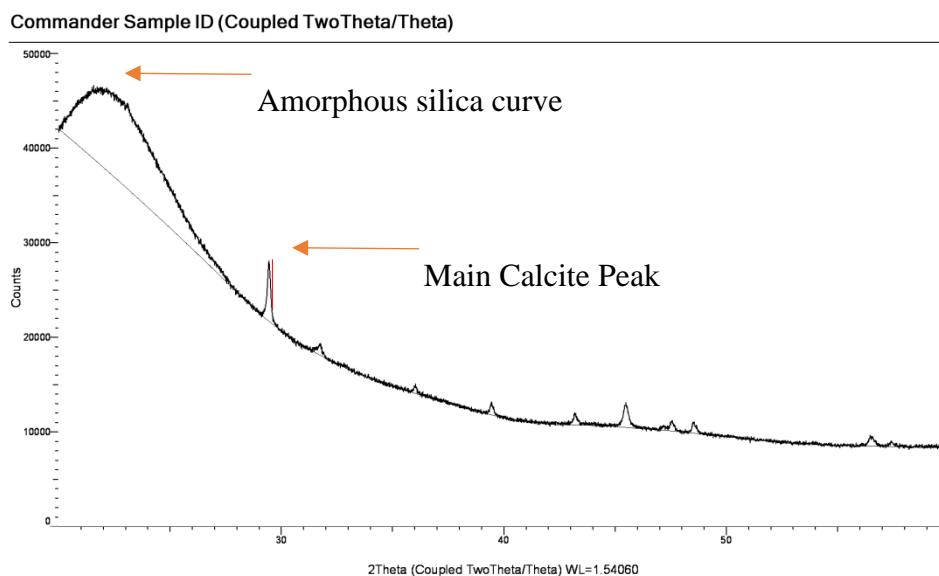


Figure 5.18: XRD results using a Goebel mirror alignment. Peaks indicate that calcite is present within colloidal silica. Colloidal silica shows as the broad peak at 23o due to its amorphous nature.

However; the Goebel mirror went out of alignment and it was necessary to switch to a twin dual optic set up. The dual optic setup changes the way the x-ray photons are collected and form the beam. The Goebel mirror gives the highest intensity, thus clearer peaks. The twin dual optics do still show the same peaks but they are less clear. Figure 5.19 b shows that the calcite peaks are still there, whilst in Grout F (Figure 5.19 a), no peaks are present. This indicates that the precipitation of the mineral (calcite) acted to limit the production of ammonium ions by bacterial ureolysis.

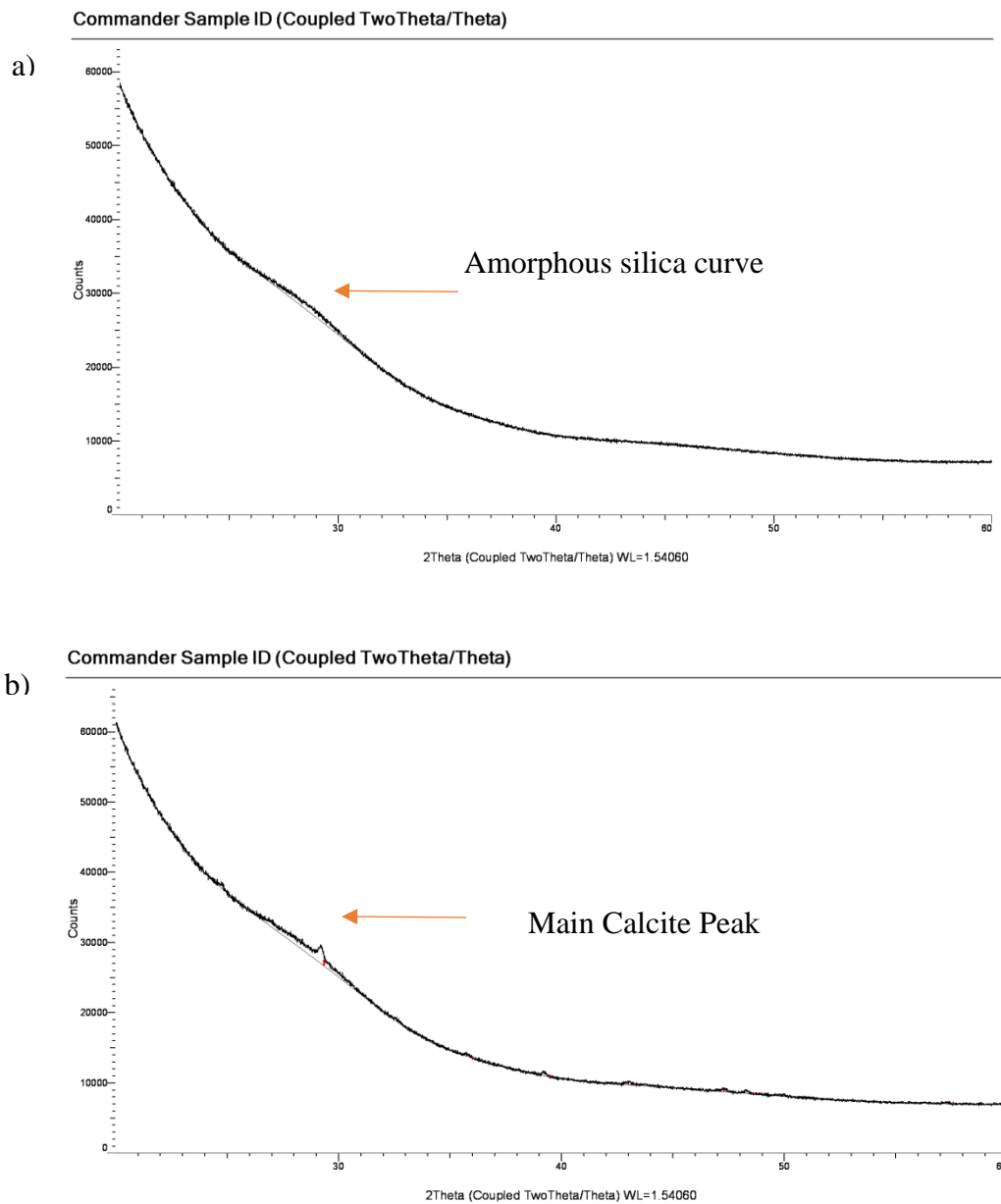


Figure 5.19: XRD results using TWIN dual optics. a) Colloidal silica shows as slight curve to its amorphous nature. b) Peaks indicate that calcite is present within colloidal silica though they are not as intense as the Goebel mirror.

5.9 Implications for grouting

When designing a rock grouting programme it is important to select a grouting material which is suitable for the nature of the fractures to be penetrated, with particular consideration to the possible fracture apertures (Fransson and Gustafson, 2003). For a successful grout injection strategy it is necessary to have good control of the properties related to the radius of penetration: (i) grout viscosity, (ii) grout setting (gel) time, (iii) injection pressure and (iv), pumping rate. For a greater penetration radius, it is desirable for the grout to be of low initial viscosity and to have a long setting (gel) time. Low injection pressures and pumping rates also can greatly facilitate the in-situ injection process. Depending on the context of the grouting scheme it will be desirable for the set grout to exhibit one or more of the following properties: (i) low hydraulic conductivity, (ii) sufficient shear strength, (iii) good adhesion to the rock surface and (iv), durability (Widmann, 1996).

It has been demonstrated here that colloidal silica gelation and the final properties of the gel are very sensitive to small changes in the composition and concentration of cations present in solution (or within the soil/rock). The direct addition of ammonium salts requires ten times the concentration, compared to CaCl_2 , to achieve similar values of shear strength, however, at this concentration it produces very short gel times, thus reducing the radius of grout penetration. At a similar molarity to ammonium chloride, sodium chloride solutions produce longer gel times and a reduction in shear strength.

Using conventional accelerators, to obtain longer gel times (greater penetration) it is necessary to reduce the molarity of the sodium chloride solution, at the cost of reducing its shear strength. The bacterial production of ammonium ions, however, enables longer gel times to be achieved whilst still producing a grout with the same shear strength as that of a traditional accelerator. This lengthening of gel times could be beneficial for penetrating greater distances into fractured rock, thus reducing the number of injection points required. Such an application could be particularly beneficial in subsurface engineering applications where large volumes of rock are required to be grouted.

5.10 Conclusion

The experimental results presented in this Chapter have shown that different accelerators can be used to destabilise colloidal silica, and that bacterial ureolysis using *S. pasteurii* can gel colloidal silica via production of ammonium accelerator in situ. The different accelerators influence the gel time of the silica grout, the rate of gelation and also the shear strength of the gelled grout. These results illustrate for the first time the potential for using bacterially-induced gelation of colloidal silica within the context of grouting rock fractures. The main conclusions are:

Due to its divalent ions, colloidal silica is very sensitive to calcium chloride accelerators, with much lower concentrations (almost one tenth) required to achieve gel times similar to the more common sodium chloride accelerator.

Ion specificity has been shown to strongly influence gelation and the gel properties, with ammonium ions resulting in shorter gel times and faster gelation rates and higher shear strength than compared to silica grouts destabilized by sodium ions. These properties can be explained by considering the smaller hydration sphere of ammonium ions (compared to sodium ions), which are preferentially adsorbed onto silica particles, with a resulting stronger attractive force.

Using bacterial ureolysis only (Grout F) as a means of destabilising colloidal silica, appears to be a very efficient accelerator as it leads to longer gel times than for direct addition of monovalent ions at the same concentration. Furthermore; this slowing down of the gelation process had no associated reduction in shear strength (after 7 days) of the gelled grout when compared to the standard accelerator NaCl (Grout A).

Grout G combined inducing gelation of colloidal silica via bacterial ureolysis and inducing microbial calcite precipitation within the grout. Grout G demonstrated a slower gel time than for bacterial ureolysis alone (Grout F) and a slower rate of gelation. This appears to be due to encapsulation of the bacteria by the calcite precipitated. Future experiments should investigate changes in bacterial density with different calcium chloride concentration and lower colloidal silica concentrations. It may be possible to engineer a combined grout where colloidal silica is used to immobilise the bacteria and reduce permeability whilst the production of calcite could increase the shear strength of the grout.

6. DISCUSSION FOR INDUSTRIAL APPLICATIONS

6.1 what current grouting problems could this research solve?

The most likely cause of radionuclides being released back to the biosphere from geological storage is the re-saturation of a repository and leaching of the radionuclides. Preventing unwanted fluid migration via fracture networks in otherwise low permeability strata is a priority. Low pH (<11) microfine cementitious grouts for apertures <100 μ m are required for the geological storage of nuclear waste due to the adverse impacts of a higher pH on the bentonite backfill and the resulting potential to accelerate the release of uranium (Bodén and Sievänen, 2005). However; a low pH cementitious grout acts like a Bingham fluid thus; it does not penetrate the same fractures as water does. Hence, when using it as a barrier it is difficult to ensure you have sealed smaller aperture fractures. With both MICP and a silica bio-grout, however; the solutions flow at a very similar viscosity to that of water (and hence as pollutants that travel in water). This means that the permeability reduction after grouting is more reflective of the sealing of pollutant transport pathways.

Low pH cementitious grouts also require additives that reduce the percentage of cement within the grout, these can be blast furnace slag, fly-ash or silica fume. SKB and Posiva have ruled out the use of both blast furnace slag and fly-ash, focusing on silica fume as the blending agent (Bodén and Sievänen, 2005). However; the use of silica fume can result in practical difficulties such as agglomeration during mixing, poor flow ability and shrinkage (Glasser, 1996). Shrinkage may not be conducive to achieving the very low hydraulic conductivities required for the geological disposal of nuclear waste. Due to its crystalline nature MICP does not undergo shrinkage whilst under saturated conditions, Axelsson (2006) demonstrated that with a colloidal silica grout shrinkage is only 2%.

The ease of application of a grout is also of great importance. Cementitious grouts tend to start setting as soon as they are mixed which decreases the time available for the application whilst also requiring increasing pumping pressure. To improve the workability of low pH grouts requires the addition of superplasticisers. There is some doubt regarding the use of superplasticisers for nuclear waste storage as they are

organic additives that have the potential to complex with radionuclides and enhance their mobility (Young et al, 2013). Although both MICP and the Silica Bio-grout require the growth of *Sporosarcina Pasteurii*, the bacterium can last several days before their ureolytic activity decreases (Whiffin, 2004).

The uncompressed confined strength of non-cohesive strata cemented by MICP process was shown to be 470kPa (Salifu et al, 2016), whilst the unconfined compressive strength of a standard low pH cementitious grout is 10MPa after 90 days curing (Kim et al, 2011). The strength of colloidal silica is much lower than low pH cementitious grouts and MICP. Dave et al (2010) showed that the unconfined compressive strength of non-cohesive strata cemented with colloidal silica was 290 kPa after 90 days.

Any grout used must also be able to prevent the ingress of water during construction and operation of the site as well as being able to isolate the radioactive waste for tens of thousands of years. Calcite precipitates have been found within fractures on the surface and at depth in natural systems with ages of up to 500,000 years (Paces et al, 2001). Bacteria have also been correlated with the formation of calcite veins within fractures in natural systems (Pedersen et al, 1997; Bons & Montenari, 2005; Hofmann & Farmer, 2000; Budai et al, 2002) indicating that calcite can be very durable as long as groundwater conditions are not highly acidic. There is a problem regarding the durability of chemical and cementitious grouts, which is at a maximum of 25 years for chemical grouts (Whang, 1995) and 150 years for cementitious grouts (Pusch, 2008).

Table 6.1 summarises the performance criteria of MICP, cementitious grouts and a colloidal silica bio-grout as discussed above. The performance criteria in Table 6.1 along with the research showing how to improve the distribution of MICP in Chapter 4, shows that MICP could be effective as a niche grout for specialist low volume applications such as the sealing of small apertures within crystalline rock for the geological storage of nuclear waste.

Table 6.1: performance criteria of MICP, colloidal silica and OPC.

<i>Performance Criteria</i>	<i>MICP</i>	<i>Silica Biogrout</i>	<i>Cementitious Grouts</i>
Permeability Reduction	High	High	Low
Application Ease	Moderate	Moderate	High (with plasticisers, otherwise Low)
Shrinkage Potential	Low	Low – High depending upon saturation	Moderate to High
Shear Strength	Moderate	Low	High
Durability	High	Low	Low - Moderate
Application Speed	Low	High	High

It is not only fractures within the deep subsurface that both MICP and a silica bio-grout may be suitable for, they can also be applied to many near subsurface porous strata that require a reduction in permeability. One such example would be the internal erosion of soils. This involves the relocation and the evacuation of fine particles in the ground by water. Fine grains are loosened from soil by the flowing water and transported through the existing pore space. The loss of fines from a soil can cause an increase in the hydraulic conductivity of the soil and a reduction in its shear strength. These changes to the soil structure can lead to leakage into underground structures such as tunnels and the erosion of transport embankments.

When untreated leakage occurs in concrete tunnels, structural deterioration can occur. Laver et al (2013) found that over 70 years, concrete can lose as much as 2 orders of magnitude in permeability, and its porosity can increase by more than 30%. Leaks within concrete tunnels are generally sealed using grouts such as shotcrete or latex (ITA, 2001). However; this does not remove the water and/or harmful chemicals from the area surrounding the tunnel thus leaks will continue to occur, incurring further remediation costs.

Chemical grouting into the surrounding soil can be applied from the surface or from the tunnel itself. The most commonly used grouts are sodium silicate based or acrylamide. However, these grouts are not ideal, sodium silicate grouts are susceptible to syneresis and there are longevity issues. Some of the organics that are used for gelling of the sodium silicate grout can also have toxic corrosive and environmental effects (Karol, 1983). Acrylamide grouts come closest to the needs of the “ideal grout” described in Chapter 1; however, there are risks to aquatic organisms and workers (RPA, 2000).

MICP has been investigated by other authors for the use of increasing the shear strength of soils, with positive results and only minimal decreases in permeability (DeJong et al., 2006; Whiffin et al., 2007; Van Paassen et al., 2010; Harkes et al., 2010). Improving the shear strength of transport embankments with MICP could be a durable, environmentally friendly method of stabilising these structures without too much reduction to its permeability. MICP has also been able to reduce the permeability of soils and fractures (Gollapudi et al., 1995; Cuthbert et al., 2013). With as much as 99% of the pore space being filled, however there were issues with the distribution of precipitate. The work in Chapter 4 shows that it is possible to improve the distribution of precipitate by appropriate control of the fluid velocity, making MICP a more effective grout. The main drawback of MICP is that it could take from several days to weeks to seal a site. Experimental results in Chapter 4 show that 9 cycles of MICP are required to achieve over two orders of magnitude reduction in permeability. The minimum duration for a cycle is 24 hours. The other limitation of the experimental setup is the small fracture surface area and the parallel flow from inlet to outlet. In a real grouting scenario, it is likely that injection would be through boreholes spaced several meters apart and that flow would be radial close to each injection point. Radial flow has the property of decreasing velocity with increasing distance from the point of injection, thus providing an ideal opportunity to prevent clogging of the fracture immediately adjacent to the injection hole. The flow velocity could then be reduced in stages with the aim of sealing the fracture back towards the injection borehole. This design distance could potentially be quite significant, meaning that grouting larger rock volumes might be possible from a single injection point.

Colloidal silica could be a much quicker alternative to MICP, where hydraulic conductivity can be reduced to at least 10^{-9} m/s (Butron et al., 2010; Noll et al., 1992) and can achieve good results within a day. The penetrability of the colloidal silica grout is related to the gel induction time, in Chapter 5 it was shown that by using bacterial ureolysis as the accelerator, the gel induction time can be delayed with no negative effects on its shear strength (compared to the standard sodium chloride accelerator) thus increasing its penetrability.

When structures already exist or there is a limited working space on granular soils, permeation grouting is a preferred method of stabilisation. This limits the types of grouts that can be used to either fine particulate cements which can be subject to filtration and agglomeration or chemical grouts which can have a poorly controlled gel time, limited penetration or be susceptible to degradation (MacCartney et al, 2011; Karol, 2003). Both MICP and Bacterially Induced Colloidal silica grout could be used as permeation grouts either independently or potentially together. Further research will be required for both of these grouts together but there is potential there to create a grout which can reduce permeability within 1 day unlike MICP then increase in strength (due to the precipitation of calcite) and have more durability than the bacterially induced colloidal silica grout would have itself.

6.2 What further research is required to enable this work to be applied at a field scale?

This research has worked on the technical challenges in the application of MICP include design of the injection rates and aqueous chemistry (e.g. calcium, carbonate, urea, pH buffer and microbial nutrients) in order to control the timing and rate of calcite precipitation to generate the desired spatial distribution. However, there are still properties and processes that still need to be understood.

Mitchell and Ferris (2006) found that the rate of bacterial ureolysis was 10 times greater at 20°C than at 10°C, delaying the onset of precipitation but not impacting the rate of calcite precipitation as temperature had little effect on ureolysis. However; at lower temperatures CO₂ is more soluble thus increasing carbonic acid content which can dissolve calcite also the dissolution of carbonate minerals is exothermic meaning

this reaction is favoured at lower temperatures. Langmuir (1997) states, that there is a fourfold difference 0°C than at 50°C . Again, for geological storage a better understanding of the effects of temperature both on the durability of the grout and the timing of precipitation (necessary to understand the time required for the grouting procedure) are needed before utilisation of MICP for the sealing of fractures.

Colloidal silica has shown great promise as a hard rock grout for the reduction in permeability of fine aperture fractures and has had many of its mechanical properties analysed (Funehag and Axelsson., 2003; Axelsson., 2006; Funehag and Gustafson., 2008; Butron et al., 2008). Further work is still required though. Knowledge is needed on how a bacterially induced colloidal silica grout seals a fracture and how much of an impact time has on the stability of the flowing grout and how the presence of groundwater with varying ion composition and concentration in the fractures affects the final distribution and strength of the grout. Bolisetti (2009) showed that breakthrough fingering of colloidal silica occurred as gelation occurred in sands, it is important to determine if this occurs in fractures and if there is any effect on the shear strength of the grout.

The durability of colloidal silica also needs to be examined further. Yonekure and Miwa (1993) found that no syneresis occurred when using colloidal silica as a grout occurred under saturated conditions. Whang (1995) states that due to the lack of syneresis under saturated conditions a colloidal silica grout should remain stable for more than 25 years. However, colloidal silica is a costly grout at an estimated cost of \$1321 per m^3 (Gallagher et al., 2013), to make it a more popular grout rather than a specialised niche grout, its durability must be known and preferably greater than 25 years and for nuclear waste storage it must be at least 150 years (the lifetime of cementitious grouts).

6.3 How would this research be applied at a field scale?

To use MICP at a field scale there are three important factors; an ability to grow the bacteria economically, a high level of urease activity and a need for the bacteria to be grown in a clean but not necessarily sterile environment. *Sporosarcina pasteurii* fits all three of these factors.

Due to its ammonium requirements, *Sporosarcina pasteurii* produces one of the highest amount of the urease enzyme (Benini, et al. 1999) and shows no inhibition by ammonium unlike other species. Before MICP can be used at a site it must first be grown, this could be either be achieved through the use of a biotechnology company such as Fermensys S.A. France as used by Van Paassen et al (2011) or it could be grown on site, which may be more economic and reduce the need for transportation. The cost of the bacterial growth medium is the most expensive part of the process. Brain heart infusion non-sterile powder costs £3.35 per litre, with potentially thousands of litres required for a large-scale grouting project. Another possibility comes from the research of Achal et al (2009). They looked at producing a growth medium which could be used economically on an industrial scale. Lactose mother liquor is a dairy industry waste; which was used as the sole source of nutrients for the growth of *Sporosarcina pasteurii*. No significant difference in microbial growth or pH was found and although it had the lowest urease production, statistically this was not significant.

Although the bacteria used in this research were all prepared using sterile growth media, Whiffin (2004) tested several batch cultures which had been contaminated with wastewater sludge micro-organisms. After 48 hours incubation, the level of urease activity in cultures with up to 50% contamination was similar or higher than the control culture (0% contamination). This is most likely down to the high pH that the bacterium creates which can disrupt the plasma membranes of other bacterial species, denaturate proteins, and reduce the availability of nutrients (Prescott 2005). Thus it is possible to grow the bacteria on site under clean but not necessarily sterile conditions with a growth medium prepared from a powder. Once the bacteria have been grown, it will be necessary to separate them from the growth medium so that they can be re-suspended in water to the required optical density and prevent bio clogging (Cuthbert et al, 2013). Cationic polyacrylamide flocculants are routinely used in the wastewater treatment industry for concentration of large volumes of cells and could be used to separate the bacteria from the growth medium.

Although the sealing of fractures using MICP may take longer than cementitious grouts, it has greater longevity than cementitious grouts. Once a cement grout has been prepared it sets within a few hours thus must be used or disposed of

incurring further expense. However; bacteria can be viable for several days at 4°C and up to 25 days with no negative effect on urease activity (Whiffin, 2005).

The technology required, for both colloidal silica and MICP grouting could be similar to that of current chemical grouting methods, however with MICP utilising *Sporosarcina pasteurii*, waste ammonium needs to be extracted.

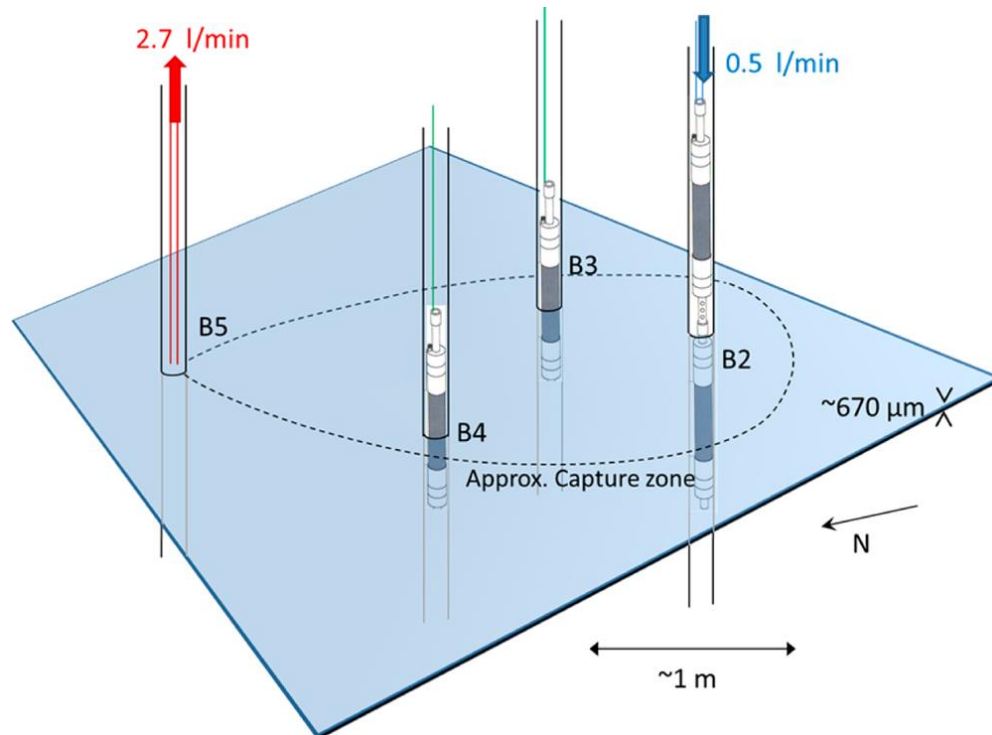


Figure 6.1: Method used by Cuthbert et al (2013) to extract ammonium from a small scale MICP field sealing experiment. The fracture plane is shown in blue; B2 is the injection borehole, B5 the extraction borehole and boreholes B3 & B4 were used for hydraulic testing.

Cuthbert et al (2013) used the set up in Figure 6.1 to extract ammonium. Although this study only involved the sealing of one fracture it shows that low pressure permeation grouting is a viable method for MICP. Extraction of ammonium is required as high concentrations can result in eutrophication of water bodies which receive the discharged groundwater.

7 CONCLUSIONS AND FUTURE WORK

7.1 Conclusions

Geological repositories are being considered as the best feasible solution for the storage of hazardous materials such as high level nuclear waste throughout the world including the UK. However; when crystalline rock is the chosen storage medium, the construction of the underground tunnels and caverns can enhance discontinuities within the rock. These discontinuities can be pathways by which radio-nuclides can reach the biosphere, due to their higher permeability, connectivity and density (Blyth and Freitas, 1992). Thus, depending on aperture, density and predicted travel times, it may be necessary to grout all fractures, even small aperture ones, which over thousands of years can contribute significantly to subsurface flow.

Conventional cementitious and chemical grouts are unsuitable within some regions of a geological disposal facility due to concerns regarding longevity, toxicity, reactions with other barriers and or workability issues. The four main requirements of a grout are; to be of low viscosity as the lower the viscosity the easier it is to achieve good penetration, to have a controllable gel time, as the longer the gel time the greater the penetrability, to be chemically inert to prevent reactions within the subsurface or have any toxic consequences during preparation, and to be durable thus able to withstand exposure to varying physic-chemical condition.

The biological process of calcite precipitation, where bacteria alter their local environment resulting in the precipitation of calcite in calcium rich waters has been sped up and researched for many applications such as the repair of building materials (Van Tittleboom et al, 2009; Sarda et al,2009), the immobilization of contaminants in groundwater, the consolidation of loose soils (Dejong et al, 2006; Van der Ruyt and Van der Zon, 2009; Whiffin et al, 2007; Achal et al, 2009), as a method of reducing the permeability of in-situ strata (Cunningham et al, 2009; Cunningham et al, 2011)) and as a method of strontium immobilization (Warren et al, 2001; Mitchell and Ferris, 2006). This process is generally known as biomineralisation or Microbially Induced Calcite Precipitation (MICP). MICP research has been predominantly focussed on its application in sediments rather than fractures, however, it has shown promise for sealing fractures within rock.

This research initially examined the influence of hydraulic controls (velocity, flow rate, aperture) on the spatial distribution of microbially induced calcite precipitation (MICP) within simulated fractures using flocculated *Sporosarcina pasteurii*. The experimental results showed that under flowing conditions, the spatial distribution of microbially induced calcite precipitate on fracture surfaces was controlled by fluid velocity. Even for a uniform initial fracture aperture with a steady flow rate, a feedback mechanism existed between velocity and precipitation that resulted in a mineral fill distribution that focussed flow into a small number of self-organizing channels which remained stable. Ultimately, this feedback mechanism controlled the final aperture profile which governed flow within the fracture. Calcite nucleated upon the bacterial cell surface and that the transport of flocculated bacteria to the fracture surface was governed by sedimentation. The microbial flocs settled out at a velocity that was dependent on the individual floc size and density. This settling velocity competes with the bed shear velocity, inhibiting deposition via entrainment. As precipitation progresses the flow becomes more channelled within the fracture, enhancing precipitation in regions of low flow and inhibiting it in the remaining high velocity channels.

To use MICP for field scale sealing operations (e.g., in aquifers and host rock surrounding nuclear waste storage sites), it is important to develop an injection strategy that ensures microbially precipitated calcite is distributed homogeneously throughout the rock body to avoid preferential flow through high porosity pathways. The initial batch and flow-plate tests of Chapter 4, determined what changes in the cycle methodology were required. *Sporosarcina pasteurii* was found to be able to hydrolyse urea for several days before the bacteria became encased within calcite preventing access to the cementing fluid. The higher rates of urea hydrolysis occurred within the first 9 hours, though significant rates of urea hydrolysis still occurred after this period. These results showed that the previous methodology of a 30 minute bacteria/30minute cementing solution which was used in Chapter 3 was inefficient and that longer flowing periods for bacteria and cementing solution were required.

Tests on flow-plate 1 (previously used in Chapter 3) showed that by reducing the size of bacterial flocs it is possible to reduce the impact of sedimentation and straining promoting a more even distribution of bacteria thus calcite precipitate

throughout the plate. Under field conditions, grouting fractures will always be performed under flowing conditions. Tests were performed using a bacterial density of 0.5 OD600 with no salt addition (reduced flocculation) and pushed through for one hour followed by either a static period for two hours or continue flowing for another two hours at a flow velocity of 0.93 mm/s. Both the static and flowing bacteria methods produced a more even distribution of calcite precipitate, showing that by increasing the length of time that the bacteria flow, allows for more bacteria to become entrained upon the fracture surface giving a better distribution.

The flow velocity within flow-plate 2 was calculated to be between 0.2 mm/s to 0.71 mm/s at an rpm of 1.25. 9 cycles of the new methodology were applied to flow-plate 2 fracture before back pressure levels rose too high. Precipitation did occur throughout the full fracture with estimated thicknesses being between 0.52mm and 0.18mm changing the topography of the base-plate quite dramatically. An 84% drop in aperture was gained from a 68% (maximum) change in volume. This calculated change in aperture along with laser data showed that the distribution of calcite precipitate was improved with no evidence of channelling as found in Chapter 3. SEM analysis of precipitate samples showed that at the inlet there was a build-up of bacteria, which resulted in a lot of calcite nucleation and smaller crystal size. Further downstream towards the outlet, crystal size increased became better shaped with less evidence of bacterial presence suggesting that crystal growth rather than crystal nucleation was the dominant factor.

It took 9 cycles over 9 days to seal flow-plate 2; which is long for a grouting operation. The introduction of a filler that can also act as a nucleation site for calcite precipitation was examined as a way of reducing the time it takes for the sealing of a fracture. One such filler is colloidal silica. Both *Sporosarcina pasteurii* and colloidal silica have negative surface charges thus colloidal silica could be used as a nucleation surface, this plus its nanometre size which could allow for a better distribution could enhance calcite precipitation and its distribution.

The use of colloidal silica as a filler to enhance the distribution of calcite precipitate was examined in Chapter 5 using the same method that was used in Chapter 4 but with the addition of 25ml of colloidal silica per 1 litre of cementing solution. A clear difference in the mass of grout retained within the fracture was seen, with MICP

alone showing the greatest weight increase. During the 8 grouting cycles with MICP + colloidal silica there appeared to be pieces of calcite travelling through the open channels. This would indicate that the calcite is unable to attach to the fracture surface. When this type of combined grout was used in fine sands as in Tobler et al, MacLachlan et al (2012), the gel like colloidal silica reduced permeability at the pore throats thus retaining the bacteria and associated calcite precipitation within in the system.

The aperture of the simulated fracture was too large to retain the colloidal silica within the system resulting in not only a loss of colloidal silica but also the loss of bacteria/calcite from the system. These results showed us that adding a small amount of colloidal silica to the cementing solution as a filler was not an efficient way to produce calcite fill. However, *Sporosarcina pasteurii* produces ammonium, which as a cation can destabilise the silica sol resulting in gelation, which led to a further question, could we improve colloidal silica gelation and possibly precipitate calcite to increase the strength of a predominantly silica chemical grout?

Batch tests were used to determine what differences in gel point, gel rate and shear strength were created by different cations, including the chemical addition of ammonium ions and the biological production of ammonium ions by the bacterium. The sensitivity of colloidal silica to calcium chloride can result in dramatic differences in gel time with small changes in molarity having great impact on whether the colloidal silica gels or not.

The direct addition of ammonium salts requires ten times the concentration, compared to CaCl_2 , to achieve similar shear strength values. However; this concentration produces very short gel times, potentially reducing the radius of penetration. At similar molarities to ammonium chloride, sodium chloride solutions produce longer gel times with some reduction in shear strength. To attain longer gel times it would be necessary to reduce the molarity of the sodium chloride solution which will reduce its shear strength.

However, bacterial production of ammonium ions gives the greatest gel times yet still produces the same shear strength as that of a sodium chloride accelerator. This increasing of gel times, without adversely impacting grout properties, could be beneficial for penetrating greater distances into fractured rock reducing the number of

injection points required. This would be particularly useful for subsurface engineering applications where large volumes of rock are required to be grouted.

7.2 Future Work

The research presented in this thesis of how the sealing of fractures by MICP and the development of the combined silica Biogrout show great promise as novel, non-toxic and effective small aperture grouts. However, further work is required. Before any field scale tests, the build-up of precipitate at the inlets is problematic and needs to be examined further, also the relationship between bacterial floc size, flow velocity and fracture surface roughness needs to be better understood so that would be possible to calculate what bacterial density and flow velocity was required for the site-specific fracture surfaces and geometry.

The shear strength of MICP as a grout has not been studied in fractures. Lin et al (2014) looked at the bonding strength of calcite between glass beads and calculated the shear strength of calcite to be 616.5 kPa, whilst Verberne et al., (2014) measured the shear strength of calcite gouge to be between 33 to 56 Mpa at a hydrostatic pressure of 10-60 Mpa (equivalent to a depth below surface of 1-4 Km). Clearly, how the strength of calcite changes with depth and temperature needs to be understood, especially when considering its use for geological storage.

Although the initial combined grout did not work as efficiently as MICP alone, I believe this can be improved upon by changing the order in which things are introduced to the fracture. The colloidal silica should be mixed with the bacteria and pushed through the fracture followed by the calcium chloride and urea cementing solution. The reasoning for this change is that the bacteria will still have some urea from the growth broth thus will still produce some ammonium which will begin the gelation of the colloidal silica with the bacteria in place, before application of the cementing solution, thus increasing the number of bacteria retained within the system. Further understanding is also required on how a colloidal silica and bacterial grout seals a fracture, how much of an impact time has on the stability of the flowing grout and how the presence of groundwater with varying ion composition and concentration in the fractures affects the final distribution and strength of the grout.

This research not only furthers our understanding of how MICP can be applied to small aperture fractures but also introduces a novel application of the same bacteria involved in MICP for the improved gelation of colloidal silica as well as the potential for a combined MICP/Silica bio-grout. These avenues of further research are vital to produce a viable alternative to current grouts which have limitations when the grouting site involves hard rock and small aperture fractures.

References

- Achal, V., Mukherjee, A. Basu, P.C. and Reddy, M.S. 2009. Lactose mother liquor as an alternative nutrient source for microbial concrete production by *Sporosarcina pasteurii*. *Journal of Industrial Microbiology and Biotechnology* 36(3): 433-438.
- Achal, V., Pan, X and Ozyurt, N. 2001. Improved strength and durability of flyash-amended concrete by microbial calcite precipitation. *Ecological Engineering*; 37. pp 554 - 559.
- Arnold, J. 2007. *Ureolytic CaCO₃ Precipitation for Immobilization of Arsenic in an Aquifer System*, University of Saskatchewan: 132.
- ASTM D4016 .1993. Standard Test Method for Viscosity of Chemical Grouts by Brookfield Viscometer (Laboratory Method). ASTM International, West Conshohocken, PA, 1993.
- ASTM. 2002. ASTM D2938-95(2002) Standard Test method for Unconfined Compressive Strength of Intact Rock Core Specimens. ASTM International, West Conshohocken, PA, 2002, DOI: 10,1520/D2938-95R02. www.astm.org
- Axelsson, M., 2006. Mechanical tests on a new non-cementitious grout, silica sol: A laboratory study of the material characteristics. *Tunnelling and Underground Space Technology*. 21(5), 554-560.
- Axelsson, M., Gustafson, G., Fransson, Å. and Funehag, J. 2008. Design criteria for permeation grouting in hard rock at great depths. *World Tunnel Congress 2008 - Underground Facilities for Better Environment and Safety – India*.
- Bang, S.S., Galinat, J.K., Ramakrishnan, V., 2001. Calcite precipitation induced by polyurethane-immobilized *Sporosarcina pasteurii*. *Enzyme Microb. Technol.* 28, 404–409.
- Barouki T.H., Martinez B.C., Mortensen B.M., Weathers T.S., DeJong J.D. Ginn T.R., Spycher N.F., Smith R.W. and Fujita Y. (2011) Forward and inverse bio-geochemical modelling of microbially induced calcite precipitation in half-meter column experiments. *Transport in porous media* 90 Special Issue, 23-39

BASF. 2009. Meyco MP320 Solvent-free, low viscosity, hydrophilic grout for rock injection and consolidation of sand and silt strata. See http://www.meyco.basf.com/en/meyco_solutions/TDS/Injection/mineralgrouts/MP320/Documents/TDS_MEYCO_MP_320.pdf . Accessed 8/06/2012.

Benini, S., Rypniewski, W., Wilson, K., Miletti, S., Ciurli, S., and Mangani, S., 1999. A new proposal for urease mechanism based on the crystal structures of the native and inhibited enzyme from *Bacillus pasteurii*: why urea hydrolysis costs two nickels: *Structure*, v. 7, pp 205-216.

Berry, R. S., Rice, S. A. and Ross J. 2000. *Physical Chemistry*, 2nd ed. Oxford University Press, New York.

Beveridge, T.J. and R. J. Doyle. 1989, *Metal ions and bacteria*, Wiley Interscience, 461p.

Bodén, A. & Sievänen, U. 2005. Low-pH injection grout for deep repositories, Summary report from a co-operation project between NUMO (Japan), Posiva (Finland) and SKB (Sweden), SKB Report R-05-40, Swedish Nuclear Fuel and Waste Management Co., Stockholm Sweden.

Bolisetti, T., Reitsma, S. and Balachandar, R., 2009. Experimental investigations of colloidal silica grouting in porous media. *Journal of geotechnical and geoenvironmental engineering*, 135(5), pp.697-700.

Bradford, S. A., J. Simunek, M. Bettahar, M. T. van Genuchten and S. R. Yates. 2006. Significance of straining in colloid deposition: Evidence and implications, *Water Resour. Res.* 42, W12S15,doi:10.1029/2005WR004791.

Brinker C.J., and Scherer G.W. 1990. *Sol-Gel Science - The Physics and Chemistry of Sol-Gel Processing*. Academic Press Limited. London. 457 – 461.

BS 1377-7:1990. Methods of test for soils for civil engineering purposes. Shear strength tests (total stress). British Standards Institution. 62 pages. ISBN: 0580182649

Budai, J. M., A.M. Martini, L.M. Walter, T.C.W. Ku. 2002. Fracture-fill calcite as a record of microbial methanogenesis and fluid migration: a case study from the Devonian Antrim Shale, Michigan Basin, *Geofluids*, 2, 163-183.

Butron, C., Gustafson, G. & Funehag, J. 2008. Grouting in the Nygård Tunnel: Pre-Grouting design for Drip Sealing and Evaluation. Chalmers University of Technology, Department of Civil and Environmental Engineering, Division of GeoEngineering, Engineering Geology Research Group. Report No 2008:2.

Butrón, C., Gustafson, G., Fransson, Å. and Funehag, J., 2010. Drip sealing of tunnels in hard rock: A new concept for the design and evaluation of permeation grouting. *Tunnelling and Underground Space Technology*, 25(2), pp.114-121.

Cheng, H., X. Zhang, and H. Song .2014. Morphological Investigation of Calcium Carbonate during Ammonification-Carbonization Process of Low Concentration Calcium Solution, *J. Nanomater.*, 1–7, doi:10.1155/2014/503696. 376

Cheong, W. C., P. H. Gaskell and A. Neville. 2013. Substrate effect on surface adhesion/crystallisation of calcium carbonate, *Journal of crystal growth*, 363:7-21.

Crawford, A. and Groskopf, G. 1984. Groutability ratio for filter blocking of joints in rock, *Proceedings of the 25th Symposium on Rock Mechanics*, Evanston, Illinois, American Institute of Mining, Metallurgical and Petroleum Engineers, New York, pp. 899–906.

Cunningham, A.B., Gerlach, R., Spangler, L., and Mitchell, A.C., 2009, Microbially enhanced geologic containment of sequestered supercritical CO₂: *Energy Procedia*;1, pp 3245-3252.

Cunningham, A.B., Gerlach, R., Spangler, L., Mitchell, A.C., Parks, S and Phillips, A. 2011. Reducing the risk of well bore leakage of CO₂ using engineered biomineralization barriers. *Energy Procedia*; 4. pp 5178 - 5185.

Cuthbert, M. O., M. S. Riley, S. Handley-Sidhu, J. C. Renshaw, D. J. Tobler, V. R. Phoenix, and R. Mackay. 2012. Controls on the rate of ureolysis and the morphology of carbonate precipitated by *S. Pasteurii* biofilms and limits due to bacterial encapsulation, *Ecol. Eng.*, 41, 32–40, doi:10.1016/j.ecoleng.2012.01.008.

Cuthbert, M. O., L. A. McMillan, S. Handley-Sidhu, M. S. Riley, D. J. Tobler, and V. R. Phoenix. 2013. A field and modeling study of fractured rock permeability reduction using microbially induced calcite precipitation., *Environ. Sci. Technol.*, 47(23), 13637–43, doi:10.1021/es402601g.

DeJong, J.T., Fritzges, M.B. and Nusslein, K. 2006. Microbially Induced Cementation to Control Sand Response to Undrained Shear. *Journal of Geotechnical and Geoenvironmental Engineering*; 132. pp 1381 - 1392.

De Muynck, W., De Belie, N., Verstraete, W., 2010. Microbial carbonate precipitation In construction materials: a review. *Ecol. Eng.* 36, 118–136.

De Muynck, Willem, Leuridan, S., Van Loo, D., Verbeken, K., Cnudde, V., De Belie, N., & Verstraete, W. 2011. Influence of Pore Structure on the Effectiveness of a Biogenic Carbonate Surface Treatment for Limestone Conservation. *Applied and Environmental Microbiology* 77, No. 19, 6808–6820

Derjaguin, B. V., and Landau, L. 1941. Theory of the stability of strongly charged lyophobic sols and the adhesion of strongly charged particles in solutions of electrolyte, *Acta Physicochimica (URSS)*, Vol. 14, pp. 633–662.

DeNovio, N. M., J. E. Saiers and J. N. Ryan. 2004. Colloid movement in unsaturated porous media: recent advances and future directions, *Vadose Zone Journal* 3, 338-351, doi:10.2113/3.2.338.

De Schryver, P., R. Crab, T. Defoirdt, N. Boon and W. Verstraete. 2008. The basics of bio-flocs technology: The added value for aquaculture, *Aquaculture* 277, 125–137.

Dupraz, C., Reid, R.P., Braissant, O., Decho, A.W., Norman, S.R. and Visscher, P.T. 2010. Processes of carbonate precipitation in modern microbial mats. *Earth-Sci. Rev.*, 96, 141–162.

Ehrlich, H.L., 2002. *Geomicrobiology* (4th ed.). Marcel Dekker, New York, pp. 768–800.

Eklund D, Stille H. 2008. Penetrability due to filtration tendency of cement-based grout. *Tunn Undergr Space Technol* 23:390–397

El Mountassir, G., R. J. Lunn, H. Moir, and E. MacLachlan. 2014. Hydrodynamic coupling in microbially mediated fracture mineralization: Formation of self-organized groundwater flow channels, *Water Resour. Res.*, 50(1), 1–16, doi:10.1002/2013WR013578.

Emmelin, A., Brantberger, M., Eriksson, M., Gustafson, G. and Stille, H. 2007. Rock grouting: Current competence and development for the final repository. SKB Report R-07-30, Swedish Nuclear Fuel and Waste Management Co., Stockholm Sweden.

Eriksson, M. & Lindström, L. 2008. KBS-3H post-grouting. Mega-Packer test at -220 m level at Äspö HRL. Svensk Kärnbränslehantering AB Report R-08-42. December 2008.

Ferris, F.G., Stehmeier, L.G., 1992. Bacteriogenic mineral plugging. Patent 5,143,155, U.S. Patent Office, Washington, DC.

Ferris, F.G., Stehmeier, L.G., Kantzas, A., Mourits, F.M., 1996. Bacteriogenic mineral plugging. *J. Can. Petrol. Technol.* 13, 57–67.

Ferris, F. G., V. R. Phoenix, Y. Fujita, and R. W. Smith. 2003. Kinetics of calcite precipitation induced by ureolytic bacteria at 10 to 20°C in artificial groundwater, *Geochemica Cosmochim. Acta*, 67(8), doi:10.1016/S0016-7037(00)00503-9. 392

Forbes, T.Z., Radha, A.V. and Navrotsky, A., 2011. The energetics of nanophase calcite. *Geochimica et Cosmochimica Acta*, 75(24), pp.7893-7905.

Fortin D., Ferris F. G., Beveridge T. J. 1997. Surface-mediated mineral development by bacteria. *Rev. Mineral.* 35, 161–180

Follmer, C., Real- Guerra, R., Wasserman, G.E., Olivera-Severo, D. and Carlini, C.R. 2004. Jackbean, soybean and *Bacillus pasteurii* ureases: Biological effects unrelated to ureolytic activity. *European Journal of Biochemistry* 271: 1357-1363.

Fujita, Y., Redden, G.D., Ingram, J.C., Cortez, M.M., Ferris 2004. Strontium incorporation into calcite generated by bacterial ureolysis. *Geochimica et Cosmochimica Acta* 68(15): 3261-3270.

Fujita, Y., J. L. Taylor, T. L. T. Gresham, M. E. Delwiche, F. S. Colwell, T. L. McLing, L. M. Petzke, and R. W. Smith. 2008. Stimulation Of Microbial Urea Hydrolysis In Groundwater To Enhance Calcite Precipitation, *Environ. Sci. Technol.*, 42(8), 3025–3032, doi:10.1021/es702643g.

Funehag, J. & Axelsson, M. 2003. Hydrogeological characterisation and sealing of narrow fractures in hard rock – A case study. *RMZ-Materials and Geoenvironment* 50, No. 1, 121–124.

- Funehag, J. & Gustafson, G. 2008. Design of grouting with silica sol in hard rock: New design criteria tested in the field, part I. *Tunnelling and Underground Space Technology* 23, No. 1, 1-8.
- Gadd, G. M. 2010. Metals, minerals and microbes: geomicrobiology and bioremediation, *Microbiology*, 156,609-643, doi:10.1099/mic.0.037143-0.
- Gallagher, P. M., and Mitchell, J. 2002. Influence of colloidal silica grout on liquefaction potential and cyclic undrained behaviour of loose sand: *Soil Dynamics and Earthquake Engineering*, v. 22, p. 1017-1026.
- Gallagher, P. M., and S. Finsterle. 2004. Physical and numerical model of colloidal silica injection for passive site stabilization. *Vadose Zone J.*3(3): 917-925.
- Gallagher, P.M., Pamuk, A., Abdoun, T., 2007. Stabilization of liquefiable soils using Colloidal silica grout. *J. Mater. Civil Eng.* 19, 33–40.
- Gallagher, P. M., and Lin, Y. 2010. Colloidal Silica Transport through Liquefiable Porous Media. *Journal of Geotechnical and Geoenvironmental Engineering*; 135. pp 1702 - 1712.
- Gallagher, P. M., S. Spatari, and J. Cucura. 2013. Hybrid life cycle assessment comparison of colloidal silica and cement grouted soil barrier remediation technologies, *J. Hazard. Mater.*, 250-251, 421–430, doi:10.1016/j.jhazmat.2013.01.065. 399
- Gargiulo G, S. Bradford, J. Simunek, P. Ustohal, H. Vereecken and E. Klumpp. 2007. Bacteria transport and deposition under unsaturated conditions: the role of the matrix grain size and the bacteria surface protein, *J Contam Hydrol.* 92(3-4):255-73.
- Glasser, F.P. 1996, Properties of cement waste composites. *Waste Management*: 16, 1-3.
- Gollapudi, U.K., Knutson, C.L., Bang, S.S., Islam, M.R., 1995. A new method for controlling leaching through permeable channels. *Chemosphere* 30, 695–705.
- Gothäll R, Stille H. 2009. Fracture dilation during grouting. *Tunn Undergr Space Technol* 24:126–135

- Hamdan, N., Kavazanjian, E. Jr, Rittmann, B. E., and Karatas, I. 2011. Carbonate mineral precipitation for soil improvement through microbial denitrification. *ASCE Geo Frontiers* 2011: *Adv. Geotech. Eng.*, 211, 3925-3934.
- Hammes, F., Seka, A., van Hege, K., van de Wiele, T., Vanderdeelen, Siciliano, S.D., Verstraete, W., 2003. Calcium removal from industrial wastewater by biocatalytic precipitation. *J. Chem. Technol. Biotechnol.* 78, 670–677.
- Harkes, M. P., L. A. van Paassen, J. L. Booster, V. S. Whiffin, and M. C. M. van Loosdrecht. 2010. Fixation and distribution of bacterial activity in sand to induce carbonate precipitation for ground reinforcement, *Ecol. Eng.*, 36(2), 112–117, doi:10.1016/j.ecoleng.2009.01.004.
- Henn R.W. 2010. *Practical Guide to Grouting of Underground Structures*. American Society of Civil Engineers ISBN: 9780784411322.
- Hernqvist L, Fransson Å, Gustafson G, Emmelin A, Eriksson M, Stille H. 2008. Analyses of the grouting results for a section of the APSE tunnel at Äspö hard rock laboratory. *Int J Rock Mech Min Sci* 46:439–449
- Hilgers C, and J. L. Urai. 2002. Experimental study of syntaxial vein growth during lateral flow in transmitted light: first results. *Journal of Structural Geology*, 24, 1029–43.
- Hofmann, B.A. and Farmer, J.D., 2000. Filamentous fabrics in low-temperature mineral assemblages: are they fossil biomarkers? Implications for the search for a subsurface fossil record on the early Earth and Mars. *Planetary and Space Science*, 48(11), pp.1077-1086.
- Holmqvist, P., M. P. Lettinga, J. Buitenhuis, and J. K. G. Dhont. 2005. Crystallization kinetics of colloidal spheres under stationary shear flow, *Langmuir* 21, 10976-10982, doi. 10.1021/la051490h.
- Iler, R. K. 1979. *The Chemistry of Silica; Solubility, Polymerization, Colloid and Surface Properties, and Biochemistry*. Wiley-Interscience Publication, John Wiley & Sons Inc, New York. p.866.

- Karatas, I., Kavazanjian, E. Jr., and Rittmann, B. E. 2008. Microbially Induced Precipitation of Calcite Using *Pseudomonas Denitrificans*. Proceedings of the First International Conference on Biogeotechnical Engineering, Technical University of Delft, Delft, The Netherlands.
- Karol, R. H. 1983. Chemical Grouting. Marcel Dekker Inc., New York. ISBN 0-8247-1835-6
- Karol, R.H. 2003. Chemical Grouting and Soil Stabilization. Marcel Dekker Inc., New York. 3rd Ed, Revised and Expanded, 2003.
- Kim M, Corapcioglu MY. 2002. Gel barrier formation in unsaturated porous media. *Journal of Contaminant Hydrology*. 56: 75-98. PMID [12076024](#) DOI: [10.1016/S0169-7722\(01\)00204-2](#)
- Kim, JS., Kwon, SK., Sanchez, M., Cho, GC. 2011. Geological storage of high level nuclear waste. *KSCE J Civ Eng* 15: 721. doi:10.1007/s12205-011-0012-8
- Kirby B. J. and E. F. Hasselbrink Jr. 2004. Zeta potential of microfluidic substrates: 2. Data for polymers, *Electrophoresis*, 25, 203–213.
- Konhauser, K. 2007. Introduction to geomicrobiology, Blackwell, Oxford.
- Laaksoharju M, Wold S. (2005). The colloid investigation conducted at the Äspö Hard Rock Laboratory during 2000-2004. SKB Technical Report TR-05-20.
- Langmuir, D. 1997. Aqueous Environmental Geochemistry, Prentice-Hall, Upper Saddle River, NJ 600 pp
- Laver, R.G., Soga, K., Wright, P. and Jefferis, S., 2013. Permeability of aged grout around tunnels in London. *Geotechnique*, 63(8), p.651.
- Leopold, L. B. and M. G. Wolman. 1957. River Channel Patterns: Braided, Meandering and Straight, USGS Professional Paper 282-B: 39-103.
- Mitchell, A. C., and F. G. Ferris. 2006. The coprecipitation of Sr into calcite precipitates induced by bacterial ureolysis in artificial groundwater: Temperature and kinetic dependence, *Geochim. Cosmochim. Acta*, 69(17), 4199–4210, doi:10.1016/j.gca.2005.03.014.

- Mitchell, A.C., Dideriksen, K., Spangler, L.H., Cunningham, A.B., Gerlach, R., 2010. Microbially enhanced carbon capture and storage by mineral-trapping and solubility-trapping. *Environ. Sci. Technol.* 44, 5270–5276.
- Moridis, G.J., Persoff, P., Holman, H.-Y, Muller. S.J., Pruess K., and Radke C.J. 1993. New Barrier Fluids for Subsurface Containment of Contaminants. Proceedings of the ER '93 Environmental Remediation Conference, Augusta, Georgia, October 24th - 28th, 1993, 941-948.
- Moridis, G., Persoff, P., Finsterle, S., Apps, J., James, A., Oldenburg, C., McGrath, A., Myer, L., Pellerin, L., and Pruess, K. 1996. A Design Study for the Isolation of the 281-3H Retention Basin at the Savannah River Site Using the Viscous Liquid Barrier Technology. Lawrence Berkeley Laboratory Report LBL-38920.
- Moseley, M. P. & Kir sch. K. (eds.), 2004, Ground Improvement, 2nd Edition.
- Murphy, E. M. and T. R. Ginn. 2000. Modeling microbial processes in porous media. *Hydrogeology J.*, vol. 8 no. 1, pages. 142-158.
- Noll, M.R., Bartlett, C. and Dochat, T.M. 1992. "In situ permeability reduction and chemical fixation using colloidal silica." Proceedings of the 6th National Outdoor Action Conference, National Ground Water Association, Las Vegas, NV, pp. 443-457.
- NRC 1996. Nuclear Wastes: Technologies for Separations and Transmutation. National Research Council. Washington D.C.: National Academy Press.
- Parks, S. L. 2009. Kinetics of calcite precipitation by ureolytic bacteria under aerobic and anaerobic conditions, MSc thesis Montana State University, USA.
- Okwadha GDO, Li J. 2011. Biocontaminant of polychlorinated biphenyls (PCPs) on flat concrete surfaces by microbial carbonate precipitation. *J Environ Manag*; 92:2860–2864. doi: 10.1016/j.jenvman.2011.05.029.
- Pedersen, K., J. Arlinger, S. Ekendahl, L. Hallbeck. 1997. 16S rRNA gene diversity of attached and unattached groundwater bacteria along the access tunnel to the Äspö Hard Rock Laboratory, Sweden. *FEMS Microbiology Ecology*, 19, 249–262.
- Pedersen, K. 1997. Microbial life in deep granitic rock, *FEMS Microbiology Reviews*, 20, 399-414.

Persoff, P., Moridis, G.J., Apps, J.A., Pruess, K., and Muller, S.J. 1994. Designing Injectable Colloidal Silica Barriers For Waste Isolation at the Hanford Site, in Proceedings, 33rd Hanford Symposium on Health and the Environment, -- In-Situ Remediation: Scientific Basis for Current and Future Technologies, Part 1, p. 87-101. Lawrence Berkeley Laboratory report LBL-35447.

Persoff, P., Moridis, G. J., Apps, J. A., and Pruess, K. 1998. Technical note: Evaluation tests for colloidal silica for use in grouting applications. *Geotech. Test. J.*, 21(3), 264–269.

Microscopic Modeling of Colloidal Silica Stabilized Granular Contaminated Soils (PDF Download Available). Available from: https://www.researchgate.net/publication/245308330_Microscopic_Modeling_of_Colloidal_Silica_Stabilized_Granular_Contaminated_Soils [accessed Jun 16, 2017].

Phillips, A. J., E. Lauchnor, J. Eldring, R. Esposito, A. C. Mitchell, R. Gerlach, A. B. Cunningham and L. H. Spangler. 2012. Leakage Reduction through Biofilm-Induced Calcium Carbonate Potential CO₂ Precipitation, *Environ. Sci. Technol.*, 47, 142-149, doi: 10.1021/es301294q.

Posiva. 2012. Design of the Disposal Facility 2012 – Working Report 2013-2017. http://passthrough.fw-notify.net/download/108504/http://www.posiva.fi/files/3400/WR_2013-17.pdf Date Accessed: 15th January 2017

Prescott, L.M., Harley, J.P. and Klein, D.A. 2005. *Microbiology*, 6th Edition. 122. Boston: McGraw Hill.

Pusch R., 2008. *Geological Storage of Radioactive Waste*. Springer, ISBN 978-3-540-77332-0.

Riding, R. 2000. Microbial carbonates: the geological record of calcified bacterial mats and biofilms. *Sedimentology*; 47. pp 179 - 214.

Rodriguez-Blanco, J. D., S. Shaw and L. G. Benning. 2011. The kinetics and mechanisms of amorphous calcium carbonate (ACC) crystallization to calcite, via vaterite. *Nanoscale*, 3:265-271, doi:10.1039/c0nr00589d.

- Savarmand, S., Carreau, P.J., Bertrand, F., Vidal, D. J.-E. & Moan, M. 2003. Rheological properties of concentrated aqueous silica suspensions: Effects of pH and ions content. *Journal of Rheology* 47, No. 5, 1133 - 1149.
- Schantz Zackrisson, A., Skov Pedersen, J., & Bergenholtz, J. 2008. A small-angle X-ray scattering study of aggregation and gelation of colloidal silica. *Colloids and Surfaces A: Physicochemical Engineering Aspects* 315, 23 - 30.
- Schultze-Lam, S., D. Fortin, B. S. Davis, T. J. Beveridge. 1996. Mineralization of bacterial surfaces, *Chemical Geology* 132, 171-181.
- Schultz, L., Pitts, B., Mitchell, A.C., Cunningham, A.B., Gerlach, R. 2011. Biologically induced mineralization in fully hydrated flow systems. *Microsc. Today* 19, 12–15.
- Sievänen, U., Syrjänen, P. and Ranta-aho, S. 2005. Injection Grout for Deep Repositories – Low-pH Cementitious Grout for Larger Fractures, Field Testing in Finland, Pilot Tests, Working Report 2004-47, POSIVA, October 2005.
- SR97 – Identification and structuring of process. SKB TR 99-20, Svensk Kärnbränslehantering AB.
- Stocks-Fischer, S., J. K. Galinat and S. S. Bang. 1999. Microbiological precipitation of CaCO₃ *Biochem.* 31(11), 1563–1571.
- Summers, L. E., Purkaple, J. D. & Allison, J. D. 1988. Laboratory evaluation of crosslinked polymer gels for water diversion, in: Stahl, G. A., Schulz, D. N. (Eds.), *Water-soluble polymers for petroleum recovery. Proceedings of a National Meeting of the ACS entitled Polymers in Enhanced Oil Recovery and the Recovery of other Natural Resources*, held September 7-12, 1986, Anaheim, California, Plenum Press, New York.
- Sarda, D., Choonia, H., Sarode, D., and Lele, S. 2009. Biocalcification by *Bacillus pasteurii* urease: a novel application: *Journal of Industrial Microbiology and Biotechnology*, v. 36. pp 1111-1115.
- Tobler, D.J., Cuthbert, M.O., Greswell, R.B., Riley, M.S., Renshaw, J.C., Handley-Sidhu, S., & Phoenix, V.R. 2011. Comparison of rates of ureolysis between

Sporosarcina pasteurii and an indigenous groundwater community under conditions required to precipitate large volumes of calcite. *Geochimica et Cosmochimica Acta* 75, No. 11, 3290-3301.

Tobler, D. J., E. Maclachlan, and V. R. Phoenix. 2012. Microbially mediated plugging of porous media and the impact of differing injection strategies, *Ecol. Eng.*, 42, 270–278, doi:10.1016/j.ecoleng.2012.02.027.

Tolppanen, P. & Syrjänen P. 2003. Hard Rock Tunnel Grouting Practice in Finland, Sweden and Norway – Literature Study. Finnish Tunnelling Association, MTR Julkasut N:o 1. 82 p

Torkzaban, S., Tazekhand, S.S., Walker, S.L. and Bradford, S.A. 2008. Transport and fate of bacteria in porous media: Coupled effects of chemical conditions and pore space geometry. *Water resources Research*; 44. pp 1-12.

Trompette, J. L. & Meireles, M. 2003. Ion-specific effect on the gelation kinetics of concentrated colloidal silica suspensions. *Journal of colloid and interface science* 263, 522-527.

Trompette, J.L. and Clifton, M.J., 2004. Influence of ionic specificity on the microstructure and the strength of gelled colloidal silica suspensions. *Journal of colloid and interface science*. 276(2), 475-82.

Tufenkji, N. and M. Elimelech, 2004. Deviation from the Classical Colloid Filtration Theory in the Presence of Repulsive DLVO Interactions, *Langmuir*, 20, 10818-10828.

USACE. 1995. Engineering and Design – Chemical Grouting. EM 1110-1-3500. US Army Corps of Engineers. Washington, DC.

van der Ruyt, M. and Van der Zon, W. 2009. Biological in situ reinforcement of sand in near-shore areas. *Geotechnical Engineering*; 162. Issue GEI. pp 81 - 83.

van Paassen, L. A. 2009. Biogrout: Ground Improvement by Microbially Induced Carbonate Precipitation, Delft University of Technology.

van Paassen, L.A., Ghose, R., van der Linden, T.J.M., van der Star, W.R.L., & van Loosdrecht, M.C. 2010. Quantifying bio-mediated ground improvement by ureolysis:

a large scale Biogrout experiment. *Journal of Geotechnical and Geoenvironmental Engineering* 136, No. 12, 1721- 1728.

van Paassen, L.A. 2011. Bio-mediated ground improvement: From laboratory experiment to pilot applications, *ASCE GeoFrontiers 2011: Advances in Geotechnical Engineering*, Geotechnical Special Publication 211, pp. 4099-4108.

van Tittleboom, K., De Belie, N., De Muynck, W., and Verstraete, W., 2009, Use of bacteria to repair cracks in concrete. *Cement and Concrete Research*, v. 40. pp 157-166.

van Rijn, L. C. 1984. Sediment transport Part 1: Bed load transport, *Journal of Hydraulic Engineering*, 110(10), 1431-1456.

Verberne, B.A., Spiers, C.J., Niemeijer, A.R., De Bresser, J.H.P., De Winter, D.A.M. and Plümper, O., 2014. Frictional properties and microstructure of calcite-rich fault gouges sheared at sub-seismic sliding velocities. *Pure and Applied Geophysics*, 171(10), pp.2617-2640.

Verwey, E. J. W., and Overbeek, J. Th. G. 1948. *Theory of the Stability of Lyophobic Colloids*, Elsevier, Amsterdam.

Warren, L., P. Maurice, et al. 2001. "Microbially mediated calcium carbonate precipitation: implications for interpreting calcite precipitation and for solid-phase capture of inorganic contaminants." *Geomicrobiology Journal* 18(1): 93-115.

Widmann, R. 1996. International society for rock mechanics commission on rock grouting. *Int. J. Rock Mech. Min. Sci. & Geomech. Abstr.* Vol. 33, No. 8. pp. 803-847.

Wan, J., T. K. Tokunaga and C.-F. Tsang. 1995. Bacterial sedimentation through a porous medium, *Water Resources Research*, 31(7), 1627-1636.

Whiffin, V.S. 2004. *Microbial CaCO Precipitation for the Production of Biocement*. Science and Engineering School of Biological Sciences and Biotechnology. Murdoch University. PhD thesis.

Whiffin, V. S., L. a. van Paassen, and M. P. Harkes. 2007. Microbial Carbonate Precipitation as a Soil Improvement Technique, *Geomicrobiol. J.*, 24(5), 417–423, doi:10.1080/01490450701436505.

Yao, K. M., M. T. Habibian, and C. R. O'Melia .1971. Water and waste water filtration: Concepts and applications, *Environ. Sci. Technol.* 5, 1105– 1112.

Young, A. J., Warwick, P., Milodowski, A. E. & Read, D. 2013. Behaviour of radionuclides in the presence of super plasticiser. *Advances in Cement Research* 25, No. 1, 32-43.